DOCTORAATSPROEFSCHRIFT

2010 | Faculteit Wetenschappen

Polymer-fullerene bulk heterojunctions : morphology and its implications on the performance and stability of photovoltaic devices

Proefschrift voorgelegd tot het behalen van de graad van
Doctor in de Wetenschappen, Fysica, te verdedigen door:

Sabine BERTHO

Promotor: prof. dr. Jean Manca
Copromotoren: prof. dr. Dirk Vanderzande
dr. Jan D'Haen

D/2010/2451/32

universiteit hasselt

Chairman	Prof. dr. Marc Gyssens, UHasselt
Promotor	Prof. dr. Jean Manca, UHasselt
Co-promotors	Prof. dr. Dirk Vanderzande, UHasselt
	Dr. Jan D'Haen, UHasselt
Members of the jury	Prof. dr. René A. J. Janssen, TU Eindhoven
	Prof. dr. Guy Van Assche, VUB
	Dr. Wibren Oosterbaan, UHasselt
	Dr. Tom Aernouts, IMEC

Dankwoord

Vijf jaar doctoreren aan het IMO, het zit erop! Toen ik eraan begon leek dit moment nog immens veraf en maar het is omgevlogen. Tijdens deze periode hebben veel mensen mij met raad en daad bijgestaan en hiervoor verdienen zij een bedankje.

Op de eerste plaats wil ik mijn promotor, prof. dr. Jean Manca, bedanken. Tijdens mijn afstudeerstage op het IMO had je genoeg vertrouwen in mij om me te helpen met een FWO aanvraag en zo mijn doctoraat te beginnen. Tijdens mijn doctoraat was het soms een uitdaging om je te vinden maar als dit lukte resulteerde dit altijd in verhelderende antwoorden, nieuwe ideeën en motiverende woorden. Je wist altijd mijn enthousiasme voor het onderzoek terug op te krikken als dit even nodig was. Ook mijn co-promotoren heb ik van tijd tot tijd lastig gevallen met vragen. Voor scheikundige vragen kon ik terecht bij prof. dr. Dirk Vanderzande die mij af en toe deed verbazen van de mogelijkheden binnen de scheikunde. Met morfologie gerelateerde vragen kon ik altijd bij dr. Jan D'Haen terecht. Jan, jouw deur stond altijd open (behalve in de winter als het koud was) en ook al had je het druk met je andere opdrachten, toch maakte je tijd voor mijn vragen. Dikwijls kwam ik binnen met 1 vraag waar je mij vlot mee verder hielp en ging ik buiten met 3 vragen die ik verder kon gaan onderzoeken. Je stimuleerde mij altijd om nieuwe dingen te proberen.

Collega-doctoraatsstudenten zijn ook dikwijls heel behulpzaam geweest. Degene die mij het meeste heeft geholpen is ongetwijfeld Ilse. We hebben 4 jaar een bureau gedeeld. Je hebt mij de beginselen van de TEM bijgebracht en later nog dikwijls geholpen met TEM-vraagjes. Het was fijn dat ik met mijn 'domme' vragen niet onmiddellijk naar Jan moest gaan maar het gewoon samen met jou kon oplossen. Als bureaugenootje was je ook altijd de eerste om mij op te krikken als ik het onderzoek even niet meer zag zitten. We hebben bovendien samen een aantal congressen mogen bijwonen en deze behoren ongetwijfeld tot de mooiste momenten van de afgelopen 5 jaar. En zelfs nu mag ik je nog lastigvallen met vraagjes over het onderzoek tijdens

onze wekelijkse 'lunch-date', ook al is je doctoraat al een tijdje afgerond. Nog iemand van de 'oude garde' die een bedankje verdient is Ann. Ann, je hebt mij onder je hoede genomen tijdens mijn afstudeerstage en voor het eerst mijn interesse in morfologie opgewekt. We hebben de laatste jaren regelmatig gelijkaardige dingen meegemaakt waardoor je één van mijn favoriete gesprekspartners bent. Ik ben blij dat ik je op het IMO heb leren kennen!

Ondertussen zijn er heel wat nieuwe collega's bijgekomen. Jean-Christophe heeft het plaatsje van Ilse overgenomen en ik had geen betere vervanger kunnen wensen. JC, jij bent de meest ijverige, plichtsbewuste onderzoeker die ik ken. Ik bewonder je onuitputtelijke motivatie die af en toe aanstekelijk kan werken. Je hebt bovendien de unieke gave om mij van tijd tot tijd met mijn 2 voetjes op de grond te zetten als ik even het noorden kwijt bent. Ook Bert wil ik bedanken. Ik heb Bert mogen begeleiden tijdens zijn ingenieursstage en dat bleek een heel gemakkelijke opdracht. Bert is volgens mij als onderzoeker geboren; heel stipt en ongelooflijk gedreven. Dankuwel voor het fitten van de degradatiecurves! De andere nieuwe leden van de ONE groep (Fortunato, Donato, Tine, Jeroen, Gopala, Wim, Wouter en Koen) zorgen voor een aangename sfeer in de groep en verdienen hier uiteraard ook een bedankje voor.

Op het IMO zitten ook een paar onmisbare vaste medewerkers. Ik zou niet weten wat ik zonder Johnny had gedaan. Hij heeft meermaals bemiddeld in mijn haat-liefde verhouding met de opdamp. Ook als de spin-coater zijn dagje niet had, stond hij altijd klaar. Voor mijn degradatie-experimenten heeft hij een prachtig kamertje ontworpen. Dankuwel voor alles Johnny! Ik ben zelf geen held in het programmeren maar gelukkig kon ik daarvoor bij Jan M. terecht. Zijn Labview-programma's deden altijd perfect wat ik verwachtte en waren bovendien zeer gebruiksvriendelijk, dat heeft mij veel tijd bespaard! Voor vraagjes over de veiligheid van solventen of het bestellen van materialen stonden Christel en Hilde altijd klaar. Als fysicus was het heel fijn dat er altijd iemand in de buurt was die mij kon helpen met mijn praktische scheikundige vragen.

Natuurlijk verliet ik het IMO ook wel eens de afgelopen 5 jaar. Dan gebeurde het regelmatig dat ik ging aankloppen bij de collega's van organische scheikunde voor hulp. Wibren heeft de P3XT vezels gemaakt maar niet alleen dat; zonder uitzondering, wist hij op elke vraag over organische scheikunde een antwoord te geven. Meestal kon hij het zelfs nog illustreren met een bijpassende publicatie. Met Bert heb ik een tijdje een aangename samenwerking gehad over de gefunctionaliseerde copolymeren gebaseerd op P3HT. Jan heeft gefunctionaliseerde copolymeren gebaseerd op MDMO-PPV gemaakt. Bert en Jan, de dagen dat we samen zonnecellen hebben gemaakt waren altijd heel plezant en vooral relaxed! For the CV measurements, I could count on Elif. Thanks a lot for your help!

Ik zou ook graag de leden van de jury willen bedanken voor hun bereidheid tot het evalueren van dit werk en het Fonds voor Wetenschappelijk Onderzoek – Vlaanderen (FWO) voor de financiële steun.

Tot slot wil ik graag mijn naaste familie bedanken. Mijn ouders hebben mij alle mogelijkheden gegeven om te studeren wat ik wou en hebben mij altijd gesteund tijdens mijn doctoraat. Ze toonden altijd interesse voor mijn onderzoek ook al klonk al die fysica voor hen ongetwijfeld nogal ingewikkeld. Marijke, mijn zus, heeft af en toe haar psychiatriekunstjes op mij mogen uitoefenen als ik het even niet zag zitten. En last but not least wil ik Wim bedanken. Ik heb je vele avonden geambeteerd met mijn gezaag over onderzoek dat niet wou lukken of het gebrek aan inspiratie om te schrijven. Altijd stond je klaar, met een opbeurend gesprek of gewoon een knuffel. Er zijn periodes tijdens mijn doctoraat geweest die voor jou ook niet aangenaam waren maar je bent mij altijd blijven steunen. Ik had mij geen beter ventje kunnen inbeelden!

Dank je wel!

Sabine

Publications

*S. Bertho, I. Haeldermans, A. Swinnen, W. Moons, T. Martens, L. Lutsen, D. Vanderzande, J. Manca, A. Senes, A. Bonfiglio, "Influence of thermal ageing on the stability of polymer bulk heterojunction solar cells", Solar Energy Materials and Solar Cells 91 (2007) 385-389

R. Mens, P. Adriaensens, L. Lutsen, A. Swinnen, S. Bertho, B. Ruttens, J. D'Haen, J. Manca, T. Cleij, D. Vanderzande, J. Gelan, "NMR study of the nanomorphology in thin films of polymer blends used in organic PV devices: MDMO-PPV/PCBM", Journal of Polymer Science Part A: Polymer Chemistry 46 (2008) 138

O. Douhéret, A. Swinnen, S. Bertho, I. Haeldermans, J. D'Haen, M. D'Olieslaeger, D. Vanderzande, J. V. Manca, "High-resolution morphological and electrical characterisation of organic bulk heterojunction solar cells by scanning probe microscopy", Progress in photovoltaics: Research and Applications 15 (2007) 713

S. Bertho, W. Moons, G. Janssen, I. Haeldermans, A. Swinnen, L. Lutsen, J. D'Haen, E. Goovaerts, J. Manca and D. Vanderzande, "Degradation Kinetics of Polymer:Fullerene Bulk Heterojunction Solar Cells", Organic and Nanoparticle Hybrid Photovoltaic Devices, Mater. Res. Soc. Symp. Proc. Volume 1013E, 1013-Z01-08

*S. Bertho, G. Janssen, T.J. Cleij, B. Conings, W. Moons, A. Gadisa, J. D'Haen, E. Goovaerts, L. Lutsen, J. Manca, D. Vanderzande, "Effect of temperature on the morphological and photovoltaic stability of bulk heterojunction polymer:fullerene solar cells", Solar Energy Materials and Solar Cells 92 (2008) 753-760

S. Bertho, I. Haeldermans, A. Swinnen, J. D'Haen, L. Lutsen, J.V. Manca, D. Vanderzande, "How stable are polymer:PCBM bulk heterojunction solar cells?" Organic Optoelectronics and Photonics II. SPIE, Proceedings of SPIE 6129 (2006) 619225

K. Vandewal, A. Gadisa, W.D. Oosterbaan, S. Bertho, F. Banishoeib, I. Van

Severen, L. Lutsen, T.J. Cleij, D. Vanderzande, J.V. Manca, "The relation between open-circuit voltage and the onset of photocurrent generation by charge-transfer absorption in polymer:fullerene bulk heterojunctions solar cells", Advanced Functional Materials 18 (2008) 2064-2070

*S. Bertho, W.D. Oosterbaan, V. Vrindts, J. D'Haen, T.J. Cleij, L. Lutsen, J. Manca, D. Vanderzande, "Controlling the morphology of nanofiber-P3HT:PCBM blends for organic bulk heterojunction solar cells", Organic Electronics 10 (2009) 1248-1251

A. Gadisa, W.D. Oosterbaan, K. Vandewal, J.-C. Bolsée, S. Bertho, J. D'Haen, L. Lutsen, D. Vanderzande, J.V. Manca, "Effect of Alkyl Side-Chain Length on Photovoltaic Properties of Poly(3-alkylthiophene)/PCBM Bulk Heterojunction", Advanced Functional Materials 19 (2009) 3300-3306

D.J.M. Vanderzande, W.D. Oosterbaan, V. Vrindts, S. Bertho, J.-C. Bolsée, A. Gadisa, K. Vandewal, J. Manca, L. Lutsen, T.J. Cleij, J. D'Haen, J. Zhao, G. Van Assche, B. Van Mele, "The use of nanofibers of P3HT in Bulk HeteroJunction Solar Cells: The effect of order and morphology on the performance of P3HT:PCBM blends." Proceedings of SPIE Vol. 7416 741605-1

K. Vandewal, W.D. Oosterbaan, S. Bertho, V. Vrindts, A. Gadisa, L. Lutsen, D. Vanderzande, J.V. Manca, "Varying polymer crystallinity in nanofiber poly(3-alkylthiophene):PCBM solar cells: Influence on charge-transfer state energy and open-circuit voltage", Applied Physics Letters 95 (2009) 123303

B. Conings, S. Bertho, K. Vandewal, A. Senes, J. D'Haen, J. Manca, R.A.J. Janssen, "Modeling the temperature induced degradation kinetics of the short circuit current in organic bulk heterojunction solar cells", Applied Physics Letters 96 (2010) 163301

W.D. Oosterbaan, J.-C. Bolsée, A. Gadisa, V. Vrindts, S. Bertho, J. D'Haen, T.J. Cleij, L. Lutsen, C.R. McNeill, L. Thomsen, J.V. Manca, D. Vanderzande, "Alkyl-Chain-Length-Independent Hole Mobility via Morphological Control with Poly(3-alkylthiophene) Nanofibers", Advanced Functional Materials 20 (2010) 792

Articles with a * are presented in Appendix B-D.

Conference contributions

Oral presentations

S. Bertho, I. Haeldermans, A. Swinnen, K. Vandewal, T. Martens, L. Lutsen, J.V. Manca, D. Vanderzande, "Improved thermal stability of organic solar cells by means of a high T_g electron donor polymer", ICOE2006 International conference on Organic Electronics, 20-22 June 2006; Eindhoven, The Netherlands

S. Bertho, I. Haeldermans, A. Swinnen, W. Moons, L. Lutsen, D. Vanderzande, J.V. Manca, A. Senes, A. Bonfiglio, "Influence of thermal ageing on the stability of polymer bulk heterojunction solar cells", ECHOS'06 European Conference on Hybrid and Organic Solar Cells, 28-30 June 2006; Paris, France

S. Bertho, W. Moons, G. Janssen, I. Haeldermans, A. Swinnen, L. Lutsen, J. D'Haen, E. Goovaerts, J. Manca and D. Vanderzande, "Degradation Kinetics of Polymer:Fullerene Bulk Heterojunction Solar Cells", MRS-Spring meeting, Organic and Nanoparticle Hybrid Photovoltaic Devices, 9-13 April 2007; San Francisco, USA

S. Bertho, I. Haeldermans, A. Swinnen, J. D'Haen, L. Lutsen, J. Manca, D. Vanderzande, "Improved thermal stability of organic solar cells by means of a high T_g electron donor polymer", BSM2007, Belgian Society for Microscopy, 16 November 2007; Liège, Belgium

S. Bertho, W. D. Oosterbaan, J. D'Haen, T.J. Cleij, L. Lutsen, J. Manca, D. Vanderzande, "Study of the morphology of nanofiber-P3HT:PCBM blends used in bulk heterojunction solar cells", EUPOC2008, Europolymer Conference, 1-5 June 2008; Gargnano, Italy

S. Bertho, B. Campo, B. Conings, J. D'Haen, L. Lutsen, J. Manca, D. Vanderzande, "How to improve the thermal stability of organic solar cells?", HOPV2010, Hybrid and Organic Pholotovoltaics Conference, 23-27 May 2010; Assisi, Italy

Poster presentations

S. Bertho, I. Haeldermans, A. Swinnen, J. D'Haen, L. Lutsen, J.V. Manca, D. Vanderzande, "How stable are polymer:PCBM bulk heterojunction solar cells?" SPIE2006 Organic Optoelectronics and Photonics, 3-7 April 2006; Strasbourg, France

S. Bertho, I. Haeldermans, B. Conings, A. Swinnen, J. D'Haen, L. Lutsen, J. Manca, D. Vanderzande, "Improved thermal stability of organic solar cells by means of a high T_g electron donor polymer" EMC2008 European Microscopy Congress, 1-5 September 2008; Aachen, Germany

Table of contents

Nederlandse samenvatting

De laatste decennia is de interesse naar zonne-energie als alternatief voor de conventionele energiebronnen (aardolie, gas en steenkool) toegenomen. Silicium zonnecellen hebben hun weg naar de consumptiemaatschappij al gevonden maar zijn vrij duur. Eén van de goedkopere alternatieven zijn zonnecellen gebaseerd op organische materialen, waar polymeren gemengd met fullereenderivaten zorgen voor het fotovoltaïsch effect.

Het onderzoek naar deze familie van zonnecellen heeft de laatste jaren geleid tot een stijging in efficiëntie richting 8%. The morfologie van de actieve laag blijkt een belangrijke rol te spelen in de optimalisatie van de zonnecellen maar ook in de stabiliteit. In dit werk wordt de morfologie van verschillende polymeer:PCBM systemen bestudeerd en gecorreleerd met de corresponderende fotovoltaïsche performantie en stabiliteit. Een belangrijke, algemene conclusie van dit werk is dat polymeer:PCBM actieve lagen niet stabiel zijn. Een verhoogde temperatuur kan PCBM diffusie veroorzaken en versnellen. Enkele oplossingen voor dit probleem worden hier onderzocht.

In hoofdstuk 2 worden de technieken besproken die gebruikt zijn om de morfologie te bestuderen. Bright Field Transmissie Electronen Microscopie (BFTEM) kan de bulk morfologie van de actieve laag tonen. Selected Area Electron Diffractie (SAED) geeft informatie over de ordening in een staal. Ook UV-Vis is gebruikt in dit werk om het vezelgehalte van P3XT:PCBM oplossingen te berekenen.

Hoofdstuk 3 toont dat het mogelijk is om P3XT:PCBM zonnecellen te maken die geen post-productie thermische behandeling nodig hebben om de kristalliniteit van het P3XT te verhogen. Deze P3XT zijn PAT-vezels die zijn opgelost in een solvent. De zijketens van deze vezels hebben een lengte variërend van 4 tot 9 koolstofatomen. Een nadeel van deze methode was dat verschillende solventen gebruikt moesten worden voor de verschillende materialen om de vezels in oplossing te bekomen. De oplosbaarheid van PCBM was niet altijd optimaal in deze solventen, wat resulteerde in de vorming van grote (> 500 nm) PCBM brokken in de actieve lagen. Er wordt een methode,

gebaseerd op het opwarmen van de oplossing, voorgesteld om de vezel-inhoud van de film te controleren. Voor de P3XT:PCBM films met verschillende vezel-inhoud werden systematisch de morfologie, kristalliniteit en fotovoltaïsche eigenschappen bestudeerd. De kortsluitstroom, J_{sc}, hing grotendeels af van de morfologie van de actieve lagen. Als er een goede menging van P3XT en PCBM was, bereikte J_{sc} een maximum. De openketenspanning V_{oc} was gecorreleerd met de vezel-inhoud. Wanneer de temperatuur van de oplossing verhoogd werd, en hierdoor de vezelinhoud daalde, steeg V_{oc}. Het werd reeds eerder gezien[a] dat de aggregatie van P3HT in vezels leidt tot een verhoging van de oxidatie potentiaal van het polymeer. Aangezien V_{oc} afhangt van het HOMO level van het polymeer, werd de stijging in V_{oc} toegewezen aan de daling van de vezelinhoud bij opwarming van de oplossing. Met de gebruikte solventen varieerde de efficiëntie voor de verschillende P3XT (X = 4 tot 9) tussen 0.6% en 3.1%. P36T (met para-xylene als solvent) behaalde de beste efficiëntie. De efficiëntie bleek echter niet recht evenredig met de vezelinhoud te stijgen, integendeel, een optimum werd gevonden bij gemiddelde vezelinhoud. Dit fenomeen komt overeen met eerdere waarnemingen voor hedendaagse P3HT:PCBM zonnecellen.[b]

Efficiënties van organische bulk heterojunctie zonnecellen zijn geleidelijk gestegen de laatste jaren maar de stabiliteit van deze zonnecellen is nog vrij laag t.o.v. de silicium zonnecellen. Hoofdstuk 4 bespreekt de thermische stabiliteit van MDMO-PPV:PCBM zonnecellen. Een thermische behandeling van deze zonnecellen leidt tot de diffusie van PCBM in de actieve laag. PCBM gaat grote (>1 µm) brokken vormen waardoor het contactoppervlak tussen MDMO-PPV en PCBM kleiner wordt. Hierdoor wordt de exciton dissociatie (die plaatsvindt op het contactoppervlak) minder efficiënt en daalt de kortsluitstroom van de zonnecel. Een Arrhenius model is gebruikt om de degradatie kinetiek van de zonnecellen te beschrijven en de levensduur bij werkingstemperatuur te voorspellen. Een activatie energie van 0.87 eV is bekomen.

In hoofdstuk 5 wordt de stabiliteit van verschillende polymeer:PCBM systemen vergeleken. Als eerste was het populaire P3HT aan de beurt. Zonnecellen

gebaseerd op dit materiaal tonen initieel een verbeterde performantie tijdens een thermische behandeling (het P3HT kristalliseert wat resulteert in een beter ladingstransport) maar na een zekere tijd neemt ook hier de performantie af. Lange thermische behandelingen of behandelingen of hoge temperatuur leiden opnieuw tot de diffusie van PCBM en een daling van de kortsluitstroom. Kleine variaties in het productieproces van de zonnecellen (het gebruik van minder PCBM of het traag drogen van de actieve laag) kunnen de initiële efficiëntie van de zonnecel wel verbeteren (omdat het P3HT al kristallijn wordt tijdens de productie) maar zorgen niet voor een betere thermische stabiliteit. Het structureel veranderen van P3HT met gefunctionaliseerde zijketens bleek de stabiliteit wel te bevorderen. Slechts 10% van deze zijketens was genoeg om de diffusie van PCBM in de actieve laag te verhinderen. Deze verhoogde stabiliteit in de morfologie werd gereflecteerd in een betere stabiliteit van de kortsluitstroom van de corresponderende zonnecellen. Ook het gebruik van een polymeer met een hoge glas transitie temperatuur (hoger dan de normale werkingstemperatuur van de zonnecel) verhinderde de diffusie van PCBM in de actieve laag en resulteerde in een stabielere kortsluitstroom.

[a] T.J. Savenije, J.E. Kroeze, X. Yang, J. Loos, *Thin Solid Films* 511, **2006**, 2
[b] S. van Bavel, E. Sourty, B. de With, J. Loos, *EMC 2008, Vol. 2 Mater. Sci.*, **2008**, 795

Abbreviations and symbols

AFM	Atomic Force Microscopy
AM	Air mass
BF	Bright Field
BHJ	Bulk heterojunction
CB	Chlorobenzene
DF	Dark Field
DSC	Differential Scanning Calorimetry
E_a	Activation energy
EDX	Energy-Dispersive X-ray
FET	Field Effect Transistor
FF	Fill factor
η	Power conversion efficiency
HAADF	High Angle Annular Dark Field
HF	Hydrofluoric acid
HOMO	Highest occupied molecular orbital
HRTEM	High Resolution Transmission Electron Microscopy
I-V	Current-voltage
I_{mmp}	Current at maximum power point
I_{sc}	Short circuit current
ITO	Indium-tin-oxide
J_{sc}	Short circuit current density
k_{deg}	Degradation constant
KPFM	Kelvin Probe Force Microscopy

λ	Wavelength
LUMO	Lowest unoccupied molecular orbital
MDMO-PPV	Poly(2-methoxy-5-(3’-7’-dimethyloctyloxy)-p-phenylenevinylene)
MEH-PPV	Poly[2-methoxy-5-(2'-ethyl-hexyloxy)-p-phenylene-vinylene]
mpp	Maximum power point
M_w	Molecular weight
oCT	Ortho-chlorotoluene
odCB	1,2-dichlorobenzene
OX	Ortho-xylene
P3HT	Poly(3-hexylthiophene)
PAT	Poly-alkylthiophene
PCBM	(6,6)-phenyl C_{61}-butyric acid methyl ester
PCE	Power conversion efficiency
PD	Polydispersity
PEDOT:PSS	Poly(3,4-ethylenedioxythiophene):poly(styrene sulphonate)
PET	Poly(ethylene terephthalate)
P_{in}	Power of incident light
P_{max}	Maximum power
PPV	Poly(p-phenylene vinylene)
PV	Photovoltaics
PX	Para-xylene
SAED	Selected Area Electron Diffraction
SCLC	Space Charge Limited Current
SEM	Scanning Electron Microscopy

SNOM	Scanning Near Field Optical Microscopy
SNPM	Scanning Near Field Photocurrent Microscopy
STEM	Scanning Transmission Electron Microscopy
T_g	Glass transition temperature
TEM	Transmission Electron Microscopy
TMB	Trimethylbenzene
V_{mmp}	Voltage at maximum power point
V_{oc}	Open circuit voltage

Chapter 1

Introduction: organic bulk heterojunction solar cells

This chapter provides a general background about organic photovoltaics. First, the benefits of solar energy are discussed and the characteristic parameters of photovoltaic devices are introduced. The evolution towards the bulk heterojunction concept is elucidated and the importance of the active layer morphology is highlighted.

The materials that will be used throughout this thesis are briefly introduced together with their material properties.

1.1 Photovoltaic energy conversion

1.1.1 Why solar energy?

"*Compared with all the other technical issues facing us in the world today, why is energy the most important? I believe that energy, not the dollar, is the currency of the world. It is the joule that drives every economy and gives people a way out of poverty. Without energy, we cannot find or administer medicine to cure disease, we cannot purify water, we cannot drive our cars; we cannot go to work, operate computers, or even study at night. Because our modern lives run on various forms of energy, we need to find a way to manage our energy challenges before they begin to manage us.*" [1] With these words, Nathan S. Lewis began his talk at the Materials Research Society Spring Meeting in San Francisco (April 11, 2007). It clearly illustrated today's growing energy demand and poses the question for sustainable energy. How are we going to meet the present energy demand without compromising the ability of future generations to meet their needs?

Today's energy consumption is based primarily on nonrenewable energy sources with fossil fuels (petroleum, natural gas and coal) representing more than 80% (Figure 1-1). It is however not possible to keep relying on these fossil fuels. First of all, they are diminishing; Shafiee et al.[2] calculated that oil, coal and gas will be available for another 35, 107 and 37 years, respectively. These numbers are of course indicative but it is certain that future generations will have to learn to be less dependent on the fossil fuels. In addition, these energy sources have a huge environmental impact. We cannot yet assess the consequences of the recent BP oil disaster in the Gulf of Mexico (April 2010) that showed that the exploitation of oil wells is not always straightforward. We do know by now the detrimental effects that the combustion of the fossil fuels brings along. The byproducts of the combustion process are carbon dioxide (CO_2) and sulfur compounds (e.g. SO_2). While the former is related to the greenhouse effect leading to global warming and the rise in sea level, the latter is a cause of acid rain harming the environment. These facts make the search for renewable and ecologically sound energy sources compulsory.

A carbon-free solution for the energy problem would be nuclear power. However, the overall public opinion is concerned about nuclear power, not only because of disasters such as Tsjernobyl but also because of the unhealthy nuclear waste that it brings along.

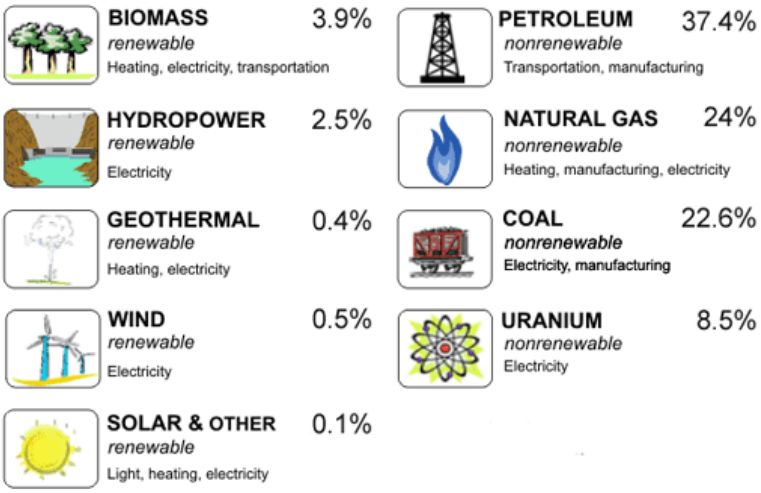

Figure 1-1 Energy consumption in the United States by source in 2008 (source: http://www.eia.doe.gov).

Several renewable and clean energy sources are used already but as Figure 1-1 indicates, they do not contribute to a large part of the energy need today. This is partly because they just cannot satisfy the large energy demand or because we have not learned yet to harvest them thoroughly. E.g. biomass now accounts for about 4% of the total energy consumption and by 2030 it should be able to account for 20%.[3] To satisfy world energy need though, 30% of the total land on Earth would have to be covered with energy farms devoted solely to producing biomass.[1] Hydropower, wind and geothermal energy all exhibit similar properties: even though they are clean and relatively cheap[4] energy sources, they just do not have the potential to fit the total energy demand.[1]

The last renewable energy source, i.e. the sun, can safely be called the champion of all energy sources. The sun provides Earth with 120 000 TW.[5] To put that another way, more energy from the sun hits the earth in one hour

than all of the energy consumed on our planet in an entire year. This poses the question that has kept scientists busy for a few decades now: "How can we harvest as much as possible of the solar energy and do this in the least expensive way?"

1.1.2 Characteristics of PV

The more solar energy is converted into electricity, the higher is the efficiency of a photovoltaic (PV) device. The standardized determination of the performance of a solar cell is done through current-voltage (I-V) recording under illumination.[6-8] In Figure 1-2, the characteristics of a solar cell are outlined on such an I-V curve. The dotted line represents the I-V curve of the cell in the dark which resembles the curve obtained by a diode. When the cell is illuminated, the I-V curve is shifted downwards (solid line).

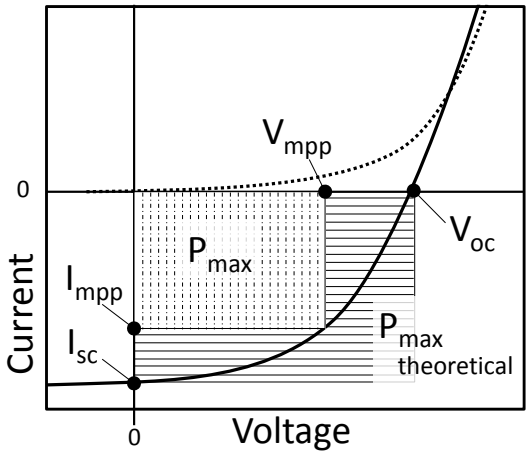

Figure 1-2 Current-voltage (I-V) curve of a photovoltaic device in the dark (dotted line) and under illumination (solid line) with the characteristic parameters.

When no external resistance is applied (i.e. when the electrodes are simply connected), the short-circuit current (I_{sc}) flows through the illuminated solar cell. I_{sc} is the maximum current that a device is able to produce. Under external load, the current will always be less. I_{sc} is proportional to the illuminated area and therefore the short-circuit current density (J_{sc}) is often used for the characterization of the solar cell. The open-circuit voltage (V_{oc}) is

the maximum voltage attainable across the cell; the voltage across the cell in sunlight when no current is flowing.

The power, generated by a photovoltaic device, is the product of current and voltage. In Figure 1-2, it can be illustrated as a rectangle with side lengths equal to a certain voltage value and its corresponding current value. At the maximum power point (mpp), the power reaches its maximum value P_{max}. This point is indicated in Figure 1-2 by its current (I_{mpp}) and voltage (V_{mpp}).

Theoretically, a solar cell could generate a power equal to the product of I_{sc} and V_{oc}. In reality this is never the case. The fill factor (FF), expresses the ratio of a photovoltaic cell's actual maximum power output to its theoretical power output. It is a measure of the 'squareness' of the I–V curve. The formula for FF in terms of the above quantities is:

$$FF = \frac{P_{\max}}{P_{theoreticd\max}} = \frac{I_{mpp}V_{mpp}}{I_{sc}V_{oc}} \qquad \text{(Eq. 1-1)}$$

The overall performance of a solar cell is usually expressed as its power conversion efficiency (PCE or η). It is the ratio of power output to power input. In other words, PCE measures the amount of power produced by a solar cell relative to the power available in the incident radiation (P_{in}). The formula for PCE, in terms of the quantities defined above, is:

$$PCE = \eta = \frac{P_{\max}}{P_{in}} = \frac{I_{mpp}V_{mpp}}{P_{in}} = \frac{I_{sc}V_{oc}FF}{P_{in}} \qquad \text{(Eq 1-2)}$$

As PCE depends on the irradiated light power, standard measurement conditions have to be used to be able to compare different devices. These exact conditions have been laid down in internationally agreed standards.[9] A solar cell should be measured at 25°C under 100 mW/cm^2 of Air Mass (AM) 1.5 radiation. The AM 1.5 radiation is a standard illumination that resembles the solar emission spectrum and intensity received on a tilted (37°) plane surface on a clear day with a solar zenith angle of 48.2°. The term air mass refers to the changes in the spectrum and intensity of the sunlight as it is

transmitted through the earth's atmosphere. AM 1.5 means that the light passes 1.5 times the atmosphere thickness before reaching the earth's surface (this corresponds to the solar zenith angle of 48.2°). The AM 1.5 solar spectrum is depicted in Figure 1-3.

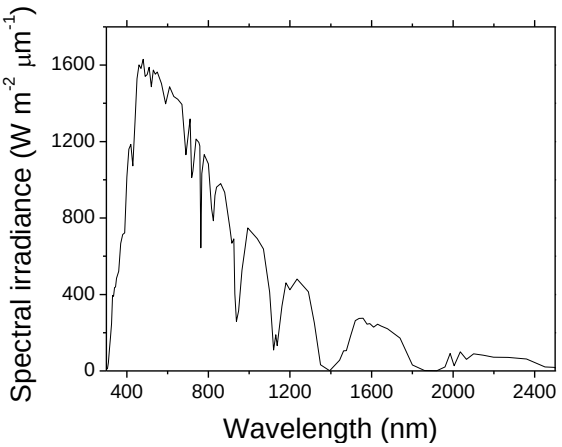

Figure 1-3 The AM 1.5 solar spectrum with a total irradiation power of 100 mW/cm^2.

1.2 Organic photovoltaics

1.2.1 Background

The discovery of the photovoltaic effect is commonly ascribed to Becquerel, who discovered a photocurrent when platinum electrodes, covered with silver bromide or silver chloride, were illuminated in aqueous solution.[10] In 1873, Smith[11] made the first report on photoconductivity working on selenium. Anthracene was the first organic compound in which photoconductivity was observed.[12] The efficiencies remained very low until the discovery of silicon (Si) solar cells by Russell Ohl in 1941.[13] Thirteen years later, the company Bell Laboratories, demonstrated a Si solar cell capable of a 6 % energy-conversion efficiency when used in direct sunlight.[14] Over the years the efficiency has reached 24% for crystalline Si solar cells in the laboratory (Figure 1-4). Today Si-based solar cells are by far the most dominating type of PVs used and account for 99% of all PVs. Fifty years of research and innovation has dramatically reduced the price of Si PVs to the lowest level possible using

existent technology. However, despite much effort of further reducing the price of Si based PVs, they still account for less than 0.1% of the total world energy production (Figure 1-1).

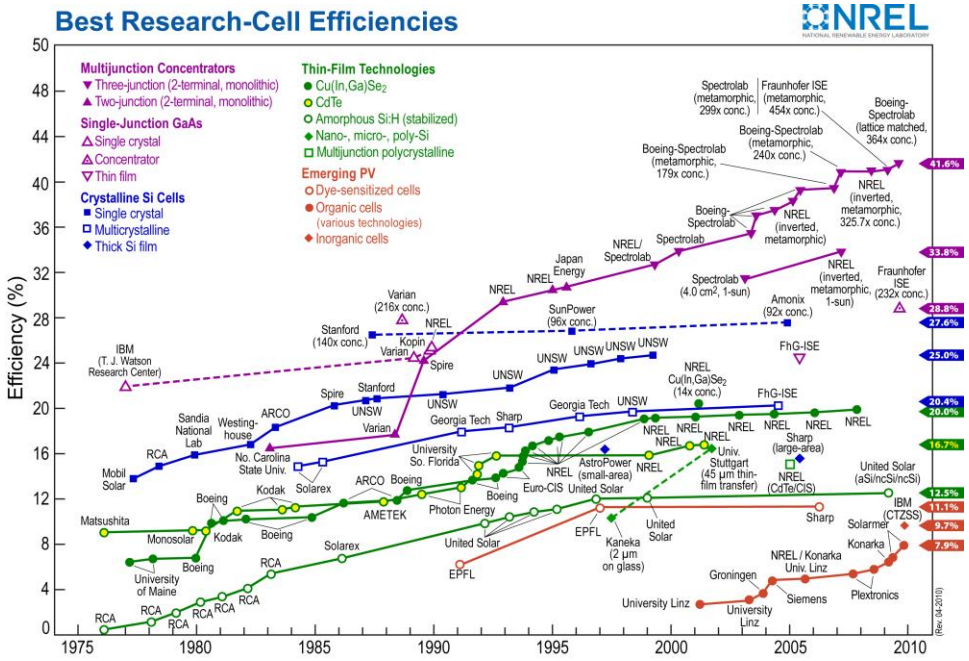

Figure 1-4 The evolution of best research-cell efficiencies.[15]

In the search for cheaper alternatives for Si solar cells, several routes are currently under investigation.[16] One of them is based on organic semiconductors which exhibit many attractive features:[17]

- the potential to be flexible and semitransparent
- the potential to be manufactured in a continuous printing process
- large area coating
- easy integration in different devices
- significant cost reduction compared to traditional solutions
- substantial ecological and economic advantages

This work will focus on fully organic solar cells that comprise of conjugated polymers and fullerene derivatives. The next sections will elucidate the progress that has been made in this area of research upon the last years.

1.2.2 The need for a bulk heterojunction

The working principle of organic solar cells[18] differs fundamentally from that of inorganic solar cells. In a classical inorganic solar cell, the absorption of sunlight generates pairs of charge carriers (electrons and holes). These two oppositely charged carriers are only weakly Coulomb bound. The potential drop at the interface between a p- and an n-doped semiconductor layer (the p-n junction), leads to their separation and subsequent transport to the respective contacts: a current flows.

In organic semiconductors, the screening of opposite charges is much weaker as the dielectric constant is lower. This leads to a stronger interaction of the photogenerated positive and negative charges. The primary optical excitation in organic materials is called an exciton, i.e. a strongly bound electron-hole pair. This binding is more difficult to overcome as compared to inorganic systems, which creates special requirements for the lay-out of organic solar cells.

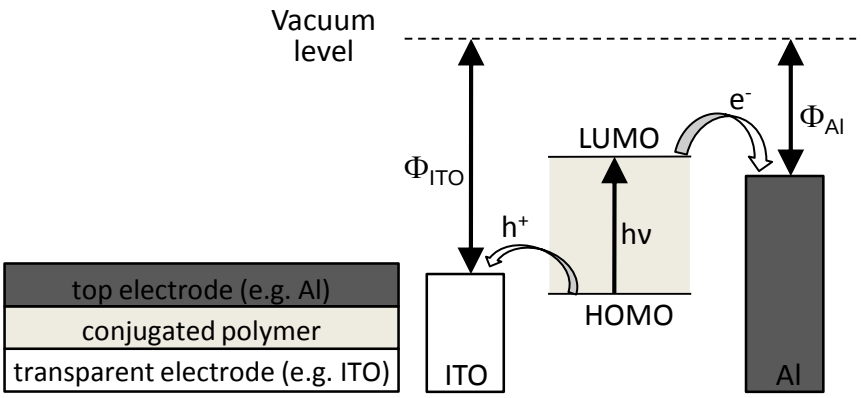

Figure 1-5 The lay-out (left) and the operating principle (right) of a single layer organic photovoltaic device. Commonly used electrodes are indium-tin-oxide (ITO) as transparent electrode and aluminium (Al) as top electrode.

The first generation of organic photovoltaic solar cells was based on a single layer of conjugated polymer sandwiched between two metal electrodes of different work functions (Figure 1-5). When light is absorbed by the polymer, an electron is promoted from the highest occupied molecular orbital (HOMO)

to the lowest unoccupied molecular orbital (LUMO); an exciton is created. To generate photocurrent, this process must be followed by exciton dissociation. Close to the electrodes, a band bending occurs at the Schottky barrier between the metal contact with the lower work funtion and the semiconducting polymer.[19] In the electric field that is created by this band bending, excitons can be dissociated. Because the exciton diffusion length for most organic solar cell materials is about 5-15 nm,[20] only those excitons generated in a small region from the contacts contribute to the photocurrent. Therefore, the power conversion efficiencies for these single layer devices were generally poor (in the range of 10^{-3} to 10^{-2} %). A remarkable high efficiency of 0.7% was reported by Morel et al who used merocyanine dyes as active materials.[21]

A step forward for organic photovoltaics came with the introduction of the bilayer heterojunction device by Tang et al.[22] that reached an efficiency of 1%. In this bilayer device, a donor and an acceptor material are stacked together with a planar interface (Figure 1-6). The charge separation occurs at this interface and is mediated by a potential drop between donor and acceptor. The bilayer is sandwiched between two electrodes matching the donor HOMO and the acceptor LUMO, for efficient extraction of the corresponding charge carriers.

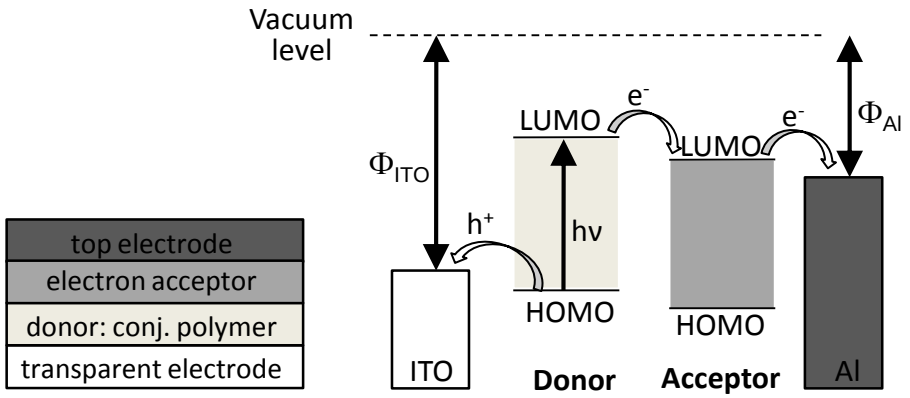

Figure 1-6 The lay-out (left) and the operating principle (right) of a bilayer organic photovoltaic device.

Although this device lay-out is an improvement compared to single layer

devices, it is still exciton diffusion limited. Only excitons in the proximity of the interface will be dissociated. Excitons created at distances further than their diffusion length, will recombine before they can reach the donor-acceptor interface. To overcome this problem, the bulk heterojunction (BHJ) concept was introduced (Figure 1-7). For these devices, donor and acceptor materials are intimately mixed and create a nano-scale interpenetrating bicontinous network within the whole photoactive layer. A large interfacial area now exists between donor and acceptor material and excitons are more likely to be dissociated than for bilayer devices. In the ideal case, the materials would be mixed on a scale smaller than the exciton diffusion length, but they would also form direct pathways to the electrodes (Figure 1-7, right). In this way, the dissociated charges would not get stuck on a loose end but instead good percolation would be possible.

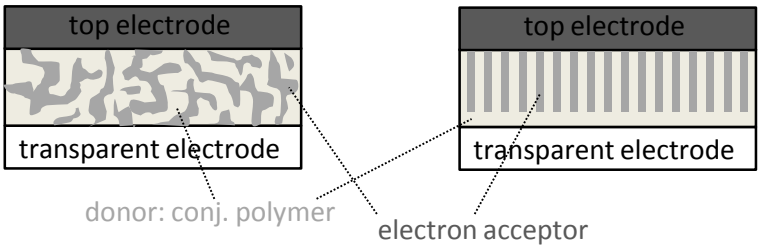

Figure 1-7 Lay-out of a common BHJ existing of donor polymer and acceptor material closely mixed (left). A 'perfect' BHJ (right) that creates 'highways' for the charges to the electrodes.

1.2.3 Physical processes in polymer:fullerene bulk heterojunction solar cells

The production of electric energy in polymer:fullerene BHJ solar cells is the result of a chain process. This section discusses the consecutive processes that (need to) take place.

Creation of excitons

To reach a high efficiency, the active layer of a solar cell should capture a large fraction of the incoming sun light. Because of the high absorption coefficient ($\sim 10^5$ cm^{-1}), [23,24] conjugated polymers absorb light very efficiently

at the maximum of their absorption spectrum. As a result a layer thickness of only a few hundred nanometer is required to absorb all the light at their peak wavelength absorption. On the other side, the absorption bands of conjugated polymers are relatively narrow; only a small region (350 – 650 nm) of the solar spectrum is covered. In addition, their bandgaps are rather high. Most solution processable semiconducting polymers have bandgaps larger than 1.9 eV (650 nm), whereas a bandgap of 1.1 eV (1100 nm) is required to cover 77% of the solar radiation on earth.[25] Developing low bandgap materials is a possibility to enhance the absorption.[26] Even better would be the development of tandem cells containing a polymer with a high bandgap as well as one with a low bandgap.[27,28]

Diffusion of excitons in conjugated polymers

Once an exciton is created upon absorption of photons with enough energy, it has to diffuse to the donor/acceptor interface before dissociation can take place. In the ideal case, the characteristic size of the polymer phase has to be smaller than the exciton diffusion distance (5-15 nm) in order to grant that all excitons can reach the donor/acceptor interface before they recombine.

Exciton dissociation at the donor/acceptor interface

For efficient electron transfer from the polymer to the acceptor, the energy levels of both materials have to be well aligned (Figure 1-6, right). A downhill energetic driving force is necessary and this driving force must exceed the Coulombic attraction of the bound electron–hole pair in the donor. Empirically, the overall energetic driving force for the electron transfer from the donor to the acceptor is represented by the energy difference between the LUMOs of the donor and acceptor.[29] A minimum energy difference of 0.3 eV is required for exciton splitting and charge dissociation.[30]

Charge transport in polymer:fullerene blends

After the electron transfer at the donor/acceptor interface, the electrons are localized in the acceptor phase whereas the holes remain in the donor polymer chains. Subsequently, the free electrons and holes must be transported via percolated pathways towards the electrodes to produce photocurrent. This

requires a morphology as indicated in Figure 1-7 were the characteristic size of the polymer phase should not exceed the exciton diffusion length (see above). Also, the hole mobility of the donor polymer as well as the electron mobility of the acceptor fullerene have to be large enough (> 10^{-4} cm^2 V^{-1} s^{-1})[30,31] to achieve effective charge transport.

Extraction of the charge carriers at the electrodes

After transportation of the charges towards the electrodes, they can be extracted. Good charge collection is obtained if the work functions of the electrodes match the HOMO of the donor and the LUMO of the acceptor.[32]

One of the electrodes has to be transparent to allow passing of the sunlight. Usually indium-tin-oxide (ITO) is chosen. To smooth the surface and to improve the hole injection, a poly(3,4-ethylenedioxythiophene):poly(styrene-sulfonate) (PEDOT:PSS) layer is spin-coated on top of the ITO.[33] The top electrode, which collects the electrons, should have a work function close to the LUMO of the acceptor material. Different materials can be used,[34] e.g. aluminum (Al), magnesium (Mg), silver (Ag),… In this work, Al (with typical thickness of 80 nm) was used as top electrode. Between the active layer and the Al, a thin (~ 20 nm) Calcium (Ca) layer, which increases the FF of the solar cells,[35] was inserted.

1.3 Interpenetrating networks and morphology

After the introduction of the BHJ concept in organic solar cells,[36] interest in the active layer morphology significantly increased. First studies on the morphology were done on systems containing poly[2-methoxy-5-(2'-ethyl-hexyloxy)-p-phenylene-vinylene] (MEH-PPV).[37,38] Yang and Heeger performed TEM on MEH-PPV:C_{60} bulk heterojunctions and observed both isolated and connected regions with characteristic size of about 10 nm, corresponding to the C_{60} phase. For increasing C_{60} content, increasing percolation and a bicontinuous network formation of the C_{60} phase within the MEH-PPV network was reported. Furthermore, the application of electron diffraction on the MEH-PPV:C_{60} blends with a weight ratio of approximately 1 : 4 revealed a crystalline organization of the C_{60}. It was concluded that C_{60} in the blend formed

nanocrystallites having sizes of roughly 10 nm.

Traditionally electron microscopy served as an exploration tool for the bulk heterojunction morphology in thin films, mainly in the form of TEM in connection with Selected Area Electron Diffraction (SAED).[39] Later on, other techniques also proved their effectiveness. Scanning Electron Microscopy (SEM) resolved the fine structure of polymer-fullerene composites.[40] Atomic Force Microscopy (AFM), especially in the non-contact mode, was applied to investigate the polymer-fullerene blend film topography.[40-42] Also more sophisticated derivatives like Kelvin Probe Force Microscopy (KPFM),[43] Scanning Near Field Optical Microscopy (SNOM) detecting photoluminescence[44] and Scanning Near-field Photocurrent Microscopy (SNPM) detecting photocurrent[45] have been used.

With all these techniques, it is possible to get a lot of information on the active layer morphology of current BHJ solar cells. The challenge still remains however to approach the optimal morphology (see Figure 1-7, right) as good as possible. The morphology of the photoactive blend is affected by several production parameters during the film formation or by post production treatments. Below, the parameters that are most significant for their influence on the nanoscale morphology are discussed.

Casting solvent

Though C_{60} had good electronic properties to serve as acceptor material in BHJ solar cells, its solubility in organic solvents was limited. When high concentration blends were used, the C_{60} had the tendency to crystallize.[36] Yu et al. overcame this problem by incorporating soluble C_{60} derivatives that were developed previously.[46] When using 1,2-dichlorobenzene (odCB) as solvent, MEH-PPV:PCBM films with a weight ratio of 1:4 could be achieved. This resulted in a significant increase of the photocurrent of the corresponding solar cells. Until today, the PCBM (1-(3-methoxycarbonyl)propyl-1-phenyl [6,6]C_{61}) that they introduced in solar cells, is still the most popular electron acceptor in organic BHJ solar cells.

Shaheen et al.[47] demonstrated the importance of the casting solvent for

MDMO-PPV:PCBM 1:4 solar cells. When they changed the solvent from toluene to chlorobenzene, the power conversion efficiency increased from 0.9% to 2.5%. This enhancement was mainly due to an increase in I_{sc} and was attributed to finer grain sizes in the thin film nanomorphology, revealed by AFM. This was confirmed by Martens et al.[48-50] with TEM (Figure 1-8). Upon increasing the PCBM concentration in the blend, an increasing number of dark clusters was observed; they were attributed to the fullerene-rich phase. Interestingly, the chlorobenzene based blends were able to incorporate more PCBM than the toluene based counterparts. In the toluene cast films, the PCBM clusters were larger in size (up to several 100 nm) as compared to chlorobenzene cast films (less than 100 nm). The morphology obtained by using chlorobenzene as casting solvent (Figure 1-8) resembles more the desired morphology in Figure 1-7. Due to the smaller grain size of PCBM, a larger interface area between polymer and PCBM exist, which is beneficial for exciton dissociation. On top of that, the PCBM clusters that serve as percolation paths for the electrons are closer together. This makes it easier for charges to reach these 'highways' before recombination occurs.

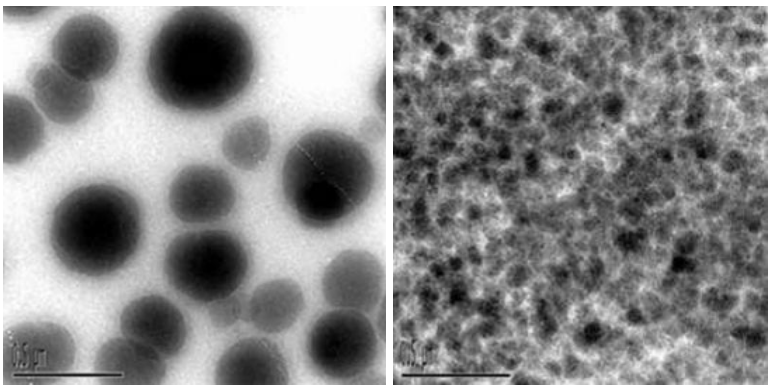

Figure 1-8 MDMO-PPV:PCBM 1:4 thin films spin-coated from toluene (left) and chorobenzene (right). Reprinted from ref 50.

For solar cells based on poly-alkylthiophenes (PAT), the solvent can also make a difference in morphology. Chang et al.[51] observed higher field-effect mobilities for P3HT (poly-3-hexylthiophene) when it was spin-coated from high boiling point solvents. This increase was attributed to a highly crystalline

morphology, with efficient interchain stacking of the polymer. Vanlaeke et al.[52] implemented this in photovoltaic devices and observed that spin-coating P3HT:PCBM 1:2 from tetrahydronaphtalene with a boiling point of 207 °C resulted in an efficiency of 3.6%, while using chlorobenzene (with a boiling point of 132 °C) with the same preparation conditions gave an efficiency of 0.25%. Due to the low boiling point of chlorobenzene the morphology of the spin-coated films was frozen very rapidly. XRD confirmed that this quick freezing deprived the P3HT of the time to self-organize into crystalline structures.

Peet et al.[53] observed the effect of using appropriate additives on the morphology of solar cells. By incorporating a few volume per cent of alkanedithiols in the solution used to spin-coat the active layers, comprising a low-bandgap polymer and a fullerene derivative, the efficiency of photovoltaic devices was increased from 2.8% to 5.5% through altering the bulk heterojunction morphology. Using a mixture of solvents, in which the donor and the acceptor had different solubilities, induced the formation of ordered aggregates directly in solution, leading to an optimally segregated donor-acceptor morphology during the film deposition.

Blending ratio of donor and acceptor material

In the first report on MEH-PPV:PCBM BHJ solar cells, the authors found the best performance for a blending ratio of 1:4 between polymer and fullerene.[36] Also for blends with the very similar MDMO-PPV, this weight ratio proved to give the best performance. Since the photoluminescence of MEH-PPV could be quenched efficiently with much smaller amounts of fullerenes (less than 5%),[54] the conclusion would be that efficient charge transport is still prohibited for smaller volume ratios of the fullerene due to insufficient fullerene phase percolation. Indeed, Yang et al. see more interconnections in the MEH-PPV:C_{60} system with increasing fullerene concentration.[38]

Van Duren et al.[55] applied a variety of techniques to relate the morphology of MDMO-PPV:PCBM blends, cast from chlorobenzene, to the solar cell's performance. They studied a wide range of MDMO-PPV:PCBM weight ratios.

For PCBM contents less than 50%, homogeneous mixing of the components was observed. At 67% PCBM content, an abrupt improvement in the device properties coincided with the onset of phase separation around 67% PCBM content. The optimum photovoltaic performance at 80% PCBM content is explained by the percolation network that is build with pathways large enough to facilitate escape from the interface. Mihailetchi et al.[56] showed that this enhanced percolation leads to the highest electron mobility at 80% PCBM content. Also the hole mobility reached an optimum at this point, with a value very close to the electron mobility. The similar mobilities of both charge carriers, prevent charge accumulation of either of the charge carriers because both will be transported with equal pace towards the electrodes.

For every different material system, other optimum weight ratios have to be found. For example, the regioregular P3HT:PCBM system, has its optimum weight ratio close to 50% PCBM content.[57,58] Cates et al.[59] suggested that this optimum weight ratio depends on the ability of the fullerene derivative to intercalate between the polymer side chain. For intercalated blends, an optimum performance would be achieved for a 1:4 polymer:fullerene weight ratio, whereas nonintercalated blends optimize at 1:1.

Concentration of the casting solution

Solutions with a constant MDMO-PPV:PCBM 1:4 mixing ratio but with different solution concentration were spin-coated from toluene by Hoppe et al.[40] AFM scans revealed that the fullerene cluster size and the average film thickness were increased with higher concentration. The extent of phase separation thus not only scales with increasing fullerene fraction but also with an increasing total concentration of the solution. To investigate whether the clusters are present already in solution or built up during film formation, identical solutions were spin-coated with different spin frequencies. For higher spin frequencies, the mean size of the clusters was reduced. This made it reasonable to assume that the phase separation is not present in the solution, but develops during film deposition. As could be expected, the film thicknesses were smaller for the films spin cast at the higher spinning frequency. Hence the cluster sizes correlate with the film thickness at constant solution concentration.

Post production treatment

When P3HT came into focus as electron donor material in BHJ solar cells, post production treatments proved their purpose. Padinger et al.[60] combined a heat treatment with the application of a dc voltage and could raise the power conversion efficiency from 0.4% to 3.5%, at that point a new record for polymer-fullerene BHJ solar cells. The better performance was explained by the crystallization of P3HT that takes place when annealed above its glass transition temperature (T_g).[61] This crystallization brings along a dramatic increase in the hole mobility of the polymer.[62] Yang et al.[63] studied this material system with TEM and SAED. They concluded that upon annealing, P3HT forms long, thin conducting nanowires in a rather homogeneous, nanocrystalline PCBM film. The improved crystallinity of P3HT but also of PCBM together with the controlled demixing at nanoscale created a better percolation network and resulted in the considerable increase of the efficiency observed in the devices. The P3HT:PCBM system has been the focus of many studies[57,64-70] and by carefully tuning the annealing conditions, efficiencies of over 5% could be reached.[71,72]

As an alternative to thermal annealing, microwave irradiation[73,74] has been recently proposed to enhance the performance of polymer solar cells. Microwave annealing induces the crystallization of the P3HT in P3HT:PCBM active layers similar to thermal annealing. This led to efficiencies up to 3%.

Another possibility to enhance active layer morphology, that does not need high temperatures, is controlling the drying time of the active layer, i.e. "solvent annealing"[75] or even "solvent vapor annealing".[76] By slowing down the drying of the P3HT:PCBM films, the system is allowed to self-organize into an ordered structure, comparable to the heat treated morphology.

Chemical structure of the materials

As mentioned above, the introduction of the more soluble C_{60} derivative PCBM allowed the incorporation of a larger fraction of fullerenes into polymer-fullerene blend films.[36] The same holds for the conjugated polymers, whose solubility also depends on the side-chains. Thus it is clear that the part of the

chemical structure that provides the solubility is an important parameter for reaching well-blended bulk heterojunctions of the constituents at the nano scale.

Another factor is the chemical compatibility between the polymer and the fullerene itself: while MDMO-PPV:PCBM 1:4 blends generally yielded the best results when spin-coated from chlorobenzene, this solvent could not deliver similar good results for an MDMO-PPV:C_{70}-PCBM 1:4 blend. Wienk et al.[77] reported that for this material system small scale phase separation occurred when ortho-dichlorobenzene was used as casting solvent instead of chlorobenzene.

Blending donor and acceptor components is currently the most effective approach for efficient power conversion efficiency. Another route towards controlled nano phase separated and bicontinuous morphology could be the synthesis of block copolymers, where the donor and acceptor component would be attached to each other. This possibility has attracted some attention but is not (yet) able to compete with the donor/acceptor blends.[78,79]

1.4 Stability

One of the general bottlenecks of organic solar cells is their poor stability. Polymers exhibit a low resistance towards oxygen in combination with UV/Vis light or high temperatures, which results in a degradation of the solar cells.[80-83] It has been reported by Neugebauer et al.[84] that the use of fullerenes in a blend with a polymer gave an improved stability compared with single component devices due to a slower degradation of the polymer in the mixture. However, the incorporation of fullerenes induces a thermal instability of the active layer morphology, yielding observations such as phase separation and PCBM clustering.[85,86] Annealing treatments bring along the demixing of polymer and PCBM, resulting in a reduced interfacial area and less efficient exciton dissociation. This instability of the active layer morphology is one of the foci of this work and will be discussed in more detail in chapters 4 and 5.

1.5 Materials

Throughout this work, different conjugated polymers will be used as donor material in organic BHJ solar cells. The fullerene derivative PCBM will always be used as acceptor material. Below, these materials will be discussed briefly.

1.5.1 MDMO-PPV

The structure of poly[2-methoxy-5-(3,7-dimethyloctyloxy)]-1,4-phenylene-vinylene or MDMO-PPV is depicted in Figure 1-9.

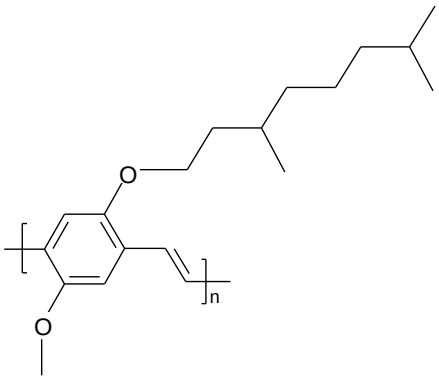

Figure 1-9 Structure of MDMO-PPV.

Characterization of MDMO-PPV was done by S. Fourier of the Organic Chemistry group at UHasselt.[87] Through a UV-Vis absorption measurement, the optical bandgap was determined to be 2.1 eV. Cyclic voltammetry showed that the HOMO level was situated at -5.3 eV and the LUMO level at -2.8 eV. This gave an electrochemical bandgap of 2.5 eV. The glass transition temperature (T_g) of MDMO-PPV was determined with the same procedure as 'High T_g PPV' (see section 1.5.4), which resulted in a value of 68 °C.

1.5.2 P3HT

The structure of poly(3-hexylthiophene) or P3HT is depicted in Figure 1-10.

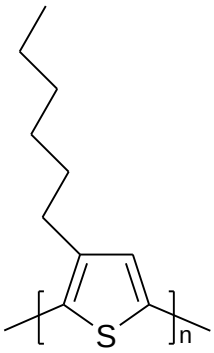

Figure 1-10 Structure of P3HT.

Cyclic voltammetry showed that the HOMO level of P3HT was situated at -5.2 eV and the LUMO level at -3.5 eV.[88] This gave an electrochemical bandgap of 1.7 eV. The optical bandgap, determined through UV-Vis, was 1.9 eV. The T_g of P3HT was determined through differential scanning calorimetry (DSC) to be 18 °C.[89]

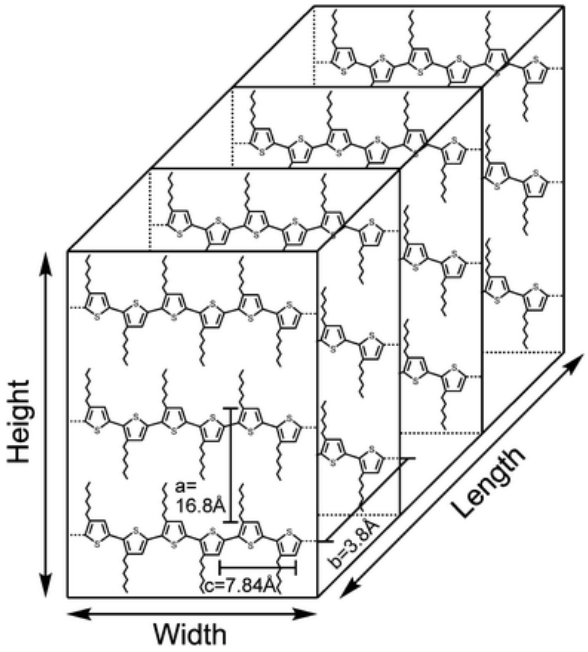

Figure 1-11 Schematic of crystalline P3HT.[90]

P3HT is a regioregular polymer, which means that it has the ability to

crystallize as opposed to the amorphous MDMO-PPV. When heated above its T_g, P3HT will form fibers as depicted in Figure 1-11. The efficient interchain stacking of the crystalline structure of P3HT results in a higher mobility as compared to the amorphous P3HT.[51]

1.5.3 P3XT

In chapter 3, poly-alkylthiophenes (PATs) with side chain lengths ranging from 4 to 9 carbon atoms, will be used. Among these materials, P3HT is also present but will be denoted as P36T to avoid confusion with the commercial P3HT. Dr. W. Oosterbaan[91] of the Organic Chemistry group at UHasselt, prepared fibers of these materials in solution which made the usual post production treatment of solar cells superfluous.

More information about this family of materials can be found in chapter 3.

1.5.4 'High T_g PPV'

'High T_g PPV' is a PPV (poly-p-phenylene-vinylene) derivative (Figure 1-12) designed by Merck OLED. 50% of this co-polymer is equal to MDMO-PPV. The other 50% consists of PPV with more complex side-chains. Because of the sterical hindrance induced by these side-chains, its glass transition temperature is much higher as compared to MDMO-PPV and P3HT. This means that its blend with PCBM allows a wide window for investigation of thermal degradation under elevated temperature conditions. However, while P3HT and MDMO-PPV are well studied materials, 'High T_g PPV', is not well known and therefore requires an appropriate introduction. The synthetic route is described by Becker et al.[92]

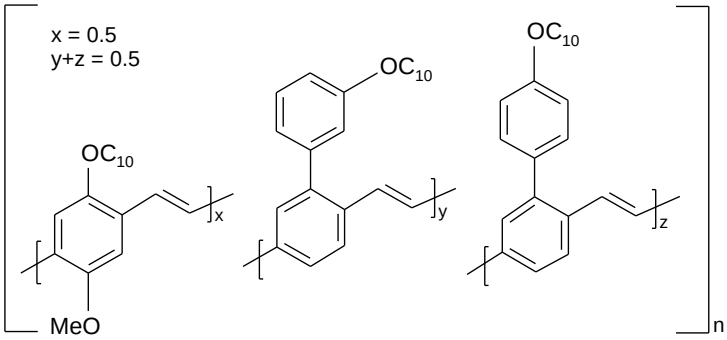

Figure 1-12 Structure of 'High T_g PPV', a copolymer designed by Merck.

T_g determination

The glass transition temperature of 'High T_g PPV' was indicated by Merck to be around 150 °C but no T_g could be observed with conventional DSC measurements. Therefore, the T_g value of 'High T_g PPV' was verified by the following method described in ref 87. Many conjugated polymers exhibit typical thermochromic properties. In PPV-type polymers, this thermochromism allows for a direct determination of previously inaccessible T_g values. This is a result of the fact that these thermochromic effects are directly correlated with temperature dependent deviations from planarity of the conjugated system, which occur above the glass transition temperature T_g. Below the T_g the backbone conformation no longer changes and as a result no thermochromism but only ground-state aggregation phenomena are observed. As a result, for PPV-type polymers an accurate value for the T_g can be determined from temperature dependent UV-Vis absorption spectra.

A T_g measurement of the 'High T_g PPV' is displayed in Figure 1-13. By plotting the wavelength λ at half maximum of the π-π^* transition as a function of temperature, two linear fits with different slopes are obtained. For these fits the measurements close to the T_g, i.e. at 130 °C and 140 °C were omitted. The intersection of the obtained fits gives an estimate of the T_g of the polymer. For 'High T_g PPV' it was determined to be 138 °C. Furthermore, from Figure 1-13 it is evident that the T_g is well defined, since the entire transition occurs within the limited temperature range of 120 °C to 150 °C.

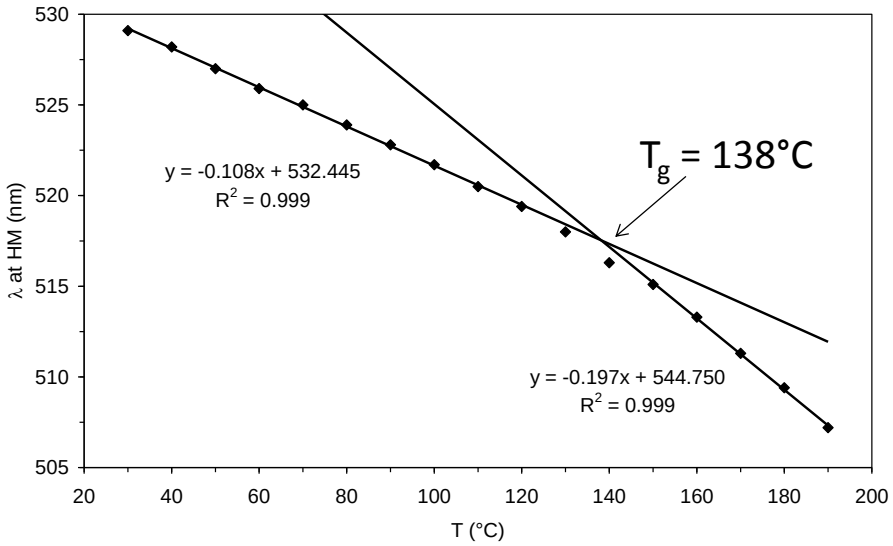

Figure 1-13 Graph of the wavelength λ at half maximum of the π-π* transition as a function of temperature, two linear fits with different slopes are obtained. The intersection of the obtained fits gives a T_g for 'High T_g PPV' of 138 °C.

UV-Vis absorption

Figure 1-14 shows the UV-Vis absorption spectrum of 'High T_g PPV'. The absorption maximum is situated at a wavelength λ_{max} of 477 nm (for MDMO-PPV: λ_{max} = 509 nm).

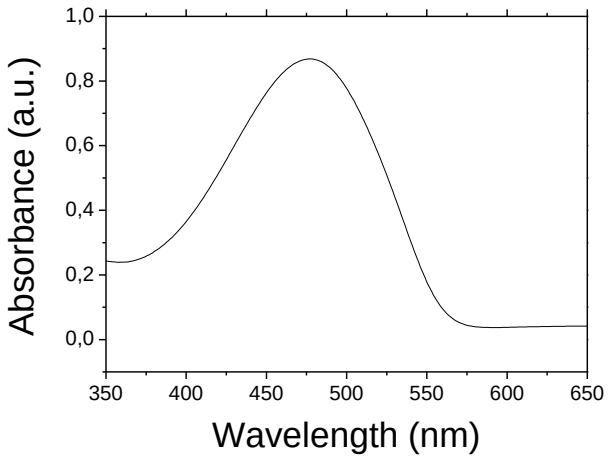

Figure 1-14 UV-Vis absorption spectrum of 'High T_g PPV'.

The onset of absorption is found around 565 nm, which corresponds to an optical bandgap of 2.2 eV.

Cyclic voltammetry

The highest occupied molecular orbital (HOMO) and the lowest unoccupied molecular orbital (LUMO) were determined through a cyclic voltammetry measurement. A conventional three-electrode cell was used: the working electrode was an ITO coated glass substrate, the counter electrode was a platinum wire and as reference electrode, a silver wire in a 0.1 M $AgNO_3$ containing electrolyte solution was used. This $Ag/AgNO_3$ 'quasi reference electrode' has an energy level of 4.93 V relative to the vacuum level. More details about this method can be found elsewhere.[87] Figure 1-15 shows the graphs obtained by cyclic voltammetry. The oxidation (at positive reference electrode voltage) and the reduction (at negative reference electrode voltage) of 'High T_g PPV' are clear from the graph. The onset of oxidation and reduction are a measure of respectively the ionisation potential and the electron affinity of the High T_g PPV. Through a linear fit, the onset of oxidation was determined to be 0.235V. This corresponds to a HOMO for High T_g PPV of:

$$HOMO = -(0.235V + 4.93V) = -5.165eV$$

The onset of reduction was determined to be -2.120V. This corresponds to a LUMO for High T_g PPV of:

$$LUMO = -(-2.120V + 4.93V) = -2.81eV$$

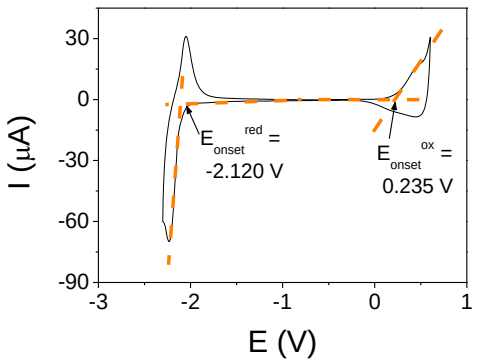

Figure 1-15 Cyclic voltammogram of 'High T_g PPV'.

The HOMO level at –5.2 eV combined with the LUMO level at -2.8 eV lead to an electrochemical bandgap of 2.4 eV.

The optical bandgap of 'High T_g PPV', determined through UV-Vis, was 2.2 eV.

1.5.5 PCBM

1-(3-methoxycarbonyl)propyl-1-phenyl [6,6]C_{61} or PCBM (Figure 1-16) is the most successful electron acceptor for over a decade already. The spatial symmetry of the C_{60} component within PCBM allows for relatively high order in the fullerene phase - even within composites.

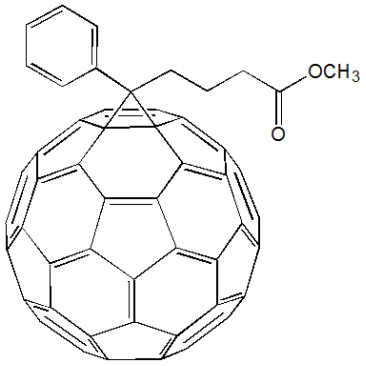

Figure 1-16 Structure of PCBM.

Cyclic voltammetry showed that the HOMO level of PCBM was situated at -6.1 eV and the LUMO level at -3.75 eV.[88] The T_g of PCBM was determined through DSC to be 131 °C.[89]

1.6 Outline

Organic BHJ solar cells offer a route towards simple and low cost photovoltaic devices. However, although they possess many attractive features (see section 1.2.1), they have to fulfill certain requirements to obtain a competitive position within the energy market. Figure 1-17 summarizes the restrictions within which organic photovoltaics can be commercialized.[17] If they are not able to satisfy the demands concerning lifetime, efficiency and cost, they will be limited to a niche market.

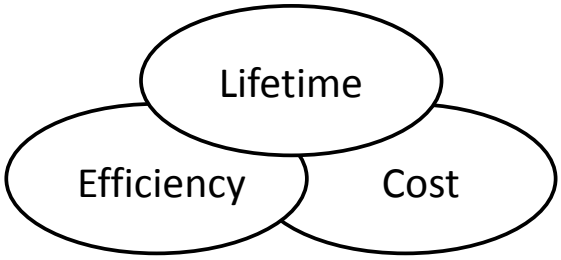

Figure 1-17 The critical triangle for photovoltaics.

This work will focus mainly on the lifetime and efficiency of solar cells and more specific on the role of the active layer morphology within this area.

The morphology of the active layer will be studied with Transmission Electron Microscopy (TEM). In chapter 2, different measuring techniques of TEM are explained and their use for organic BHJ is demonstrated. Also the calculation of the fiber content of a solution from UV-Vis measurements is explained.

Chapter 3 discusses the possibility to use fibrillar PAT-derivatives in organic BHJ solar cells. The fibers were produced in solution and upon mixing with PCBM different morphologies were obtained, depending on the used solvent.

In chapter 4, the stability of MDMO-PPV:PCBM 1:4 solar cells is investigated. This material has served as reference material since the beginning of organic photovoltaics. This makes it a good candidate to study the degradation processes. To speed up degradation, thermal annealing is used. The morphology of the active layer turns out to play a important role in the degradation of the solar cells. A model is suggested to extrapolate lifetimes for the solar cells.

Chapter 5 compares the stability of different material systems. P3HT:PCBM solar cells prepared from identical materials using different processing conditions, are compared. The effect on stability of using a polymer with high glass transition temperature as electron donor is tested. Also the implementation of P3HT with 10% functionalized side chains is verified.

Finally, chapter 6 summarizes the conclusions obtained throughout this thesis. An outlook towards future research is proposed.

1.7 References

[1] N.S. Lewis, *MRS Bull.* 32, **2007**, 808
[2] S. Shafiee, E. Topal, *Energ. Policy* 37, **2009**, 181
[3] Press release OAK RIDGE, April 21, 2005, http://www.ornl.gov/
[4] T. Konrad, '*What does clean energy cost*?' http://www.altenergystocks.com/
[5] G.W. Crabtree, N.S. Lewis, *Phys. Today* 60, **2007**, 37
[6] S. Gunes, H. Neugebauer, N.S. Sariciftci, *Chem. Rev.* 107, **2007**, 1324
[7] H. Spanggaard, F.C. Krebs, *Sol. Energy Mater. Sol. Cells* 83, **2004**, 125
[8] B.R. Saunders, M.L. Turner, *Adv. Colloid Interface Sci.* 138, **2008**, 1
[9] ASTM international, *Standard specification for solar simulation for photovoltaic testing*, E927-05, **2005**; IEC904-9, *photovoltaic devices-Part 9: Solar simulator performance requirements*, IEC904-9:1995 (E), **1995**
[10] M.E. Becquerel, *Compt. Rend. Acad. Sci.* 9, **1839**, 561
[11] W. Smith, *Nature* 7, **1873**, 303
[12] M. Volmer, *Ann. Physik* 40, **1913**, 775
[13] M. Riordan, L. Hoddeson, *IEEE Spectrum* 34, **1997**, 46
[14] D.M. Chapin, C.S. Fuller, G.L. Pearson, *J. Appl. Phys.* 25, **1954**, 676
[15] http://www.nrel.gov
[16] S. Shrestha, *Prog. Photovolt: Res. Appl.* 18, **2010**, 229
[17] C.J. Brabec, *Sol. Energy Mater. Sol. Cells* 83, **2004**, 273
[18] A. Goetzberger, J. Knobloch, B. Voss, *Crystalline Silicon Solar Cells*, Wiley, New York, **1998**
[19] H. Hoppe, N.S. Sariciftci, *J. Mater. Res.* 19, **2004**, 1924
[20] S.R. Scully, M.D. McGehee, *J. Appl. Phys.* 100, **2006**, 034907
[21] D.L. Morel, A.K. Ghosh, T. Feng, E.L. Stogryn, P.E. Purwin, R.F. Shaw, C. Fishman, *Appl. Phys. Lett.* 32, **1978**, 495
[22] C.W. Tang, *Appl. Phys. Lett.* 48, **1986**, 183
[23] H. Hoppe, N. Arnold, N.S. Sariciftci, D. Meissner, *Sol. Energy Mater. Sol. Cells* 80, **2003**, 105
[24] U. Zhokhavets, T. Erb, G. Gobsch, M. Al-Ibrahim, O. Ambacher, *Chem. Phys. Lett.* 418, **2006**, 347
[25] P.W.M. Blom, V.D. Mihailetchi, L.J.A. Koster, D.E. Markov, *Adv. Mater.* 19, **2007**, 1551
[26] E. Bundgaard, F.C. Krebs, *Sol. Energy. Mater. Sol. Cells* 91, **2007**, 954
[27] B. Minnaert, M. Burgelman, *Prog. Photovolt: Res. Appl.* 15, **2007**, 741
[28] S.R. Forrest, *MRS Bull.* 30, **2005**, 28
[29] B.C. Thompson, J.M.J. Fréchet, *Angew. Chem. Int. Ed.* 47, **2008**, 58
[30] A.C. Mayer, S.R. Scully, B.E. Hardin, M.W. Rowell, M.D. McGehee, *Mater. Today* 10, **2007**, 28
[31] M.M. Mandoc, L.J.A. Koster, P.W.M. Blom, *Appl. Phys. Lett.* 90, **2007**, 133504

[32] D. Chirvase, Z. Chiguvare, M. Knipper, J. Parisi, V. Dyakonov, J.C. Hummelen, *J. Appl. Phys.* 93, **2003**, 3376
[33] R. Steim, F. R. Kogler, C.J. Brabec, *J. Mater. Chem.* 20, **2010**, 2499
[34] Y.S. Eo, H.W. Rhee, B.D. Chin, J.-W. Yu, *Synth. Met.* 159, **2009**, 1910
[35] M.O. Reese, M.S. White, G. Rumbles, D.S. Ginley, S.E. Shaheen, *Appl. Phys. Lett.* 92, **2008**, 053307
[36] G. Yu, J. Gao, J.C. Hummelen, F. Wudl, A. J. Heeger, *Science* 270, **1995**, 1789
[37] J.J.M. Halls, C.A. Walsh, N.C. Greenham, E.A. Marseglia, R.H. Friend, S.C. Moratti, A.B. Holmes, *Nature* 376, **1995**, 498
[38] C.Y. Yang, A.J. Heeger, *Synth. Met.* 83, **1996**, 85
[39] H. Hoppe, N.S. Sariciftci, *J. Mater. Chem.* 16, **2006**, 45
[40] H. Hoppe, M. Niggemann, C. Winder, J. Kraut, R. Hiesgen, A. Hinsch, D. Meissner, N.S. Sariciftci, *Adv. Funct. Mater.* 14, **2004**, 1005
[41] S.E. Shaheen, C.J. Brabec, N.S. Sariciftci, F. Padinger, T. Fromherz, J.C. Hummelen, *Appl. Phys. Lett.* 78, **2001**, 841
[42] J. Liu, Y. Shi, Y. Yang, *Adv. Funct. Mater.* 11, **2001**, 420
[43] H. Hoppe, T. Glatzel, M. Niggemann, A. Hinsch, M.Ch. Lux-Steiner, N.S. Sariciftci, *Nano Lett.* 5, **2005**, 269
[44] T. Röder, H.-S. Kitzerow, J.C. Hummelen, *Synth. Met.* 141, **2004**, 271
[45] C.R. McNeill, H. Frohne, J.L. Holdsworth, P.C. Dastoor, *Synth. Met.* 147, **2004**, 101
[46] J.C. Hummelen, B.W. Knight, F. LeFeq, F. Wudl, J. Yao, C.L. Wilkins, *J. Org. Chem.* 60, **1995**, 532
[47] S.E. Shaheen, C.J. Brabec, N.S. Sariciftci, F. Padinger, T. Fromherz, J.C. Hummelen, *Appl. Phys. Lett.* 78, **2001**, 841
[48] T. Martens, J. D'Haen, T. Munters, L. Goris, Z. Beelen, J. Manca, M. D'Olieslaeger, D. Vanderzande, L. De Schepper, R. Andriessen, *Mat. Res. Soc. Symp. Proc.* 725, **2002**, P7.11
[49] T. Martens, J. D'Haen, T. Munters, Z. Beelen, L. Goris, J. Manca, M. D'Olieslaeger, D. Vanderzande, L. De Schepper, R. Andriessen, *Synth. Met.* 138, **2003**, 243
[50] T. Martens, T. Munters, L. Goris, J. D'Haen, K. Schouteden, M. D'Olieslaeger, L. Lutsen, D. Vanderzande, W. Geens, J. Poortmans, L. De Schepper, J.V. Manca, *Appl. Phys. A* 79, **2004**, 27
[51] J.-F. Chang, B. Sun, D.W. Breiby, M.M. Nielsen, T.I. Solling, M. Giles, I. McCulloch, H.Sirringhaus, *Chem. Mater.* 16, **2004**, 4772
[52] P. Vanlaeke, G. Vanhoyland, T. Aernouts, D. Cheyns, C. Deibel, J. Manca, P. Heremans, J. Poortmans, *Thin Solid Films* 511, **2006**, 358
[53] J. Peet, J.Y. Kim, N.E. Coates, W.L. Ma, D. Moses, A.J. Heeger, G.C. Bazan, *Nat. Mater.* 6, **2007**, 497

[54] A. Haugeneder, M. Neges, C. Kallinger, W. Spirkl, U. Lemmer, J. Feldmann, U. Scherf, E. Harth, A. Gügel, K Müllen, *Phys. Rev. B* 59, **1999**, 15346
[55] J.K.J. van Duren, X. Yang, J. Loos, C.W.T. Bulle-Lieuwma, A.B. Sival, J.C. Hummelen, R.A.J. Janssen, *Adv. Funct. Mater.* 14, **2004**, 425
[56] V.D. Mihailetchi, L.J.A. Koster, P.W.M. Blom, C. Melzer, B. de Boer, J.K.J. van Duren, R.A.J. Janssen, *Adv. Funct. Mater.* 15, **2005**, 795
[57] M. Al-Ibrahim, O. Ambacher, S. Sensfuss, G. Gobsch, *Appl. Phys. Lett.* 86, **2005**, 201120
[58] Y. Kim, S.A. Choulis, J. Nelson, D.D.C. Bradley, S. Cook, J.R. Durrant, *J. Mater. Sci.* 40, **2005**, 1371
[59] N.C. Cates, R. Gysel, Z. Beiley, C.E. Miller, M.F. Toney, N. Heeney, I. McCulloch, M.D. McGehee, *Nano Lett.* 9, **2009**, 4153
[60] F. Padinger, R.S. Rittberger, N.S. Sariciftci, *Adv. Funct. Mater.* 13, **2003**, 85
[61] Y. Zhao, G.X. Yuan, P. Roche, M. Leclerc, *Polymer* 36, **1995**, 2211
[62] J.J. Dittmer, E.A. Marseglia, R.H. Friend, *Adv. Mater.* 12, **2000**, 1270
[63] X. Yang, J. Loos, S.C. Veenstra, W.J.H. Verhees, M.M. Wienk, J.M. Kroon, M.A.J. Michels, R.A.J. Janssen, *Nano Lett.* 5, **2005**, 579
[64] R. De Bettignies, J. Leroy, M. Firon, C. Sentein, *Synth. Met.* 156, **2006**, 510
[65] V. Dyakonov, *Appl. Phys. A* 79, **2004**, 21
[66] M. Glatthaar, N. Mingirulli, B. Zimmermann, T. Ziegler, R. Kern, M. Niggemann, A. Hinsch, A. Gombert, *Phys. Stat. Sol. (a)* 202, **2005**, 125
[67] K. Inoue, R. Ulbricht, P.C. Madakasira, W. M. Sampson, S. Lee, J. Gutierrez, J. Ferraris, A. A. Zakhidov, *Synth. Met.* 154, **2005**, 41
[68] Y. Kim, S.A. Choulis, J. Nelson, D.D.C. Bradley, S. Cook, J.R. Durrant, *Appl. Phys. Lett.* 86, **2005**, 063502
[69] T.J. Savenije, J.E. Kroeze, X. Yang, J. Loos, *Thin Solid Films* 511, **2006**, 2
[70] P. Vanlaeke, A. Swinnen, I. Haeldermans, G. Vanhoyland, T. Aernouts, D. Cheyns, C. Deibel, J. D'Haen, P. Heremans, J. Poortmans, J.V. Manca, *Sol. Energy Mater. Sol. Cells* 90, **2006**, 2150
[71] W. Ma, C. Yang, X. Gong, K. Lee, A.J. Heeger, *Adv. Funct. Mater.* 15, **2005**, 1617
[72] M. Reyes-Reyes, R. Lopez-Sandoval, J. Arenas-Alatorry, R. Garibay-Alonso, D.L. Carroll, A. Lastras-Martinez, *Thin Solid Films* 516, **2007**, 52
[73] C.-J. Ko, Y.-K. Lin, F.-C. Chen, *Adv. Mater.* 19, **2007**, 3520
[74] O. Yoshikawa, T. Sonobe, T. Sagawa, S. Yoshikawa, *Appl. Phys. Lett.* 94, **2009**, 083301
[75] V.D. Mihailetchi, H. Xie, B. de Boer, L.M. Popescu, J.C. Hummelen, P.W.M. Blom, *Appl. Phys. Lett.* 89, **2006**, 012107
[76] Y. Zhao, Z. Xie, Y. Qu, Y. Geng, L. Wang, *Appl. Phys. Lett.* 90, **2007**, 043504
[77] M.M. Wienk, J.M. Kroon, W.J.H. Verhees, J. Knol, J.C. Hummelen, P.A. van Hal, R.A.J. Janssen, *Angew. Chem. Int. Ed.* 42, **2003**, 3371

[78] S. Sun, Z. Fan, Y. Wang, J. Haliburton, *J. Mater. Sci.* 40, **2005**, 1429
[79] Q. Zhang, A. Cirpan, T.P. Russel, R. Emrick, *Macromolecules* 42, **2009**, 1079
[80] H. Neugebauer, C. Brabec, J.C. Hummelen, R.A.J. Janssen, N.S. Sariciftci, *Synth. Met.* 102, **1999**, 1002
[81] F. Padinger, T. Fromherz, P. Denk, C.J. Brabec, J. Zettner, T. Hierl, N.S. Sariciftci, *Synth. Met.* 121, **2001**, 1605
[82] J.M. Kroon, M.M. Wienk, W.J.H. Verhees, J.C. Hummelen, *Thin Solid Films* 403, **2002**, 223
[83] F.C. Krebs, J.E. Carlé, N. Cruys-Bagger, M. Andersen, M.R. Lilliedal, M.A. Hammond, S. Hvidt, *Sol. Energy Mater. Sol. Cells* 86, **2005**, 499
[84] H. Neugebauer, C. Brabec, J.C. Hummelen, N.S. Sariciftci, *Sol. Energy Mater. Sol. Cells* 61, **2000**, 35
[85] X. Yang, J.K.J. van Duren, M.T. Rispens, J.C. Hummelen, R.A.J. Janssen, M.A.J. Michels, J. Loos, *Adv. Mater.* 16, **2004**, 802
[86] X. Yang, J.K.J. van Duren, R.A.J. Janssen, M.A.J. Michels, J. Loos, *Macromolecules* 37, **2004**, 2151
[87] S. Fourier, *Spectroscopy, Electrochemistry and Spectro-Electrochemistry of PPV and PTV Derivatives; the Effect of Backbone Structure and Side Chain Polarity on the Optoelectronic Properties of Conjugated Polymers*, PhD Thesis UHasselt, D/2007/2451/14, **2007**
[88] M. Al-Ibrahim, H.-K. Roth, U. Zhokhavets, G. Gobsch, S. Sensfuss, *Sol. Energy Mater. Sol. Cells* 85, **2005**, 13
[89] A. Swinnen, *Morphological, thermal and electrical characterization of organic photovoltaic blends*, PhD Thesis UHasselt, D/2007/2451/62, **2007**
[90] J. A. Merlo and C. D. Frisbie, *J. Phys. Chem. B* 108, **2004**, 19169
[91] W.D. Oosterbaan, V. Vrindts, S. Berson, S. Guillerez, O. Douheret, B. Ruttens, J. D'Haen, P. Adriaensens, J. Manca, L. Lutsen, D. Vanderzande, *J. Mater. Chem.* 19, **2009**, 5424
[92] H. Becker, H. Spreitzer, W. Kreuder, E. Kluge, H. Schenk, I. Parker, Y. Cao, *Adv. Mater.* 42, **2000**, 42

Chapter 2

Active layer morphology studied with TEM and UV-Vis

This chapter introduces the imaging modes in Transmission Electron Microscopy (TEM) that have been used further on in this work and illustrates their use for studying polymer:fullerene blends. Bright Field (BF) TEM is the most straight-forward imaging technique. Selected Area Electron Diffraction (SAED) is a useful tool to study ordering in samples.

UV-Vis absorption is used to calculate the amount of fibers present in P3XT:PCBM solutions (discussed in chapter 3). The method to determine this fiber concentration is presented here.

2.1 Transmission electron microscopy (TEM)

With the introduction of the bulk heterojunction concept in organic solar cells, it became clear that the morphology of the polymer:fullerene matrix was of crucial importance for the fabrication of high performance devices. To obtain good exciton dissociation, phase separation on a small scale is necessary to avoid recombination of the exciton within the diffusion length (~ 10 nm). After exciton dissociation, the created charges have to be able to reach the electrodes. Therefore (preferably uninterrupted) percolation paths have to be present.

In this work the morphology of the active layer of the solar cells is primarily studied with Transmission Electron Microscopy (TEM). The microscope that was used was either a Philips CM12-STEM or a FEI Tecnai G2 Spirit Twin. In TEM, several modes exist, that all give information on different properties of the morphology of a sample. This chapter introduces the main modes that have been used throughout this work. In Appendix A, some examples of other TEM modes are discussed briefly.

2.1.1 BFTEM

A schematic presentation of a TEM is depicted in Figure 2-1. The electron beam in a TEM is produced by a filament[a] that produces a stream of electrons by thermionic emission. The stream passes through two magnetic lenses (the first and second condenser lenses) that focus it into a small, coherent beam. The condenser aperture blocks the high angle electrons before the beam strikes the sample. The transmitted part of the beam is focused into an image by the objective lens. The objective aperture can block the high-angle diffracted electrons to enhance the contrast of the image. The selected area aperture can be used to specify the region of interest, when displaying diffraction patterns (see section 2.1.3). Finally, the intermediate and projector lenses enlarge the image; the beam strikes the phosphor screen and light is

[a] The Philips CM12-STEM contained a tungsten (W) filament, whereas the FEI Tecnai G2 Spirit Twin contained a lanthanum hexaboride (LaB_6) cathode

generated, allowing the user to see the image.[1]

The samples used in TEM have to be thin in order to allow the electron beam to pass through it (for organic samples, active layers are usually in the order of 100 nm thick). The beam interacts with the specimen and the resulting image gives information on the bulk morphology of the specimen.

Bright Field Transmission Electron Microscopy (BFTEM, Figure 2-1) is the most straightforward way in TEM to obtain nanostructural images. In this technique, the objective diaphragm can be chosen in order to enhance contrast. The smaller the objective diaphragm, the more diffracted electrons will be blocked and thus the higher the contrast. But due to the high amount of blocking, the intensity of the eventual image might become very low. A suitable objective diaphragm delivers images with an optimal contrast and intensity.

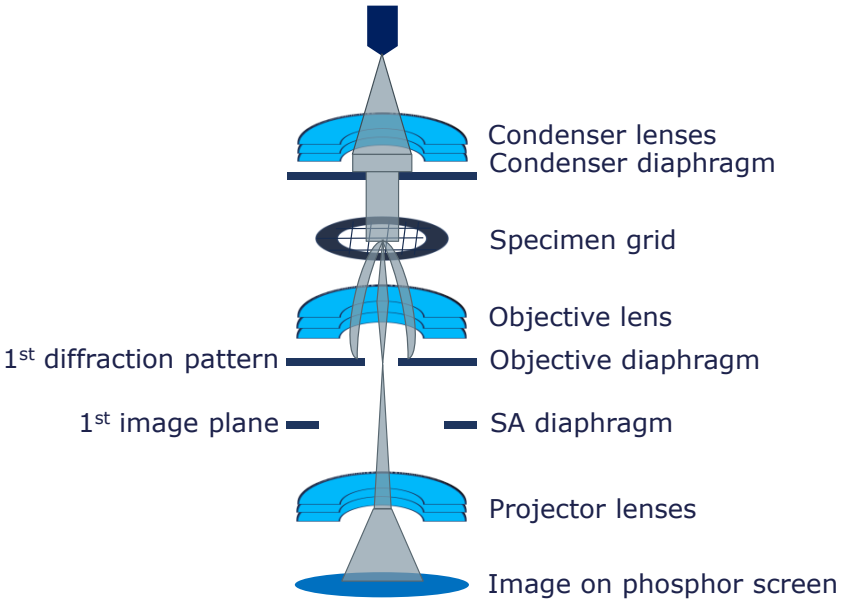

Figure 2-1 Schematic representation of a TEM operating in Bright Field mode.

When the electron beam passes through the sample, electrons scatter more from places where the sample is thicker or has a higher density. These places then appear darker in the resulting image because fewer electrons arrive at

the fluorescent screen.

This technique was for example used to explain why efficiencies of MDMO-PPV:PCBM solar cells increased from 0.9% to 2.5% when using chlorobenzene as solvent instead of toluene.[2] Martens et al.[3] showed that this was caused by the dimension of the phase separation between MDMO-PPV and PCBM (Figure 2-2). When the polymer:fullerene mixture was dissolved in toluene large (~ 200 – 500 nm) PCBM rich areas existed. When chlorobenzene was used, these PCBM rich areas were a lot smaller (~ 50 – 100 nm).

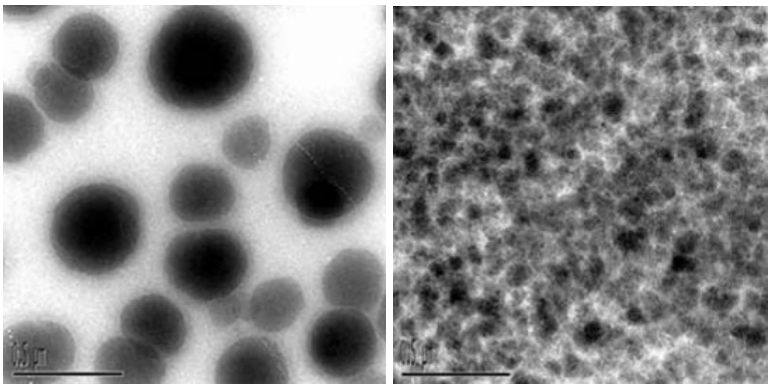

Figure 2-2 MDMO-PPV:PCBM 1:4 thin films spin-coated from toluene (left) and chorobenzene (right). Reprinted from ref 3.

2.1.2 Sample preparation

As mentioned above, TEM is a technique to visualize bulk morphology. To this end, freestanding films of the samples under investigation are prepared. The active layers of photovoltaic devices in this work are prepared through spin-coating on an ITO/PEDOT-PSS substrate (section 4.1). Layer thicknesses were in the range of 100 nm which made them suitable for TEM measurements. To facilitate the making of the TEM samples, identical layers to the active layers of the solar cells, were mostly (unless stated otherwise) spin-coated on a clean Si substrate with a 100 nm SiO_2 top layer. Upon putting the samples in hydrofluoric acid (HF), the SiO_2 layer is removed (SiO_2 + 6 HF → H_2SiF_6 + 2 H_2O) and the Si substrate sinks to the bottom. The spin-coated active layer floats in the HF and after transferring the active layer to H_20, it can be picked

up with a copper TEM grid (3.05 mm diameter, 400 mesh, supplied by EMS).

A few experiments in this work were done on the active layers that were taken directly from photovoltaic devices. In these cases, the complete solar cells (ITO/PEDOT-PSS/active layer/CaAl) were put in HF. The CaAl electrode is slowly (after ~ 1 minute) removed by the HF and the ITO substrate again sinks to the bottom. The active layer can then be put in H_2O to remove any residual PEDOT-PSS, after which it is again put on a copper TEM grid. A drawback for this second method as opposed to the first one, was that quite often some remains of the CaAl electrode stuck on the active layer, making the visualization of the active layer morphology with TEM more difficult.

2.1.3 SAED

Selected Area Electron Diffraction (SAED) is a useful tool to study ordering in samples. Figure 2-3 shows an electron beam parallel to the optic axis and incident upon the specimen. The action of forming the image brings both the transmitted and the diffracted beam to a focus in the back focal plane of the objective lens. Thus a diffraction pattern is produced there. By adjusting the projector lenses, it is possible to display this diffraction pattern instead of the image on the fluorescence screen or the CCD camera.

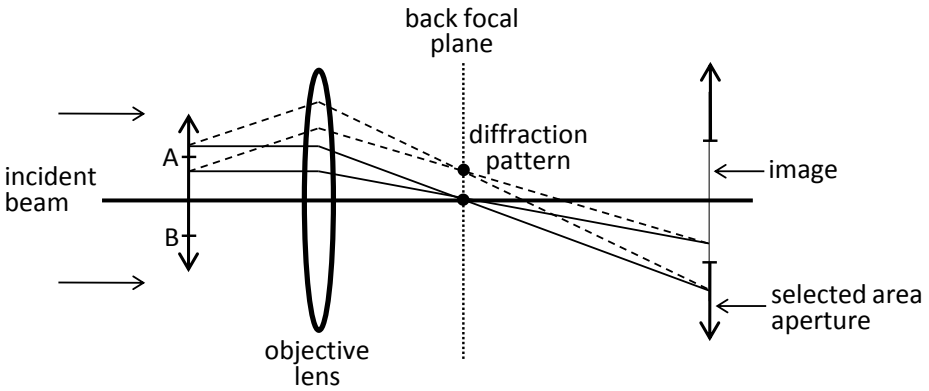

Figure 2-3 Selected Area Electron Diffraction (SAED) using the SA diaphragm to select a specific area.

Figure 2-3 also explains that it is possible to select a specific region for SAED

by inserting an aperture in the plane of the image. The incident beam covers the sample completely and all transmitted and diffracted rays contribute to the diffraction pattern in the back focal plane of the objective lens. However, if an aperture is inserted in the plane of the image, only the rays that originate from the region AB of the sample are allowed into the following magnification system. Consequently, only the electrons that pass region AB are allowed to contribute to the diffraction pattern formed on the viewing screen.

An incident electron beam that hits a sample is diffracted in all directions. In most directions, the diffracted rays cancel each other out through destructive interference. However, when the sample is crystalline, some diffracted rays will interfere constructively. The directions in which this happens are determined by Bragg's Law:

$$2d\sin\theta = n\lambda \qquad \text{(Eq. 2-1)}$$

where d is the distance between the diffracting planes, θ is the incident angle, n is an integer and λ is the wavelength of the beam[b]. These specific directions appear as spots in the diffraction patterns.

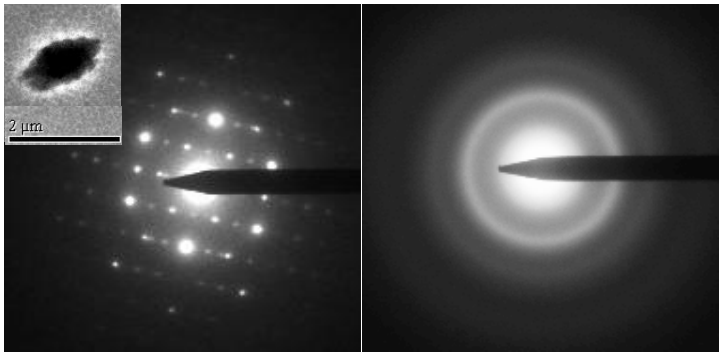

Figure 2-4 Diffraction pattern of a single PCBM crystal (left) and of a polycrystalline PCBM sample (right). Scale bar = 2 µm.

Figure 2-4 shows two possible diffraction patterns obtained by TEM. The left pattern was taken from a PCBM single crystal that was formed in an MDMO-PPV:PCBM 1:4 sample during annealing at 110°C. The right pattern was taken

[b] For a TEM working at 120 kV, the wavelength of the electrons is 3.35 pm.

from an identical sample but this time without annealing (analogous to Figure 2-2, right). The nanocrystalline PCBM was dispersed throughout the sample and oriented in all directions. This created a diffraction pattern consisting of a series of concentric rings.

2.1.4 Calculating residual intensities of SAED patterns

SAED patterns of P3HT:PCBM films resemble Figure 2-5. Two diffraction rings appear very pronounced in the image. The inner diffraction ring at a d-spacing of 4.6 Å corresponds to nanocrystalline PCBM,[4] the outer ring at 3.8 Å corresponds to crystalline P3HT.[5] The intensities of the diffraction rings relate to the amount of PCBM or crystalline P3HT in the film.

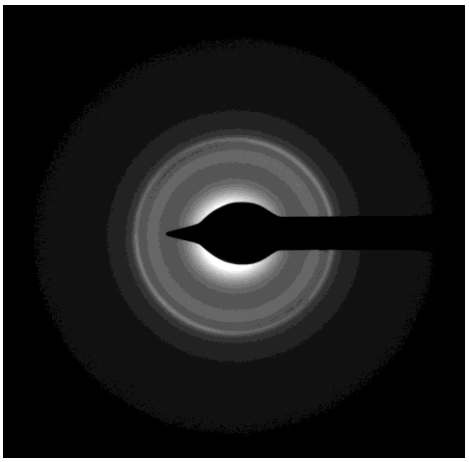

Figure 2-5 SAED pattern of a P3HT:PCBM 1:1 film.

To obtain the residual intensities of the SAED pattern, first an integration of the intensities across the pattern was performed. To this end, the intensities at a certain distance (expressed in pixels) to the centre of the pattern were added (Figure 2-6). This number was divided by the number of pixels contributing to this number to obtain the normalized intensities at each distance from the centre (Figure 2-7).

Diffraction in a TEM follows Bragg's law (Eq 2-1). For small diffraction angles, this can be written as:

$$\theta \approx \sin\theta = \frac{\lambda}{2d} \qquad \text{(Eq. 2-2)}$$

where λ is 3.35 pm for an operating voltage of 120 kV and d is the distance between the scattering planes. SAED patterns are typically calibrated with an Al specimen that has a sharp diffraction peak at a distance corresponding to 2.338 Å (d_{Al}). The scattering angle of this diffraction peak can thus be written as:

$$\theta_{Al} = \frac{\lambda_{120kV}}{2 \cdot d_{Al}} \qquad \text{(Eq. 2-3)}$$

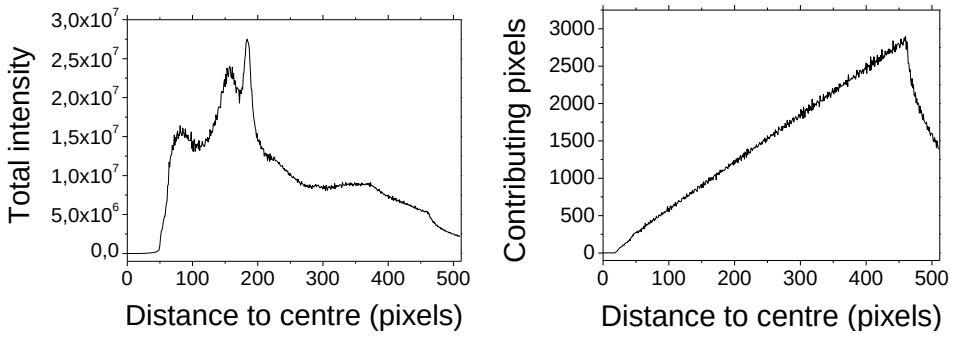

Figure 2-6 Total intensity of the SAED pattern in Figure 2-5 at a certain distance from the centre (left) and the pixels that contribute to this total intensity (right).

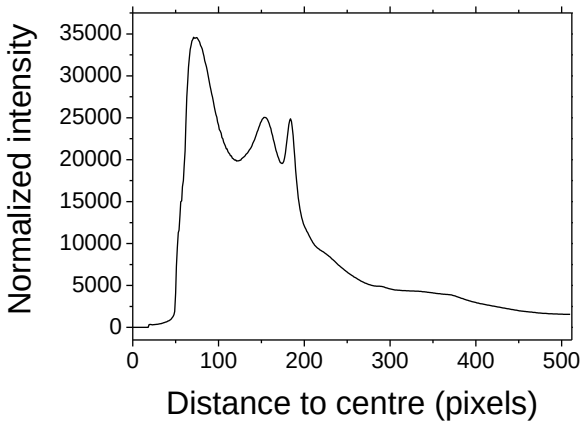

Figure 2-7 Normalized intensity of the SAED pattern in Figure 2-5 as a function of the distance to the centre.

Through a calibration experiment, the number of pixels corresponding to this scattering angle (pix_{Al}) is determined. The scattering angle θ corresponding to an arbitrary pixel value (pix) can then be calculated by:

$$\theta = \frac{pix \cdot \lambda_{120kV}}{2 \cdot pix_{Al} \cdot d_{Al}} \qquad \text{(Eq. 2-4)}$$

By inserting Eq. 2-2, the d-value for all pixels can be calculated.

In Figure 2-7, the diffraction peaks originating from PCBM or P3HT are already visible. The graph however shows a large background. This background is fitted by neglecting the pronounced peaks due to PCBM and P3HT (Figure 2-8) and performing a fitting procedure. The background originates from inelastic scattering. The intensity of the inelastically scattered beam for a certain scattering angle θ is proportional to the differential cross-section:[6]

$$I(\theta) \approx \frac{d\sigma_{inel}}{d\vartheta} = \frac{d\sigma_{inel}}{d\Omega}\frac{d\Omega}{d\theta} = \frac{Z\lambda^4\left(1+E/E_0\right)^2}{4\pi^4 a_H^2}\frac{\left\{1-\frac{1}{\left[1+\left(\theta/\theta_0\right)^2\right]^2}\right\}}{\left(\theta^2+\theta_E^2\right)^2}2\pi\sin\theta$$

(Eq. 2-5)

with $\frac{d\sigma_{inel}}{d\Omega}$ = the differential cross-section of inelastic scattering

Z = the atomic number

λ = wavelength of the incoming beam

E = kinetic energy of the incoming electron

E_0 = rest energy of an electron (= m_0c^2)

a_H = Bohr radius

θ_0 = characteristic angle for elastic scattering

θ_E = characteristic angle for inelastic scattering

Eq. 2-5 contains many constants, for fitting they can be inserted in fitting parameters. This leads to the following formula that was used for fitting the curve in Figure 2-8:

$$I = c\sin(x)\frac{1-\frac{1}{\left(1+(ax)^2\right)^2}}{\left(x^2+b^2\right)^2} \qquad \text{(Eq. 2-6)}$$

where x (= 1/d) is proportional to θ and a, b and c are the fitting parameters. The dashed line in Figure 2-8 represents a result of the fitting procedure.

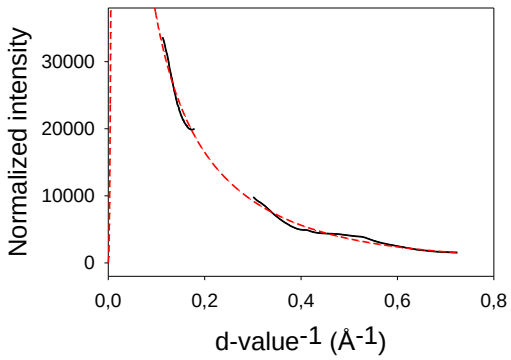

Figure 2-8 Fitted background of the SAED patterns in Figure 2-5.

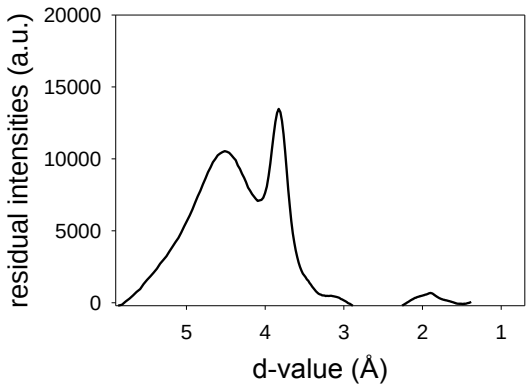

Figure 2-9 Residual intensities of the SAED patterns in Figure 2-5.

Subtracting the fitted background from the normalized intensities results in a graph where the diffraction peaks corresponding to PCBM and P3HT are very clear (Figure 2-9).

Although all samples that were used for TEM had thicknesses close to 100 nm, small differences in thickness could exist. These differences in thickness have an effect on the peak intensities in Figure 2-9. For thicker samples, more scattering will occur and the intensity of the peaks will be lower. To account for this, the intensities in Figure 2-9 were divided by the average intensity of a BFTEM image of the selected area and multiplied by the arbitrary number 10000 for simplicity. In this way, small variations in peak intensities due to thickness differences are ruled out and a comparison can be made between several samples.

2.2 UV-Vis

Ultraviolet-visible spectroscopy (UV-Vis) refers to absorption spectroscopy in the ultraviolet-visible spectral region. In Chapter 3, UV-Vis absorption measurements of solutions are used to determine the fiber concentration of those solutions. For the measurements a Cary 500 Scan UV-Vis-NIR Spectrophotometer was used, equipped with the software Cary WinUV Scan Application (May 9, 2002), version 3.00. A quartz cuvette with 1 cm path length contained the solutions during the measurements.

2.2.1 Determining fiber content of P3XT:PCBM solutions

For the P3XT:PCBM blends, that will be discussed in chapter 3, the fiber fraction of the solid state films was approximated by the fiber fraction of the dispersion from which the active layers were spin-coated. Since PCBM inhibits the crystallization of PATs[7,8] and thermal annealing or slow drying was not applied this seems a fairly good estimation.

The P3XT:PCBM solutions that were used for spin-coating, were too viscous to perform UV-Vis measurements. Therefore a small amount (≈ 50 µl) of the solution was diluted in ≈ 3 ml of the corresponding solvent that was kept at the same temperature as the solution. The absorbance of this diluted solution was measured through UV-Vis absorption spectroscopy in a range from 200 nm to 900 nm (Figure 2-10).

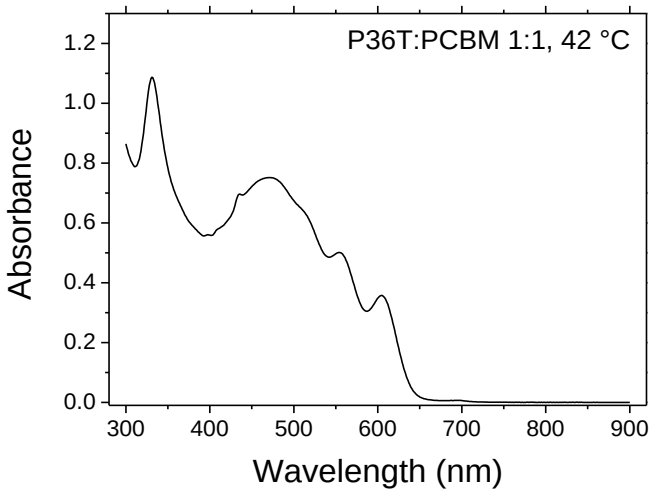

Figure 2-10 UV-Vis absorption spectrum of P36T:PCBM 1:1 for a solution temperature of 42 °C.

Beforehand, absorption spectra of the different components of the solution were recorded, i.e. the spectra of PCBM, the fully amorphous P3XT and the fully fibrillar P3XT in the corresponding solvent (Figure 2-11). These spectra were used in a fitting procedure through the formula:

$$Solution = P_1 \cdot FP3XT + P_2 \cdot AP3XT + P_3 \cdot PCBM + P_4 \qquad \text{(Eq. 2-7)}$$

where *Solution* is the absorption spectrum of the P3XT:PCBM solution (Figure 2-10), *FP3XT* is the spectrum of the fiber P3XT in Figure 2-11, *AP3XT* is the spectrum of amorphous P3XT in Figure 2-11 and *PCBM* is the spectrum of PCBM in Figure 2-11.

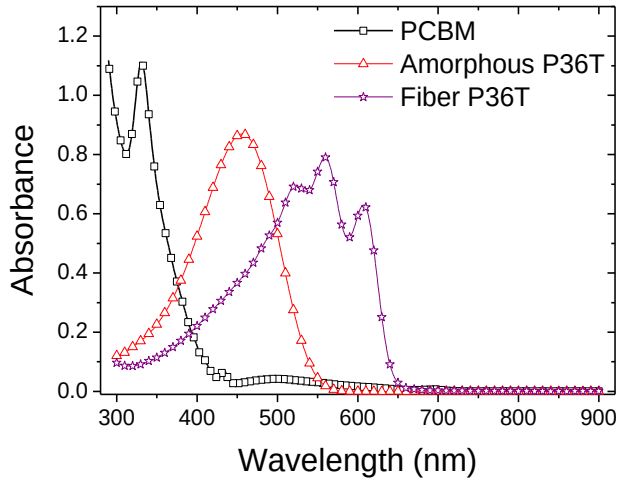

Figure 2-11 UV-Vis absorption spectra of PCBM (squares), fully amorphous P36T (triangles) and fully fibrillar P36T (stars) in pinane.

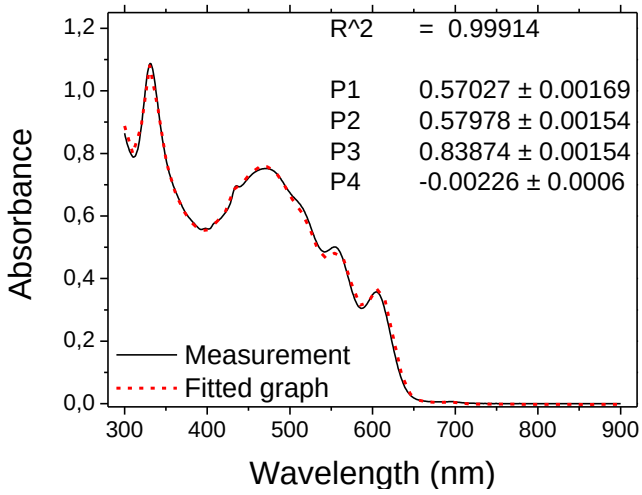

Figure 2-12 Result of the fitting procedure, described by Eq. 2-7.

The fitting procedure returns four parameters (Figure 2-12). P_4 denotes a possible small baseline of the spectrum. P_1, P_2 and P_3 respectively denote the contribution to the absorption of fiber P3XT, amorphous P3XT and PCBM. The fiber fraction of P3XT in the solution can then be calculated by:

$$Fiber\_P3XT = \frac{P_1}{P_1 + P_2} \qquad \text{(Eq. 2-8)}$$

And the amount of amorphous P3XT by:

$$Amorphous\_P3XT = \frac{P_2}{P_1 + P_2} \qquad \text{(Eq. 2-9)}$$

Note however that for the films spin-coated from pinane, this method underestimated the fiber fraction in the solid state film. This solvent evaporates slowly (boiling point = 168 °C) and in this way some P3XT has the possibility to self-organize (see section 3.2.6). A more accurate way to calculate the fiber fraction in these films would be through TEM tomography as was done before by van Bavel et al.[9]

2.3 References

[1] J.W. Edington, *Practical electron microscopy in materials science. Monograph One: The operation and calibration of the electron microscope*, Philips, **1974**

[2] S.E. Shaheen, C.J. Brabec, N.S. Sariciftci, *Appl. Phys. Lett.* 78, **2001**, 841

[3] T. Martens, T. Munters, L. Goris, J. D'Haen, K. Schouteden, M. D'Olieslaeger, L. Lutsen, D. Vanderzande, W. Geens, J. Poortmans, L. De Schepper, J.V. Manca, *Appl. Phys. A.* 79 **2004**, 27

[4] M.T. Rispens, A. Meetsma, R. Rittberger, C.J. Brabec, N.S. Sariciftci, J.C. Hummelen, *Chem. Commun.* **2003**, 2116

[5] S. Hugger, R. Thomann, T. Heinzel, T. Thurn-Albrecht, *Colloid Polym. Sci.* 282, **2004**, 932

[6] L. Reimer, *Transmission Electron Microscopy*, Springer, Berlin, **1989**

[7] P. Vanlaeke, A. Swinnen, I. Haeldermans, G. Vanhoyland, T. Aernouts, D. Cheyns, C. Deibel, J. D'Haen, P. Heremans, J. Poortmans, J.V. Manca, *Sol. Energy Mater. Sol. Cells* 90, **2006**, 2150

[8] J. Jo, S.-S. Kim, S.-I. Na, B.-K. Yu, D.-Y. Kim, *Adv. Funct. Mater.* 19, **2009**, 866

[9] S. van Bavel, E. Sourty, G. de With, J. Loos, *Nano Lett.* 9, **2009**, 507

Chapter 3

P3XT: poly-alkylthiophene fibers produced in solution

For P3HT:PCBM blends, it is necessary that P3HT is crystalline to obtain good photovoltaic performance. This chapter investigates an alternative for the traditional thermal treatment, i.e. PAT fibers in solution were prepared. PAT fibers with side chain lengths ranging from 4 to 9 carbon atoms were tested (this is denoted as P3XT where X is a number from 4 to 9). Different solvents had to be used to obtain the fibers in solution and these solvents clearly had an effect on the active layer morphology. When PCBM had a high solubility in the solvent, good intermixing of PCBM and polymer was obtained. For low PCBM solubility, the PCBM assembled in large (> 500nm) chunks. In the end, P36T, which corresponds to the popular P3HT, gave the best photovoltaic performance.

3.1 Materials

After the discovery of the dual crystallization behaviour of P3HT:PCBM blends (see also section 5.1) upon thermal treatment, other procedures were explored that could be able to deliver the ideal active layer morphology where fibrillar P3HT is mixed with PCBM. This could avoid the thermal treatment in order to be able to use flexible substrates such as PET (poly(ethylene terephthalate)), which does not resist high temperatures. One possibility was solvent annealing.[1,2] Another possibility was the production of PAT (poly-alkylthiophene) fibers in solution. Ihn et al.[3] already produced these PAT fibers in solution in 1992 but it was not until 2007 that Berson et al.[4] actually used the P3HT fibers in solution to make photovoltaic devices.

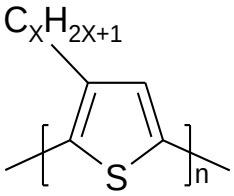

Figure 3-1 Structure of the different P3XT polymers that were produced as fibers in solution.

	M_w / 10^3	PD	Solvent
P34T	44.7	2.29	oCT
P35T	32.2	1.93	PX
P36T	42.7	1.80	PX
P37T	40.0	1.64	Pinane
P38T	46.4	1.66	Pinane
P39T	37.8	1.46	Pinane

Table 3-1 Molecular weight (M_w) and polydispersity (PD) of the PAT derivatives. Reprinted from ref 5.

Dr. W. Oosterbaan of the Organic Chemistry group at the UHasselt, made a whole set of PAT fibers in solution. The production process is discussed elsewhere.[5] PAT-fibers with side-chain lengths ranging from 4 carbon atoms to 9 carbon atoms (Figure 3-1) were prepared. The molecular weights of the materials are listed in Table 3-1. In this chapter, the materials will be called

P3XT, where X denotes the number of carbon molecules in the side chain. This means that the P36T corresponds to the popular P3HT (poly-3-hexylthiophene).

3.2 Solar cell performance and active layer morphology

Each material, presented in Figure 3-1, was used as electron donor material in bulk heterojunction solar cells. The fibers were prepared in different solvents,[5] therefore the solar cell fabrication process varied slightly for the different materials. It was found that upon heating the fibers in solution, the fiber concentration of the solution decreased (the fibers dissolved slowly and were transformed back to amorphous material). For each material, the solar cell performance was determined for several solution temperatures. The temperature range was chosen through a preceding UV-Vis experiment where the speed of the fiber decrease was estimated.

The procedure for making solar cells started always from one vial with P3XT fibers. PCBM was added to this vial to obtain the desired P3XT:PCBM weight ratio. For P34T, P35T and P36T, this solution was stirred for at least 24h. When a co-solvent was used for adding the PCBM (in the case of P37T, P38T and P39T) this solution was left to stir for one hour. After this, the solution was gradually heated until the desired temperature where it was left for at least 30 minutes. Then the active layer of the solar cell was spin-coated from the solution on an ITO/PEDOT-PSS substrate, an identical layer was spin-coated on a Si substrate to make TEM samples afterwards and a small amount of the solution was isolated to determine the fiber content at the current solution temperature. The fitting procedure for determining this fiber content is explained in section 2.2.1. The solution temperature was then increased to the next value where the whole experiment was repeated.

This section presents subsequently the photovoltaic performance of the indivicual PAT derivatives (P3XT with X = 4 to 9) and the observed changes in active layer morphology upon heating the solution. In the next section (section 3.3), a summary and discussion is provided of all the obtained results.

3.2.1 P34T

P34T-fibers were delivered in a 0.4% ortho-chlorotoluene (oCT) solution. PCBM was added to obtain a 1:1 weight ratio with the polymer. Figure 3-2 shows the evolution of the photovoltaic parameters as the temperature of the solution, containing the P34T:PCBM 1:1 mixture, is increased. The short circuit current density (J_{sc}) decreases. This can be caused by the decreasing active layer thickness (from ~265 nm at 31 °C to ~70 nm at 75 °C) due to the decreasing viscosity of the solution upon heating.

In the open circuit voltage (V_{oc}) and the fill factor (FF) an increase is observed upon heating the solution. Reyes-Reyes et al.[6] and Vanlaeke et al.[7] already observed a similar behavior of V_{oc}. They used a post-production thermal treatment on their P3HT devices, and observed a decrease of V_{oc} coinciding with an increase in the amount of crystalline P3HT. Here we did the reverse experiment. Figure 3-3 shows that the fiber concentration decreased very smoothly when the solution temperature was increased. A temperature increase from 31 °C to 75 °C leads to a decrease in fiber concentration from 90% to 20%. Savenije et al.[8] demonstrated that the aggregation of P3HT into fibers increases the polymers oxidation potential. When P3HT:PCBM blends were annealed at 80 °C, a positive shift of the HOMO level of P3HT of about 0.2 V was measured. Since V_{oc} is related to the HOMO level of the donor material,[9-13] the increase in V_{oc} is attributed to a decrease in fibrillar P34T.

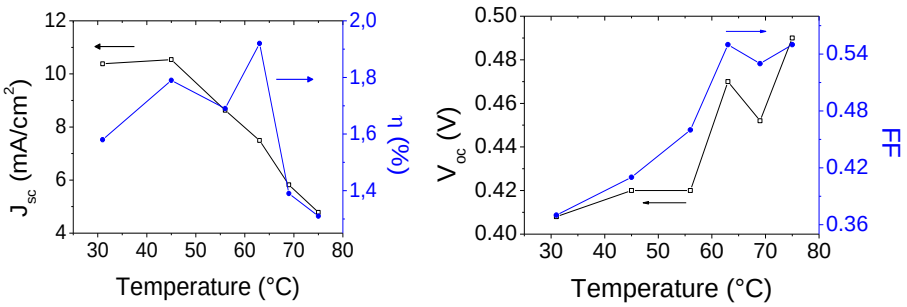

Figure 3-2 Performance of P34T:PCBM 1:1 solar cells as a function of solution temperature.

For the FF, different behavior was observed up till now. Reyes-Reyes et al.[6]

observed an increase as well as a decrease of the FF upon post-production thermal treatment. High temperature (155 °C) thermal treatment lead to a decrease of FF, low temperature (≤ 105 °C) thermal treatment lead to an increase in FF. They suggested that the increase in FF was due to better polymer chain ordering within the thin film allowing for high mobilities. Since for P34T, the amount of crystalline polymer is decreasing while FF increases, the ordering of P34T alone cannot explain the evolution of the FF.

The efficiency of the solar cells shows a rather irregular evolution. The best performance (~1.9%) is reached at a solution temperature of ~63 °C, at this point the active layer thickness was ~95 nm.

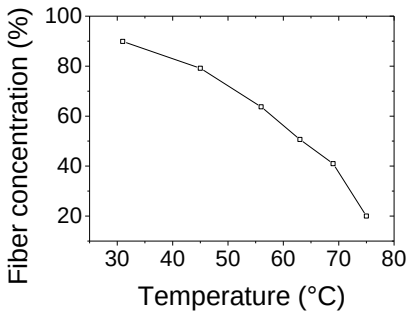

Figure 3-3 Decrease of the P34T-fiber concentration as a function of solution temperature.

BFTEM images of the active layers of the solar cells above are presented in Figure 3-4. No significant changes in the active layer morphology can be deduced upon solution heating. In the larger magnification (Figure 3-4, bottom), the P34T fibers are nicely visible. Also some darker and some lighter regions are visible. This could point to some phase separation between PCBM (darker regions) and P34T (lighter regions) because of the higher density of PCBM as compared to P34T.[14,15] However, the difference in contrast is probably more influenced by thickness variations since thickness measurements with a Dektak profilometer showed a coarse surface.

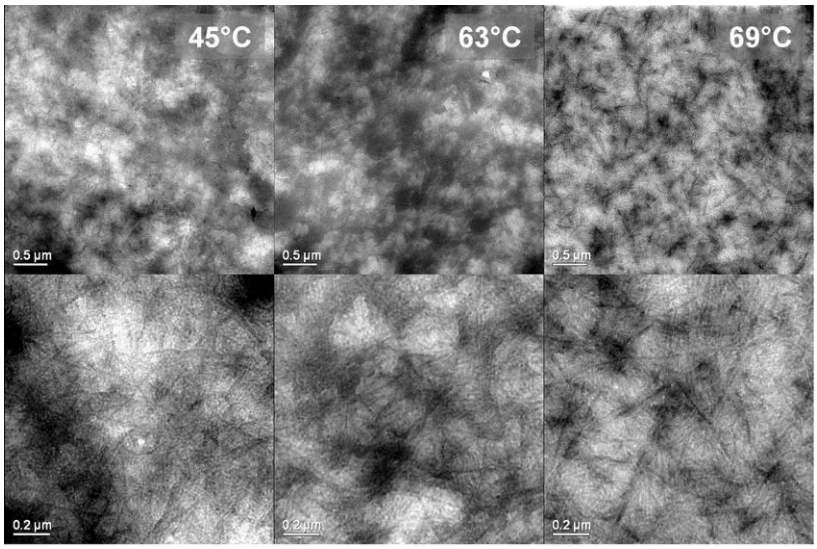

Figure 3-4 BFTEM images of the P34T:PCBM 1:1 active layer of solar cells prepared from different solution temperatures. Top images: scale bar = 0.5 µm, bottom images: scale bar = 0.2 µm.

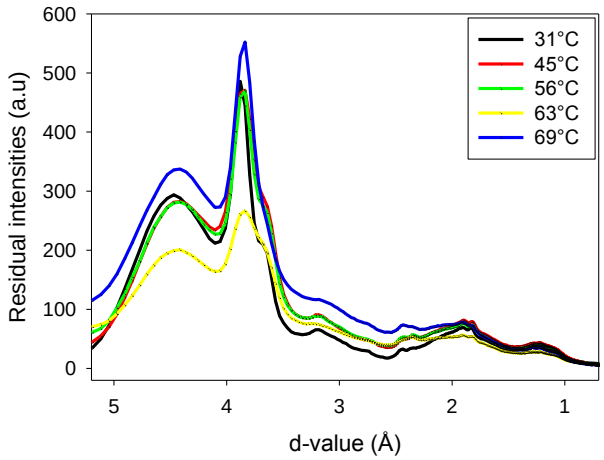

Figure 3-5 Residual intensities of SAED patterns of the P34T:PCBM matrix.

SAED patterns were taken with a SA diaphragm so that circular areas with a diameter of about 5.8 µm were used in the formation of the diffraction pattern. The residual intensities (see section 2.1.3) of these patterns are shown in Figure 3-5. The peak at 3.8 Å, corresponding to crystalline P34T, is clearly

visible. However, this peak has a shoulder at about 3.65 Å. This could point out that 2 phases of the P34T exist. At 4.6 Å, a peak corresponding to the nano-crystalline PCBM is visible. Upon heating the solution, no significant changes in the diffraction patterns can be observed. Both the peak at 4.6 Å (due to nanocrystalline PCBM) and the peak at 3.8 Å (due to crystalline P34T) are clearly present for all solution temperatures. This means that at the scale where the SAED pattern was taken PCBM is well mixed with crystalline P34T.

3.2.2 P35T

P35T fibers were delivered in a 0.6% para-xylene (PX) solution. PCBM was added to obtain a 1:1 weight ratio with the polymer. The evolution of the photovoltaic parameters as a function of solution temperature is depicted in Figure 3-6. When the solution is heated from 40 °C to 57 °C, an increase in J_{sc} is observed, and heating the solution further to 74 °C leads to a small decrease in J_{sc}. These changes in J_{sc} are however very small (at most 0.9 mA/cm^2). The evolution of V_{oc} and FF looks similar as in the case of P34T, both parameters show a gradual increase upon solution heating. Also the decrease of the P35T-fiber concentration (Figure 3-7) looks similar to the behavior of the P34T-fibers (Figure 3-3).

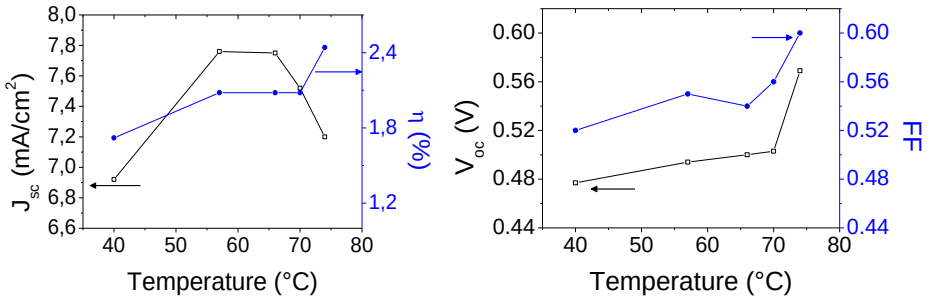

Figure 3-6 Performance of P35T:PCBM 1:1 solar cells as a function of solution temperature.

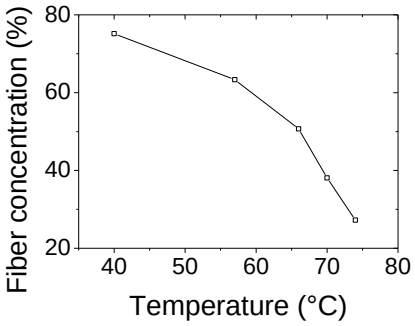

Figure 3-7 Decrease of the P35T-fiber concentration as a function of solution temperature.

BFTEM images (Figure 3-8), do not show significant changes in active layer morphology. The thickness of the active layers decreased upon heating the solution from ~195 nm (at 40 °C) to ~75 nm (at 74 °C). The thickness measurements of the films, revealed that the active layer for the solution temperature of 40 °C, was inhomogeneous. There were large (>100 nm) thickness differences within the film. This can explain the worse photovoltaic performance at this temperature. The decrease in J_{sc} when heating the solution above 70 °C can be attributed to the smaller active layer thickness.

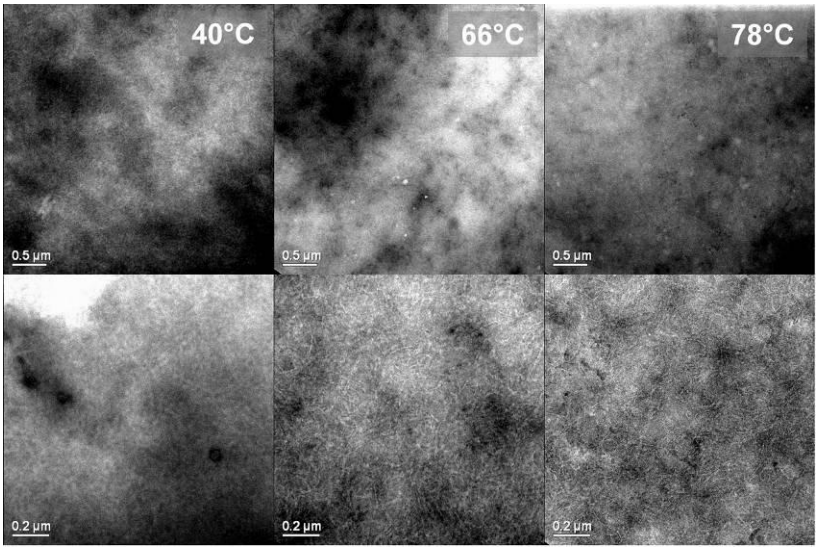

Figure 3-8 BFTEM images of the P35T:PCBM 1:1 active layer of solar cells prepared from different solution temperatures. Top images: scale bar = 0.5 µm, bottom images: scale bar = 0.2 µm.

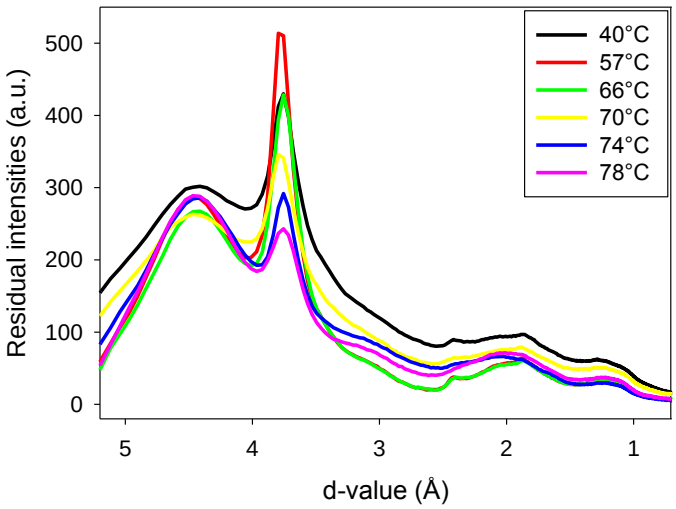

Figure 3-9 Residual intensities of SAED patterns of the P35T:PCBM matrix.

The residual intensities of the SAED patterns, made from the P35T:PCBM active layer (Figure 3-9) reflect the decreasing fiber concentration in the solution. The higher the solution temperature, the smaller the peak at 3.8 Å (due to crystalline P35T).

3.2.3 P36T

P36T fibers are a specific appearance of the popular P3HT, which will be discussed in chapter 5. The use of these fibers in photovoltaic devices was studied here in several weight ratios with PCBM to obtain an optimum in solar cell performance.

The first batch of P36T-fibers was delivered in a 0.7% para-xylene solution. PCBM was added to this solution to obtain three different P36T:PCBM weight ratios, namely 1:0.65, 1:0.8 and 1:1. For each weight ratio a set of solar cells was made while the solution temperature was again increased gradually (Figure 3-10). Apparently, there is not a big difference between the 1:0.65 and the 1:0.8 weight ratio. For all 4 photovoltaic parameters (J_{sc}, V_{oc}, FF and η), the results are close together. The 1:1 weight ratio differs a lot from the other two weight ratios. V_{oc} and FF rise as a function of solution temperature,

like they did for the 1:0.65 and the 1:0.8 weight ratios but the course of the curves is rougher. The biggest difference is found in J_{sc}: for the 1:1 solar cells, it seems that J_{sc} displays a quadratic dependence on temperature (fit is shown in Figure 3-10). The course of J_{sc} is reflected in η.

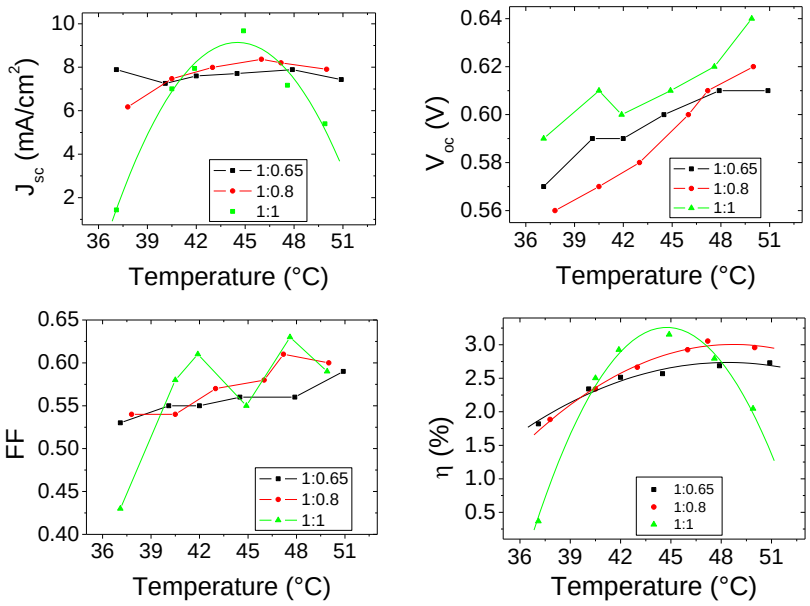

Figure 3-10 Performance of P36T:PCBM solar cells with different weight ratios.

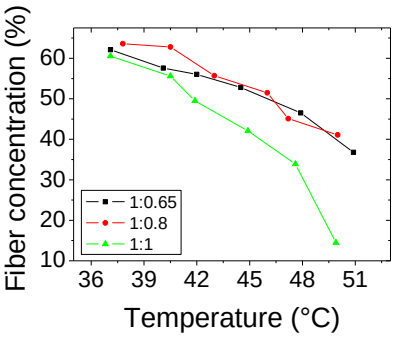

Figure 3-11 Decrease of the P36T-fiber concentration as a function of solution temperature.

The decrease of the fiber concentration is again very similar for the 1:0.65 and 1:0.8 solar cells. The fiber concentration in the 1:1 blend decreases a little bit faster.

The highest efficiency, obtained with these solar cells, was over 3%. This efficiency was reached for the 1:1 solar cells at a solution temperature of ~45 °C. The fiber concentration at this solution temperature was 42%.

For the P36T:PCBM 1:1 devices, a strong connection between their performance and their active layer morphology is present. Figure 3-12 shows BFTEM images of the active layers. The active layer spin-coated from a solution at a relatively low temperature (37 °C) shows large (up to 50 µm) needles. Spots in the SAED patterns of the needles confirm that they are PCBM single crystals.[16] In between the needles, fibers of P3HT are visible. They appear dark against a light background.

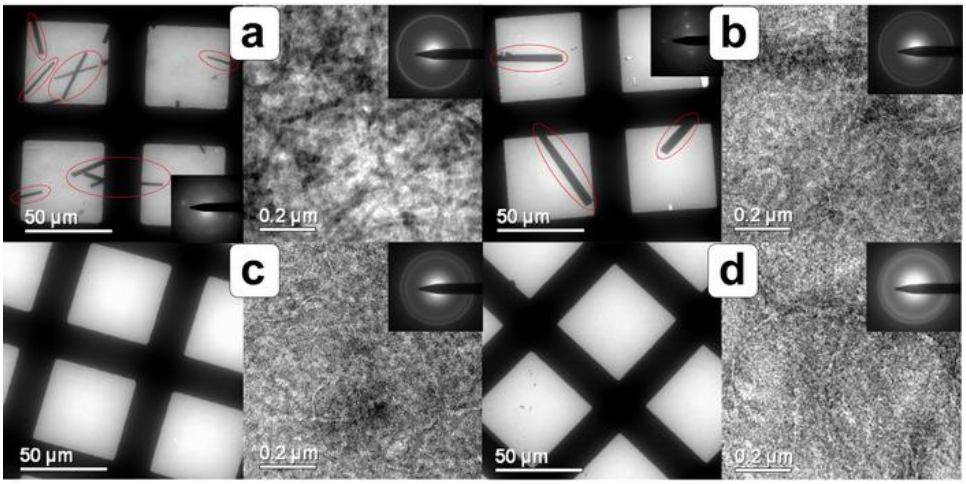

Figure 3-12 BFTEM images of P36T:PCBM 1:1 spin-coated from a solution at 37.1 °C (a), 40.5 °C (b), 41.9 °C (c) and 49.9 °C (d). The insets show the SAED patterns of either the PCBM needles (a and b, left) or the homogeneous P3HT:PCBM regions in between the needles (right). Scale bar = 50 µm (left) of 0.2 µm (right).

SAED also gives information about this part of the active layer. In Figure 3-13, the residual intensities of the SAED patterns of the homogeneous areas of the active layers are shown (the area in between the PCBM crystals). For the film spin-coated at 37 °C, the residual intensities of the SAED pattern show a clear peak at 3.8 Å (due to crystalline P3HT). The remainder of the SAED pattern appears featureless and no peaks corresponding to PCBM can be distinguished. This indicates that the major part of PCBM is assembled in the needles.

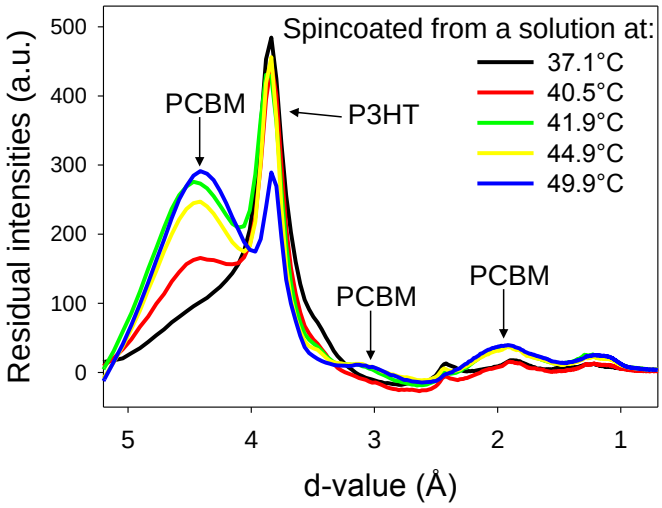

Figure 3-13 Residual intensities of the SAED patterns of the P36T:PCBM matrix for several solution temperatures.

By slightly increasing the solution temperature to ~ 40 °C, a change in morphology is immediately observed. The PCBM needles have grown larger (Figure 3-12). The long (> 48 h) stirring of the solution at room temperature and at elevated temperatures make it plausible that the PCBM needles were formed in the casting solution. The spin-coating takes less than 120 s, which does not leave much time for the formation of such large needles. The long time available during stirring together with the perfect crystal shape and dependence of the crystal size on the temperature of the casting solution, all indicate that the crystals were formed during stirring of the casting solution by an Ostwald ripening process.[17]

For the solution temperature of ~ 40 °C, a small increase in the diffraction intensity at 4.6 Å can be seen in the SAED pattern of the area in between the needles (Figure 3-13). This small peak indicates that some amount of nano-crystalline PCBM[18] is now present in between the fibers. Apparently a small part of the PCBM has dissolved in the p-xylene at this temperature; the PCBM is no longer completely grouped in the needles. This gives a higher yield of exciton dissociation at the polymer:PCBM interface and thus a better solar cell performance (Figure 3-10). As opposed to the film made from a solution at

37 °C, the P3HT fibers are now visible as light areas in the Bright Field TEM image (Figure 3-12). This is caused by the presence of PCBM with a higher density in between the polymer matrix.

A further increase of the solution temperature leads to the disappearance of the PCBM needles (Figure 3-12). For solution temperatures of ~ 42 °C, ~ 45 °C (Figure 3-13) and ~ 48 °C (not shown) strong peaks corresponding to both P3HT (at 3.8 Å) and PCBM (at 2 Å, 3.1 Å and 4.6 Å[16]) are present. These temperatures also correspond to the best photovoltaic performances (Figure 3-10). Good charge transport due to crystalline P3HT, in combination with a large interfacial area between polymer and PCBM render good solar cells. At a solution temperature of ~ 50 °C, there is a slight drop in solar cell efficiency. At this point the fiber content has decreased strongly (Figure 3-11 and Figure 3-13), which will likely result in less efficient hole transport.

The active layer thickness of these devices was rather low (about 90 nm for the best performing solar cell). Therefore an attempt was made to increase the active layer thickness by increasing the concentration of the P36T-fibers in solution from 0.7% to 1%. Figure 3-14 shows the performance of solar cells that were made starting from this solution. The temperature of the solution was chosen in the range where the previous P36T:PCBM photovoltaic devices performed the best (40 °C – 48 °C).

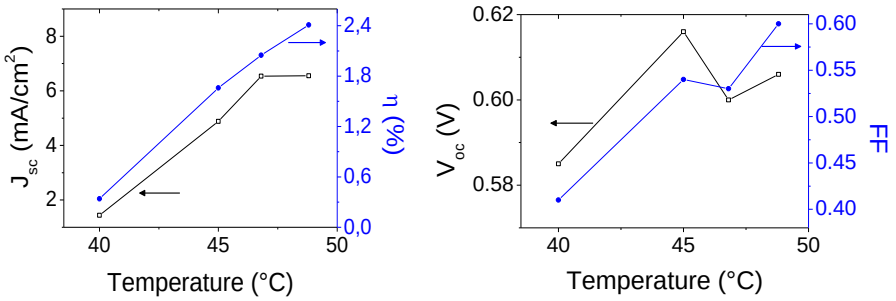

Figure 3-14 Performance of P36T:PCBM 1:1 solar cells as a function of solution temperature.

The decrease in fiber content (Figure 3-15) for this solution is comparable to the evolution seen in Figure 3-11. The performance of these solar cells is not

better than the performance of the solar cells made with the solution of 0.7%. At 48 °C, the efficiency is still rising but the relatively small increase in active layer thickness (~100 nm) as opposed to the previous solar cells (~90 nm) and the decrease of fiber content below 40% make it plausible that the efficiency of the solar cells will not increase much further upon heating the solution.

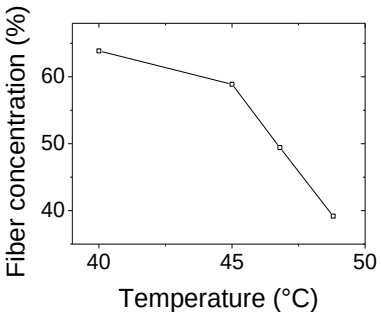

Figure 3-15 Decrease of the P36T-fiber concentration as a function of solution temperature.

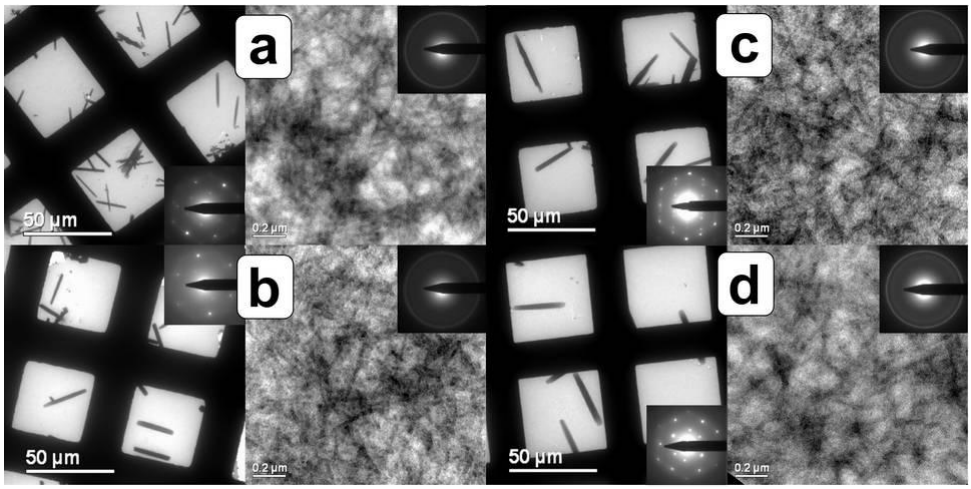

Figure 3-16 BFTEM images of P36T:PCBM 1:1 spin-coated from a solution at 40.0 °C (a), 44.5 °C (b), 46.6 °C (c) and 48.3 °C (d). The insets show the SAED patterns of either the PCBM needles (left) or the homogeneous P3HT:PCBM regions in between the needles (right). Scale bar = 50 µm (left) of 0.2 µm (right).

Apparently, the higher concentration of the solution, induces a more pronounced Ostwald ripening for the PCBM as is clear from Figure 3-16. PCBM

again forms needles like it did in Figure 3-12. The residual intensities of the areas in between the needles (Figure 3-17) indicate that the PCBM dissolves more slowly. Upon heating, some evolution can be observed at 4.6 Å, this means that some part of the PCBM dissolves into the polymer matrix. The peak at 4.6 Å is however never as pronounced as in Figure 3-13, which means that a big part of the PCBM is still assembled in the needles.

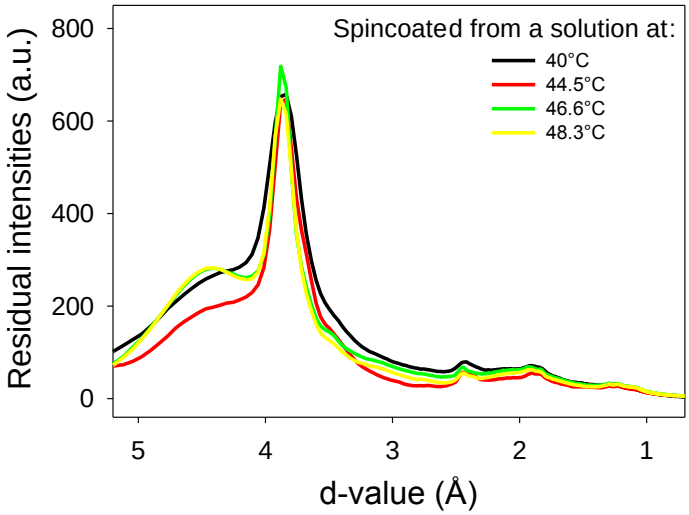

Figure 3-17 Residual intensities of the SAED patterns of the P36T:PCBM matrix for several solution temperatures.

3.2.4 P37T

P37T fibers were delivered in a 0.25% pinane solution. The initial solar cells made from the P37T:PCBM 1:1 solution were short circuited at low solution temperature. BFTEM images (Figure 3-18, left) revealed large (>500 nm) PCBM chunks, indicating that the PCBM did not intermix with P37T fibers in the pinane solution. Upon heating the solution, the PCBM chunks became smaller and functioning photovoltaic devices with an efficiency of about 0.22% (at a solution temperature of 64 °C) could be produced.

In an attempt to solve the dissolution problem of PCBM in pinane, a co-solvent was used. After comparison of several solvents (see section 3.2.5), the use of a 4% PCBM solution in 1,2,4-trimethylbenzene (1,2,4-TMB) seemed the most

appropriate choice. The concentration of the initial solution was also increased to 1.25% to obtain thicker active layers.

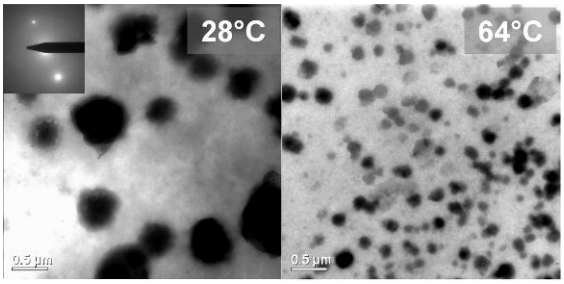

Figure 3-18 BFTEM images of the P37T:PCBM 1:1 active layer of solar cells prepared from different solution temperature. At low temperatures (e.g. 28 °C), PCBM forms large chunks in pinane, at higher temperatures (e.g. 64 °C) the chunks become smaller. Scale bar = 0.5 µm.

The photovoltaic parameters of these solar cells are depicted in Figure 3-19. At room temperature it was still not possible to obtain a homogeneous spin-coated film. Upon dropcasting, the film looked rather homogeneous at first sight but the photovoltaic device was still short-circuited. The solution was then heated and around 50 °C it became spin-coatable. J_{sc} then increased gradually and obtained a maximum at 60 °C after which it stayed rather constant. At this point, the maximum efficiency of 1.8% was reached. For higher solution temperature, the FF decreased and with it also the efficiency fell down. The active layer thicknesses for solutions of 56 °C or higher were between 120 nm and 140 nm.

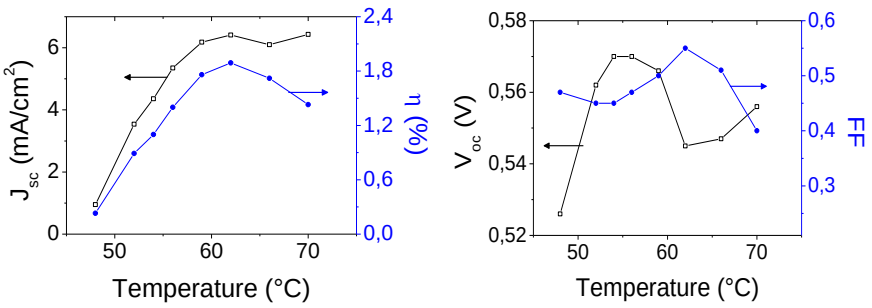

Figure 3-19 Performance of P37T:PCBM 1:1 solar cells as a function of solution temperature.

The morphology of the drop-casted film and the film spin-coated at 48 °C could not be investigated with TEM because they were too thick. Figure 3-20 shows the morphology for a few other solution temperatures. It is clear that P37T and PCBM are much better mixed than in Figure 3-18. No chunks of PCBM are visible.

For P37T, it was not possible to calculate the fiber-concentration of the solutions because of the presence of 2 phases of the polymer. Because the 2 phases could not be separated completely, it was not possible to do a fitting as described in section 2.1.4. However, analogous to the other P3XT fibers, the residual intensities of the SAED patterns of the P37T:PCBM films (Figure 3-21) indicate that the amount of fibers decreases for higher solution temperatures (peak at 3.8 Å becomes smaller).

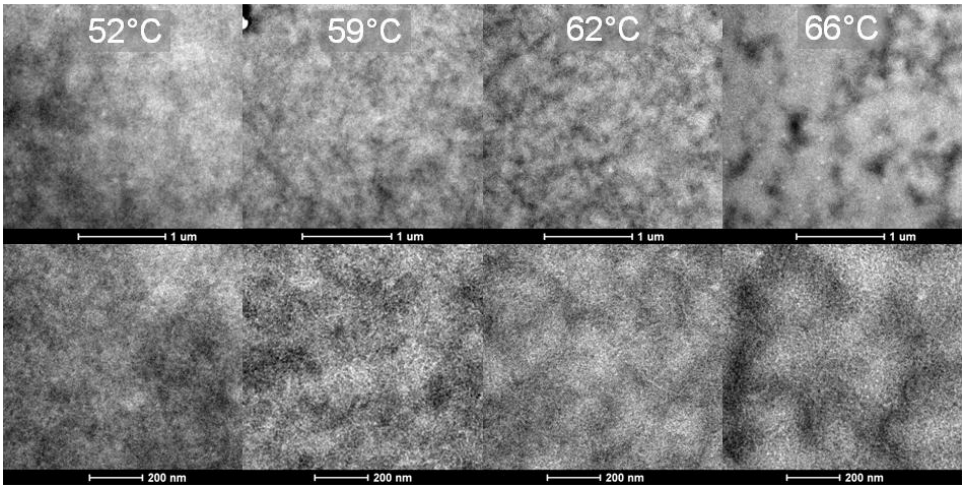

Figure 3-20 P37T:PCBM 1:1 active layer morphology when the PCBM is added from a 4% solution in 1,2,4-TMB. Scale bar = 1 µm (top), scale bar = 200 nm (bottom).

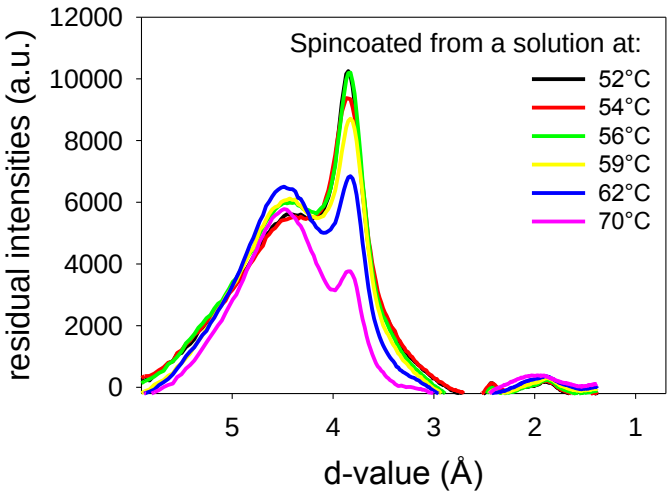

Figure 3-21 Residual intensities of the SAED patterns of P37T:PCBM 1:1 films.

3.2.5 P38T

P38T fibers were delivered in a 0.25% pinane solution. When adding PCBM to this solution, the behaviour of the solution was comparable to the P37T solution. The efficiency of the solar cells did not exceed 0.2% and BFTEM images again showed PCBM chunks that decreased in size upon heating the solution (Figure 3-22).

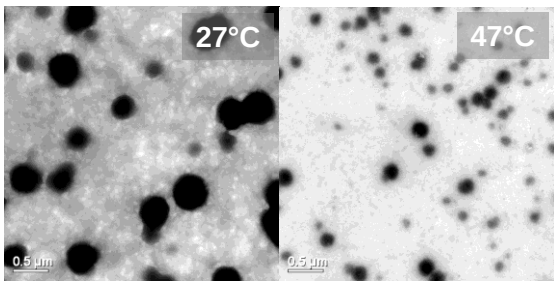

Figure 3-22 BFTEM images of the P38T:PCBM 1:1 active layer of solar cells prepared from different solution temperature; PCBM forms chunks. Scale bar = 0.5 µm.

Because of the bad dissolution of PCBM in pinane, a co-solvent was introduced in which PCBM dissolved good. Another condition for the co-solvent was that the fibers should not dissolve in it. 3 co-solvents were tested, namely

dichlorobenzene (DCB), ortho-xylene (OX) and 1,2,4-trimethylbenzene (1,2,4-TMB). The test was done by adding PCBM that was dissolved in the co-solvent to the P38T solution in pinane in such a way that a P38T:PCBM 1:1 weight ratio was obtained. After the addition of PCBM, UV-Vis spectra were recorded at regular time intervals and the decrease of the fiber content could be obtained by fitting these spectra. The curves that represent this experiment are shown in Figure 3-23.

It is immediately obvious that DCB is not suitable as co-solvent; the fiber content decreased within less than 15 minutes to below 20%. Both OX and 1,2,4-TMB perform a lot better, after a first rapid decrease of the fiber content, it stays rather constant. It is also clear that the higher the PCBM concentration in the co-solvent is (hence the closer PCBM comes to its solubility limit), the lower is the decrease in P38T fibers upon addition of the co-solvent. In this experiment, a 4% solution of PCBM in 1,2,4-TMB performed very well (the fiber content stayed above 90% after 1 hour). Therefore, 1,2,4-TMB was chosen as co-solvent in the subsequent fabrications of photovoltaic devices based on a solution in pinane.

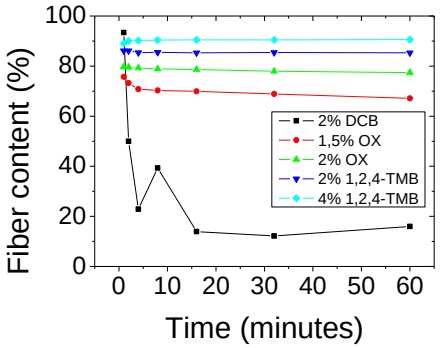

Figure 3-23 Decrease of the P38T fiber content in time upon addition of several co-solvents.

The use of the co-solvent 1,2,4-TMB immediately led to an improvement of the photovoltaic performance. Because of the better dissolution of PCBM the concentration of the P38T fibers in pinane was increased to 0.7%. Figure 3-24 shows that efficiencies of over 1% could now be reached. The active layer

thickness of these solar cells was about 140nm.

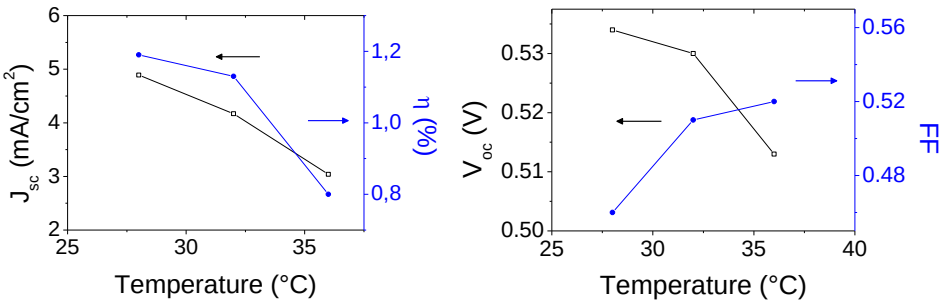

Figure 3-24 Performance of P38T:PCBM 1:1 solar cells as a function of solution temperature.

Figure 3-25 shows the decrease in P38T-fiber concentration. The P38T fibers are a lot more sensitive to the temperature treatment than the fibers with shorter side-chains.

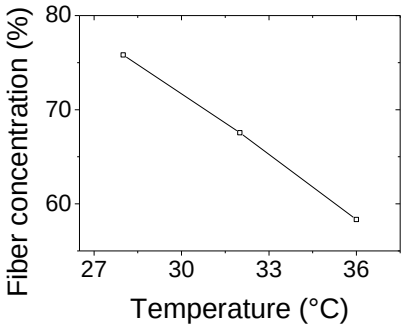

Figure 3-25 Decrease of the P38T-fiber concentration as a function of solution temperature.

The active layer of the solar cells still shows phase separation between P38T and PCBM but now the PCBM areas are smaller and more evenly spread throughout the polymer matrix (Figure 3-26). This gives a larger contact area between the polymer and PCBM, which improves the photovoltaic performance. At rare positions in the films, PCBM single crystals (>2 µm) were formed (see inset in Figure 3-26). Apparently the formation of a few rare PCBM crystals does not render bad solar cells, there is still enough PCBM present in the polymer matrix to obtain sufficient charge separation.

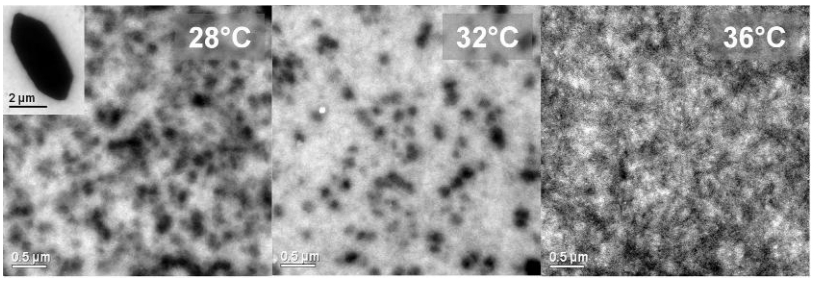

Figure 3-26 BFTEM images of the P38T:PCBM 1:1 active layer, PCBM was added from 1,2,4-TMB. Scale bar = 0.5 µm.

In the last attempt to increase the photovoltaic performance even further, the concentration of the P38T solution in pinane was increased to 1.75% and at the same time, the weight ratio of P38T:PCBM was reduced to 1:0.65 (to avoid the clustering of PCBM). The initial fiber solution looked very viscous at first glance. Upon adding the solution of PCBM in 1,2,4-TMB, the solution became a bit less viscous but it was still to thick to spin-coat a homogenous layer. The P38T:PCBM 1:0.65 solution was then heated very slowly until it was possible to spin-coat a homogeneous layer. This experiment led to a solar cell efficiency of over 2% (Figure 3-27).

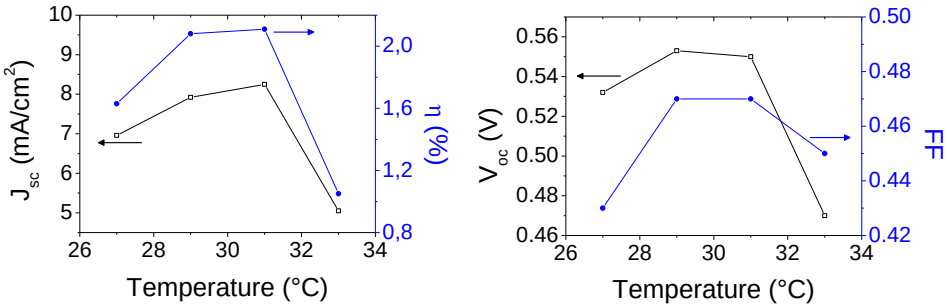

Figure 3-27 Performance of P38T:PCBM 1:0.65 solar cells as a function of solution temperature.

The fiber content for this experiment (Figure 3-28) decreased faster than in the previous experiment (Figure 3-25). This is probably caused by a larger amount of 1,2,4-TMB that had to be added to the fiber solution because of the high P38T concentration (1.75%) of this solution.

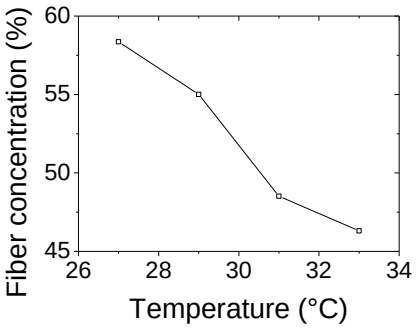

Figure 3-28 Decrease of the P38T-fiber concentration as a function of solution temperature.

BFTEM images show that for these solar cells, again phase separation between PCBM and P38T is present (Figure 3-29). At 27 °C, the PCBM chunks are quite large (> 500 nm). Slightly increasing the solution temperature gives a better mixing of polymer and PCBM with smaller PCBM domains. At 33 °C, Ostwald ripening was again visible. A few nicely shaped PCBM crystals have formed at this temperature (see inset Figure 3-29).

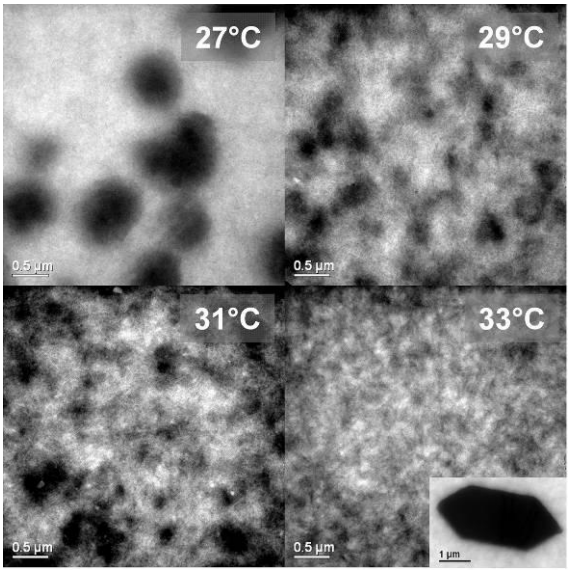

Figure 3-29 BFTEM images of the P38T:PCBM 1:1 active layer, P38T fibers were prepared in a 1.75% pinane solution, PCBM was added from 1,2,4-TMB. Scale bar = 0.5 µm.

3.2.6 P39T

Solar cells from P39T fibers were prepared similarly as P38T:PCBM solar cells. The fibers were delivered in a 1.75% solution in pinane. PCBM was added from a 4% solution in 1,2,4-TMB to obtain a 1:0.65 weight ratio with respect to the polymer. The highest efficiency obtained with this material was 1.3% (Figure 3-30). This efficiency was obtained at the highest solution temperature in this experiment (31 °C). The fiber concentration of the P39T:PCBM solution decreased slowly with the solution temperature (Figure 3-31) and became less than 3% for a solution at 31 °C. The active layer thickness of the best solar cell was ~ 70 nm. This rather low thickness, together with the very low fiber concentration make it plausible that J_{sc} will not increase a lot anymore upon heating the solution (upon heating, the active layer will become even thinner).

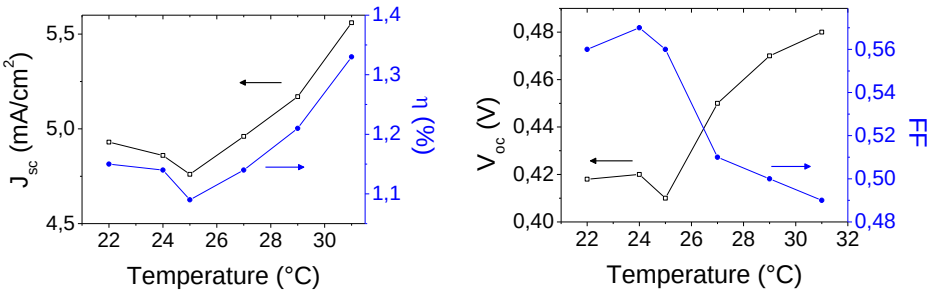

Figure 3-30 Performance of P39T:PCBM 1:0.65 solar cells as a function of solution temperature.

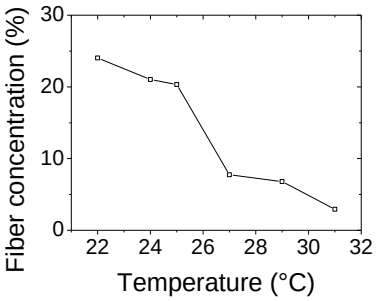

Figure 3-31 Decrease of the P39T-fiber concentration as a function of solution temperature.

The morphology of the active layer for a low solution temperature (i.e. 22 °C) is similar as for P37T and P38T. Small spherical clusters of PCBM are present

in the active layer. This indicates that the joint solvent of P37T, P38T and P39T, namely pinane, has a big influence on this morphology.

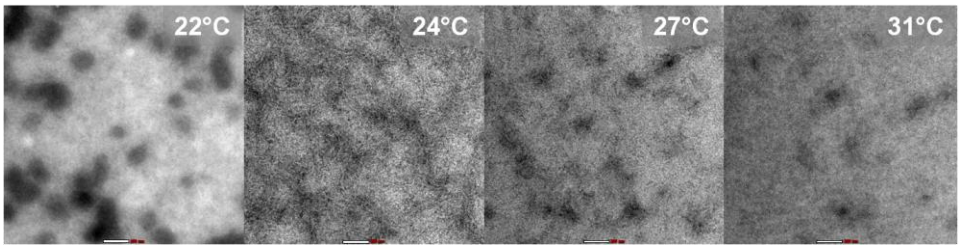

Figure 3-32 BFTEM images of P39T:PCBM 1:0.65 films spin-coated from different solution temperatures. Scale bar = 0.2 µm.

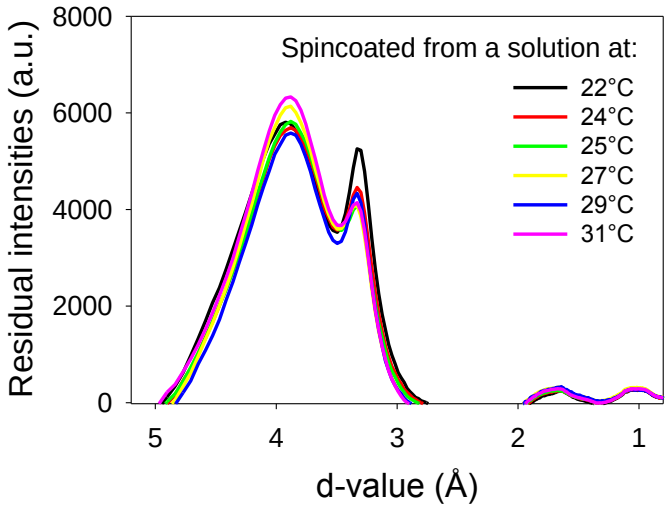

Figure 3-33 Residual intensities of the SAED patterns of P39T:PCBM 1:0.65.

The residual intensities of the P39T:PCBM 1:0.65 films (Figure 3-33) show a small decrease in P39T fibers. The P39T peak at 3.8 Å becomes slightly smaller as compared to the PCBM peak at 4.6 Å for solution temperatures above 24 °C. The effect is however not very significant. Figure 3-31 indicated that the fibers in the solution were almost completely dissolved (the concentration decreased to less than 3% for a solution temperature of 31 °C). The SAED patterns indicate however that there is still some fibrillar P39T present in the layer. The fairly high boiling point of pinane (168 °C) induces some self-organization of the P39T.

3.3 Summary on P3XT-fibers in organic solar cells

The JV-curves of the best performing solar cell for the 6 materials discussed above are represented in Figure 3-34. These PAT's have again shown that a lot of parameters are involved in making photovoltaic devices with high efficiencies.

A very important factor is proven to be the solvent that is used. In the most ideal case, it renders a small (at the scale of the exciton diffusion length, ~10nm) phase separation and it is even better if both solar cell components (donor and acceptor) form crystalline electron- and hole-'highways' towards the electrodes. For the PATs in this study, there was often a phase separation where PCBM assembled into too large (>500 nm) domains. Through heating of the solvent it was possible to either get good intermixing without visible phase separation of PCBM and the polymer (in the case of P36T) or it was possible to reduces the size of the PCBM domains to about 100nm (in the case of P38T and P39T).

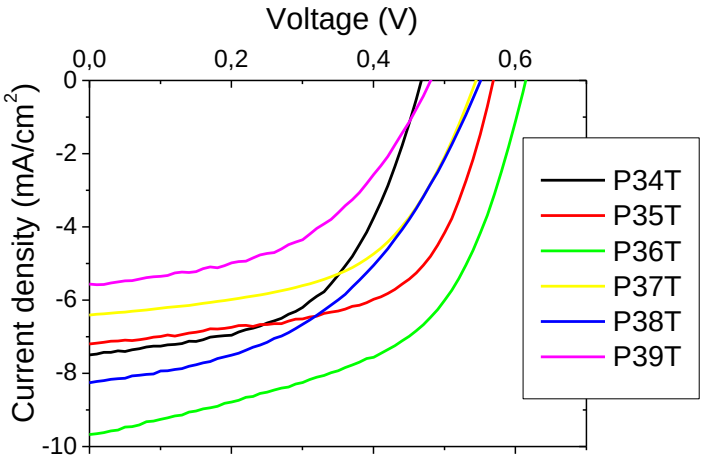

Figure 3-34 J-V curves of the best performing solar cells made with the different PAT's.

A side effect of the solution heating was the decreasing fiber content in the solution. An optimal temperature had to be discovered where the PCBM domains were as small as possible and the P3XT fiber content was as high as possible. From Table 3-2, it is clear that the best performing solar cells do not

have the highest possible fiber content, on the contrary, average fiber contents between 42 % and 51 % were found for the best devices. Only for P35T, the fiber content of the best solar cell was lower. It should be noted however that for P35T also a very good solar cell was made with a fiber content of 50.7%. This device had a J_{sc} of 7.75 mA/cm^2, a V_{oc} of 0.50, a FF of 0.54 and an η of 2.08%. From these observations, it seems as though the 'ideal' fiber content is situated somewhere around 45%. For state of the art P3HT:PCBM solar cells Bavel et al.[19] calculated the fiber content of the active layer using BFTEM tomography. Also the fiber content that they found was not 100 % but in the order of 60 % (slightly higher than the value obtained here).

Material (solvent)	J_{sc} (mA/cm^2)	V_{oc} (V)	FF	η (%)	Fiber content (%)
P34T (oCT)	7.49	0.47	0.55	1.90	50.7
P35T (p-xylene)	7.20	0.57	0.60	2.40	27.2
P36T (p-xylene)	9.67	0.61	0.55	3.15	42.1
P37T (pinane)	6.41	0.55	0.55	1.89	?
P38T (pinane)	8.25	0.55	0.47	2.10	48.5
P39T (pinane)	5.56	0.48	0.49	1.33	43.4

Table 3-2 Photovoltaic parameters of the solar cells in Figure 3-34.

Upon heating the solution, an increase in open circuit voltage (V_{oc}) was often observed in the results above. A similar behavior was already found before.[6,7] A post-production thermal treatment of P3HT:PCBM devices led to a decrease of V_{oc} coinciding with an increase in the amount of crystalline P3HT. Here we did the reverse experiment. Upon increasing the solution temperature, the fiber concentration decreased smoothly. Savenije et al.[8] demonstrated that the aggregation of P3HT into fibers increases the polymers oxidation potential. Since V_{oc} is related to the HOMO level of the donor material,[9-13] the increase in V_{oc} for the P3XT:PCBM solar cells is attributed to a decrease in fibrillar P3XT upon solution heating.

Comparing the performance of the different PATs in Figure 3-34, the best performing material is still P36T. Both for longer and for shorter side chains of

the polymer, the performance gradually decreases. For P34T, the lower efficiency could be caused by the tendency of these fibers to orient parallel to the substrate. The other P3XT, also have this tendency but for P34T it is more pronounced.[20] This parallel orientation of the fibers leads to a high FET (Field Effect Transistor) mobility, in the plane parallel to the substrate, but a low SCLC (Space Charge Limited Current) mobility, perpendicular to the plane of the substrate. For photovoltaic devices, this last mobility is the most important, high SCLC mobilities are favorable for good solar cell performance. P34T, with its parallel orientation, thus shows a lower SCLC mobility than the other P3XT fibers, which could explain its lower efficiency.

For longer side chains (P37T, P38T and P39T), the poorer performance is probably caused by the morphology which has proven to be difficult to tune. Though the use of a co-solvent greatly reduced the size of the PCBM clusters, they still remained too big (> 100 nm) to achieve good efficiencies.

3.4 References

[1] P. Vanlaeke, G. Vanhoyland, T. Aernouts, D. Cheyns, C. Deibel, J. Manca, P. Heremans, J. Poortmans, *Thin Solid Films* 511, **2006**, 358

[2] V.D. Mihailetchi, H. Xie, B. de Boer, L.M. Popescu, J.C. Hummelen, P.W.M. Blom, *Appl. Phys. Lett.* 89, **2006**, 012107

[3] K.J. Ihn, J. Moulton, P. Smith, J. Polym. Sci., Part B: Polym. Phys. 31 (1992) 735

[4] S. Berson, R. De Bettignies, S. Baily, S. Guillerez, Adv. Funct. Mater. 17 (2007) 1377

[5] W.D. Oosterbaan, V. Vrindts, S. Berson, S. Guillerez, O. Douheret, B. Ruttens, J. D'Haen, P. Adriaensens, J. Manca, L. Lutsen, D. Vanderzande, *J. Mater. Chem.* 19, **2009**, 5424

[6] M. Reyes-Reyes, K. Kim, D.L. Carrol, *Appl. Phys. Lett.* **2005**, *87*, 083506

[7] P. Vanlaeke, A. Swinnen, I. Haeldermans, G. Vanhoyland, T. Aernouts, D. Cheyns, C. Deibel, J. D'Haen, P. Heremans, J. Poortmans, J.V. Manca, *Sol. Energy Mater. Sol. Cells.* **2006**, *90*, 2150

[8] T.J. Savenije, J.E. Kroeze, X. Yang, J. Loos, *Thin Solid Films* 511, **2006**, 2

[9] C.J. Brabec, A. Cravino, D. Meissner, N.S. Sariciftci, T. Fromherz, M.T. Rispens, L. Sanchez, J.C. Hummelen, *Adv. Funct. Mater.* 11, **2001**, 374

[10] N.S. Sariciftci, *Mater. Today* Sept **2004**, 36

[11] G. Dennler, N.S. Sariciftci, *Proc. IEEE* 93, **2005**, 1429

[12] M.C. Scharber, D. Muhlbacher, M. Koppe, P. Denk, C. Waldauf, A.J. Heeger, C.J. Brabec, *Adv. Mater.* 18, **2006**, 789
[13] K. Vandewal, A. Gadisa, W.D. Oosterbaan, S. Bertho, F. Banishoeib, I. Van Severen, L. Lutsen, T.J. Cleij, D. Vanderzande, J.V. Manca, *Adv. Funct. Mater.* 18, **2008**, 2064
[14] X. Yang, J. Loos, S.C. Veenstra, W.J.H. Verhees, M.M. Wienk, J.M. Kroon, M.A.J. Michels, R.A.J. Janssen *Nano Lett.* **2005**, *5*, 579
[15] T.J. Prosa, M.J. Winokur *Macromolecules* **1992**, *25*, 4364
[16] M. T. Rispens, A. Meetsma, R. Rittberger, C. J. Brabec, N. S. Sariciftci, J. C. Hummelen, *Chem. Commun.* **2003**, 2116
[17] R. Boistelle, J. P. Astier, *J. Cryst. Growth* **1988**, *90*, 14
[18] X. Yang, J. K. J. van Duren, M. T. Rispens, J. C. Hummelen, R. A. J. Janssen, M. A. J. Michels, J. Loos, *Adv. Mater.* **2004**, *16*, 802
[19] S. van Bavel, E. Sourty, G. de With, J. Loos, *Nano Lett.* 9, **2009**, 507
[20] W.D. Oosterbaan, J.-C. Bolsée, A. Gadisa, V. Vrindts, S. Bertho, J. D'Haen, T.J. Cleij, L. Lutsen, C.R. McNeill, L. Thomsen, J.V. Manca, D. Vanderzande, *Adv. Funct. Mater.* 20, **2010**, 792

Chapter 4

Stability of MDMO-PPV:PCBM solar cells

The active layer morphology of organic BHJ solar cells has proven to be a vital factor in obtaining good photovoltaic performance. This chapter investigates whether the stability of organic solar cells is influenced by changes in the morphology. To induce degradation, annealing at elevated temperatures (from 50 °C to 110 °C) is used. In the active layer, the polymer and PCBM tend to cluster upon annealing. The decrease in interfacial area between both components can explain the decrease of the short circuit current of the solar cells. An Arrhenius analysis is proposed to extrapolate the results to a larger temperature range.

4.1 General procedure to prepare solar cells

All solar cells in this work were prepared according to a standard procedure. Glass substrates coated with an indium tin oxide (ITO, 100 nm) pattern (Figure 4-1) were cleaned successively in soap, demineralised water and acetone, each for 10 minutes in an ultrasonic bath. This was followed by cleaning in boiling isopropanol for 10 minutes. A 25 nm thick poly(3,4-ethylenedioxythiophene–polystyrenesulfonate (PEDOT–PSS (Bayer)) layer was spin-coated on the clean glass/ITO substrates. The substrates were dried for 20 min on a hot plate at 120°C. After this, the substrates were transferred to a glovebox with nitrogen atmosphere where the preparation of the solar cells was finished and the measurements were done.

The active layer (conjugated polymer:PCBM) was spin-coated from a solution in chlorobenzene (unless stated otherwise). Spin-coating parameters were chosen to obtain a layer thickness of ~ 100 nm (verified with a Sloan Dektak^3 ST surface profiler). After depositing the active layer, the devices were put in a vacuum chamber (10^{-6} mbar) where the counter electrode was evaporated. This electrode consisted of a calcium layer (~ 25 nm) with an aluminum layer (~ 70 nm) on top.

At the end of this process, each substrate contained 4 identical solar cells with an active area of 25 mm^2 (Figure 4-1).

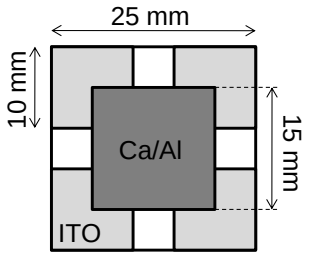

Figure 4-1 Each ITO substrate contains 4 identical solar cells of 25 mm^2.

4.2 Ex-situ degradation measurements

Thermal ageing of the photovoltaic parameters of solar cells was examined

through a three-stage experiment. Firstly, a set of identical solar cells (with an active layer of MDMO-PPV:PCBM 1:4) was prepared and immediately after preparation IV-characterization was performed to obtain the initial values of the photovoltaic parameters. Secondly, each device was annealed (at 100 °C or 110 °C) for a specific time interval (between 0 and 16 hours). This was done in the dark, in a nitrogen atmosphere to prevent degradation due to UV-radiation and oxygen. As a third and final step, when all annealing treatments were finished, IV-characterization of all solar cells was redone. The final solar cell parameters were normalized with respect to the initial values. The curves representing the relative decay of the photovoltaic parameters vs. the annealing time are shown in Figure 4-2.

The curves corresponding to an annealing temperature of 100 °C (squares in Figure 4-2) are first discussed. The first point in the curves corresponds with a solar cell that was not annealed. It was kept in the dark at room temperature during the full experiment to determine the shelf life degradation of the photovoltaic parameters. Apparently, even without a thermal treatment, there is already a small decay in the photovoltaic parameters. This indicates that even without annealing, the solar cells are not stable.

From the second point of the curves onwards, the effect of the annealing on the solar cell parameters can be seen. The annealing results in a significant decay of the solar cell parameters. The short circuit current (I_{sc}) shows a rather exponential decay. After 16 hours of annealing, it has dropped to about 75% of its initial value. The decay in fill factor (FF) has roughly the same behaviour as the decay in I_{sc}. The open circuit voltage (V_{oc}) seems to be less sensitive to a thermal treatment than I_{sc} and FF. The efficiency (η) of the solar cells, being proportional to the product of the other 3 photovoltaic parameters, obviously has the largest decay. Its value drops below 50% of its initial value. These results clearly show that annealing has a dramatic influence on the performance of this type of solar cells.

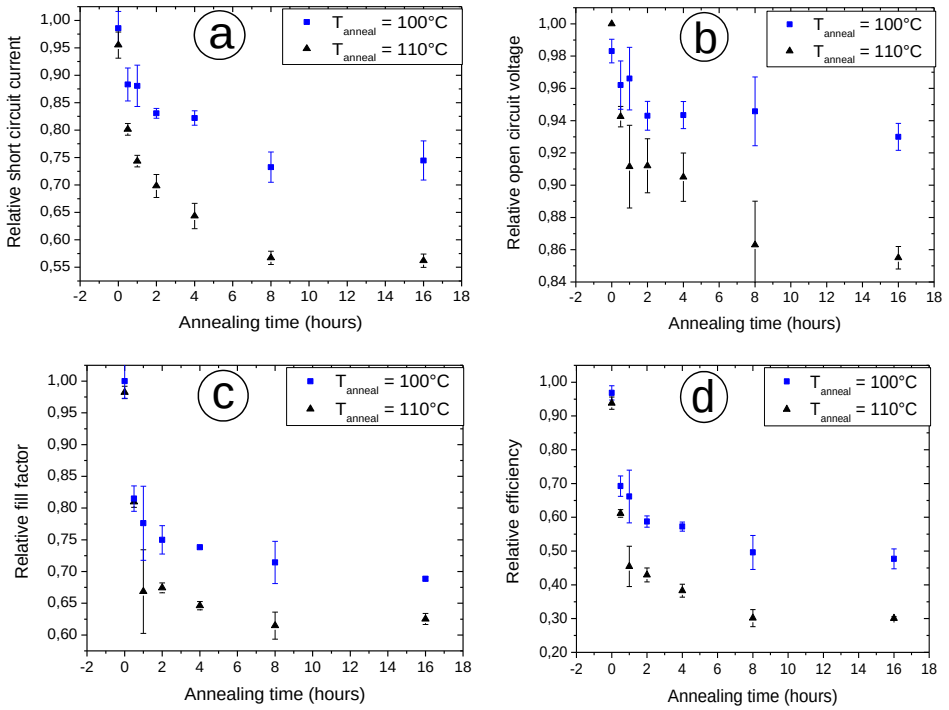

Figure 4-2 Decay of the relative short circuit current (a), the open circuit voltage (b), the fill factor (c) and the efficiency (d) as a result of annealing at 100 °C (squares) and 110 °C (triangles) of MDMO-PPV:PCBM (1:4) solar cells.

When the annealing temperature is raised to 110 °C (triangles in Figure 4-2), the decay characteristics of the photovoltaic parameters change slightly. The small difference between the first points in the 100 °C-curve and the 110 °C-curve is caused by a different time period between the initial and final IV-characterization (30 hours for the 100 °C-curve vs. 42 hours for the 110 °C-curve). Looking at the further course of the curves, the decay in photovoltaic parameters occurs faster for an annealing temperature of 110 °C than for an annealing temperature of 100 °C. This could be expected since for higher annealing temperatures, more energy is supplied. This is also illustrated in paragraph 4.4 where the morphology of active layer is presented. If a rough Arrhenius analysis is performed on these results, an activation energy of around 1 eV is obtained. As a rule of thumb: for an activation energy of 1 eV, one can expect that an increase in temperature of 10 °C would accelerate the

degradation with a factor of 2. For a detailed Arrhenius analysis, a set of in situ experiments should be performed at various temperatures. For this purpose, in situ measurements were done at several temperatures (see next paragraph).

4.3 In-situ measurements

In the following, several experiments are performed at elevated temperatures to speed up the degradation processes inside solar cells. The difference with the previous paragraph is that now the behaviour of a single solar cell is followed within a certain time span.

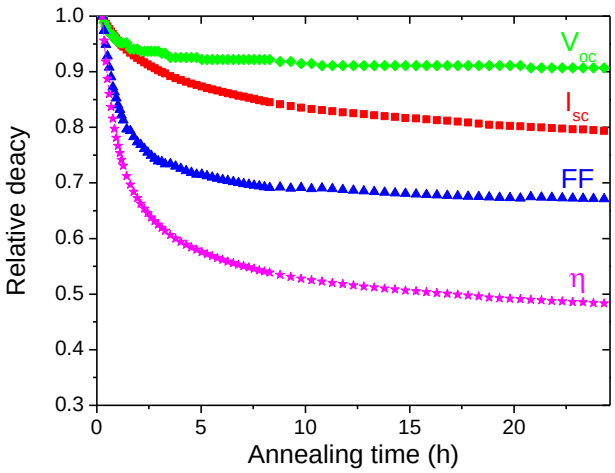

Figure 4-3 Relative decay of the short circuit current (Jsc), open circuit voltage (V_{oc}), fill factor (FF) and efficiency (η) of an MDMO-PPV:PCBM 1:4 solar cell at 110°C.

Figure 4-3 shows the relative decay of the photovoltaic parameters of a solar cell with an MDMO-PPV:PCBM 1:4 blend as active layer for an annealing temperature of 110 °C. As can be inferred from the figure, the open circuit voltage (V_{oc}) is barely sensitive to the thermal treatment performed over a long period of time. This is consistent with the fact that V_{oc} mainly depends on material properties, namely the ionization potential of the donor polymer and electron affinity of the acceptor fullerene molecule. Only a relatively small decrease in V_{oc} (less than 10%) is observed. A larger decrease is observed in

the short circuit current (I_{sc}) and the fill factor (FF). The efficiency of the solar cell, proportional to I_{sc}, V_{oc} and FF, shows the largest decrease. Figure 4-4 again illustrates that for higher annealing temperatures, the decay happens faster.

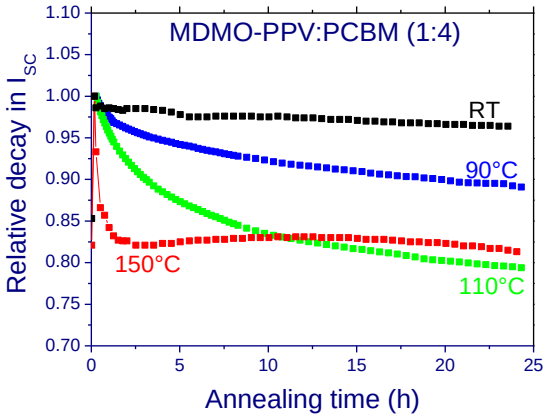

Figure 4-4 Relative decay of I_{sc} for MDMO-PPV:PCBM 1:4 solar cells at different annealing temperatures.

4.4 Degradation reflected in morphology

For pristine MDMO-PPV:PCBM, it was already shown that the performance is strongly linked to the morphology.[1,2] At a 1:4 weight ratio of MDMO-PPV to PCBM, the solar cells performed the best. A phase separated morphology appeared. This morphology could be fine tuned by using chlorobenzene as solvent instead of toluene. This resulted in smaller (~ 50 nm) phase separated regions and better photovoltaic performance. Here we will demonstrate that the behavior of the short circuit current upon annealing (depicted in paragraphs 4.1 and 4.3) can also be linked to morphology changes taking place in the active layer. Figure 4-5 shows Bright Field TEM-images of the evolution of the active layers of MDMO-PPV:PCBM (1:4) during annealing at 100°C and 110°C. Large clusters are formed upon annealing. The Selected Area Electron Diffraction (SAED) patterns of these clusters (insets in Figure 4-5) indicate that they are in fact groups of PCBM-crystals.[3] Annealing gives the PCBM molecules, within the MDMO-PPV:PCBM matrix, the opportunity to

assemble in large clusters. At 110 °C, the PCBM clusters are formed faster than at 100 °C.

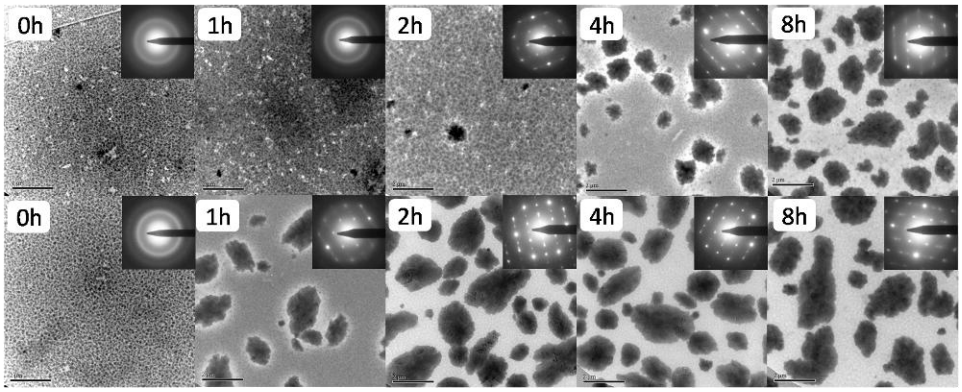

Figure 4-5 Morphology changes in the active layer of MDMO-PPV:PCBM 1:4 during annealing at 100 °C (top) and at 110 °C (bottom). Annealing resulted in the formation of PCBM-clusters. At 110 °C, these clusters were formed faster than at 100 °C (scale bar: 2µm).

Figure 4-6 gives more information about the area in between the clusters in Figure 4-5. After 1 hour of annealing at 110 °C, the clusters had a bright border around them and a grey area in between (Figure 4-5). A larger magnification reveals that this grey area resembles the phase separated MDMO-PPV:PCBM blend of non-annealed samples (Figure 4-6). The residual intensities of the SAED pattern of this area contain distinct peaks corresponding to the nano-crystalline PCBM. After 2 hours of annealing at 110 °C, the area in between the PCBM clusters has become completely bright (Figure 4-5). The BFTEM image in Figure 4-6 now shows a completely different morphology than the initial phase separated blend. The residual intensities of the SAED pattern of this area form a rather flat graph without distinct peaks. This indicates that the PCBM has diffused out of this area.

This demixing of MDMO-PPV and PCBM reduces the interfacial area between both components, leading to less efficient exciton dissociation and a lower short circuit current. At 110 °C, this diffusion of PCBM out of the polymer matrix happens faster than at 100 °C (Figure 4-5). This explains the faster decrease in short circuit current at 110 °C that was observed in Figure 4-2.

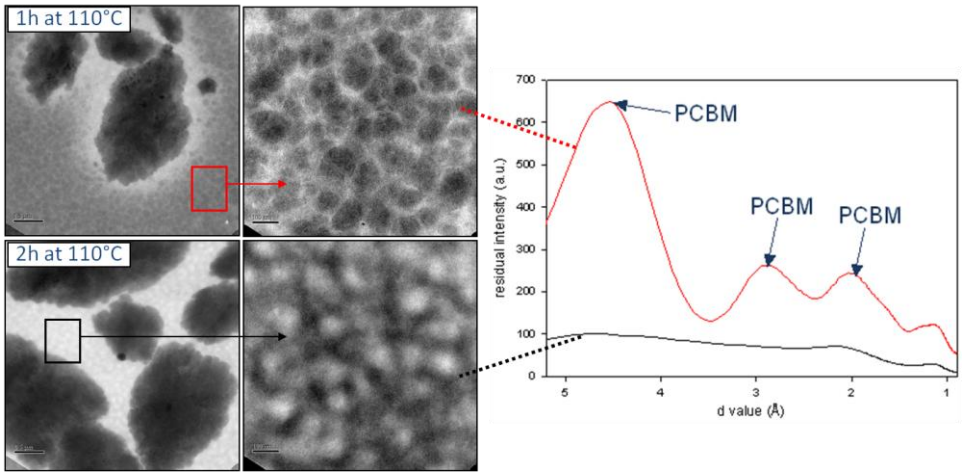

Figure 4-6 BFTEM images of MDMO-PPV:PCBM 1:4 after an annealing treatment at 110 °C, scale bar = 0.5 µm (left) and 100 nm (right). The corresponding SAED patterns of the area in between the clusters are shown in the graph.

4.5 Modeling of the short circuit current decay

The previous sections indicate that MDMO-PPV:PCBM solar cells deteriorate upon annealing at higher temperatures. With higher annealing temperatures, the degradation of the photovoltaic performance happened faster. Usually solar cells operate at lower temperatures than mentioned above, for outdoor applications the maximum operating temperatures are around 70 °C. To get better insight into the degradation at these temperatures, longer degradation measurements at lower temperatures were performed.[4] The results of these measurements are shown in Figure 4-7 (colored curves).

Previous studies on degradation of solar cells,[5,6] use linear and first order exponential models to fit the degradation data. The curves in Figure 4-7 point to an exponential behaviour. Moreover, J_{sc} seems to stagnate at the same value for all annealing temperatures. These observations lead to a model described by the following equation:

$$J_{sc}(t) = J_{sc}(\infty) + J_{sc}(0)\exp(-k_{\deg}t) \qquad \text{(Eq. 4-1)}$$

where $J_{sc}(\infty)$ resembles the stagnation value of J_{sc} after a long annealing time,

k_{deg} is a rate constant that is connected to the degradation kinetics.

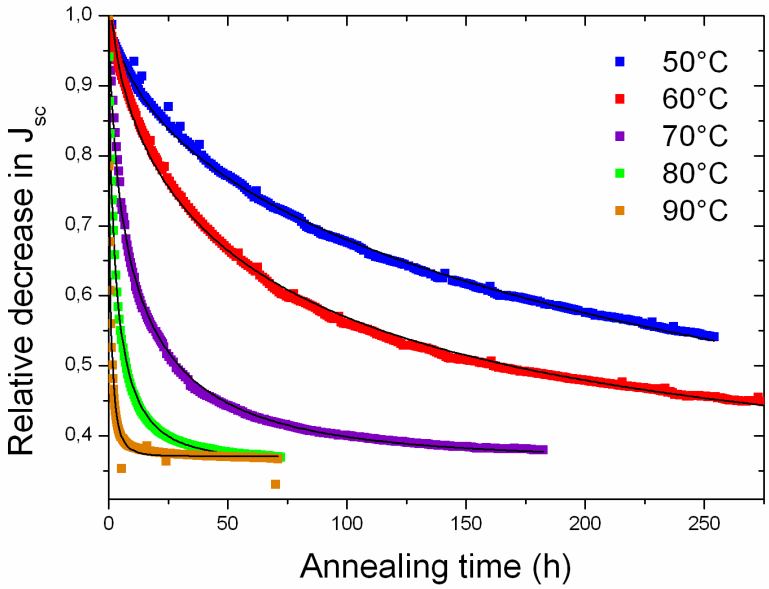

Figure 4-7 Relative decrease in J_{sc} of MDMO-PPV:PCBM solar cells at different annealing temperatures. The solid lined represents the fitted data.

In the previous sections, a strong connection between the decrease in J_{sc} and the clustering of PCBM in the active layer of solar cells, was demonstrated. It seems that the diffusion of PCBM largely determines the degradation of the solar cells. Diffusion processes commonly follow a $\sqrt{t}$ behavior.[7] Therefore Eq. 4-1 was slightly adjusted:

$$J_{sc}(t) = J_{sc}(\infty) + J_{sc}(0)\exp(-k'_{\mathrm{deg}}\sqrt{t}) \qquad \text{(Eq. 4-2)}$$

The degradation curves in Figure 4-7 were fitted simultaneously to this equation (solid lines in Figure 4-7). The fitted results correspond very well to the experimental data. For each annealing temperature, a different k'_{deg} is obtained. Through the Arrhenius model,[8] these rate constants can be used to calculate the activation energy E_a:

$$k'_{\mathrm{deg}} = A\exp(-E_a / k_B T) \qquad \text{(Eq. 4-3)}$$

with k_B the Boltzmann constant (8.62 x 10^{-5} eV/K) and T the annealing temperature.

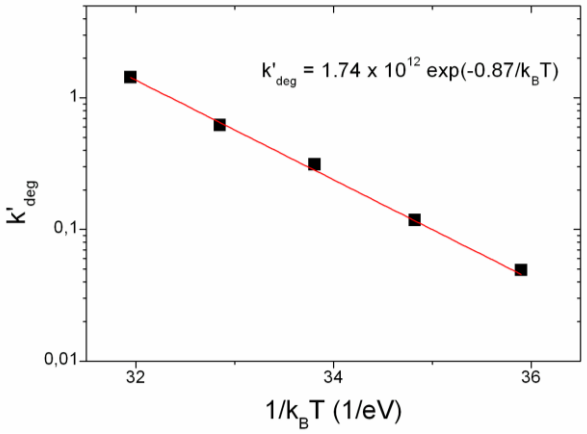

Figure 4-8 Fitting the rate constant k'_{deg} leads to an activation energy of 0.87eV.

Figure 4-8 shows a graph of the rate constant k'_{deg} plotted on a logarithmic scale. The results were fitted with Eq. 4-3 and the activation energy E_a was determined to be 0.87 eV (R^2 = 0.9986).

With the activation energy, acceleration factors K for arbitrary temperatures T_1 and T_2 can be calculated by:

$$K = \frac{k_{deg}(T_2)}{k_{deg}(T_1)} = \exp\left[\frac{E_a}{k_B}\left(\frac{1}{T_1} - \frac{1}{T_2}\right)\right] \qquad \text{(Eq. 4-4)}$$

For the temperature range in Figure 4-7, this acceleration factor lies between 2.6 (for low temperatures) and 2.2 (for high temperatures) for an increase of 10 °C in temperature. Since the $\sqrt{t}$ behavior was introduced to obtain better fitting, this means that on average the degradation happens about 5.5 times faster when the temperature is increased with 10 °C.

4.6 Influence of the electrode on the stability of the morphology

The TEM samples that are depicted in Figure 4-5, were prepared from the photovoltaic devices in Figure 4-2 but for easy processing (see section 2.1.2), they were made from the active layer beside the top electrode. One can ask whether the changes in active layer morphology are the same below or next to the electrode, therefore this experiment was done.

Again MDMO-PPV:PCBM 1:4 solar cells were made and annealed for several times at 110°C. This time, TEM samples were prepared from the active layer below the electrode as well as next to the electrode for comparison. As shown in Figure 4-9, it was sometimes even possible to see the transition of the electrode in the samples. Below the electrode, the PCBM clusters, created upon annealing at 110°C, seem slightly bigger and the contrast is less in this area (Figure 4-9). This is caused by the hindrance of the CaAl electrode which prevents the PCBM clusters to grow upwards. Instead they seem to spread out a little bit more.[9]

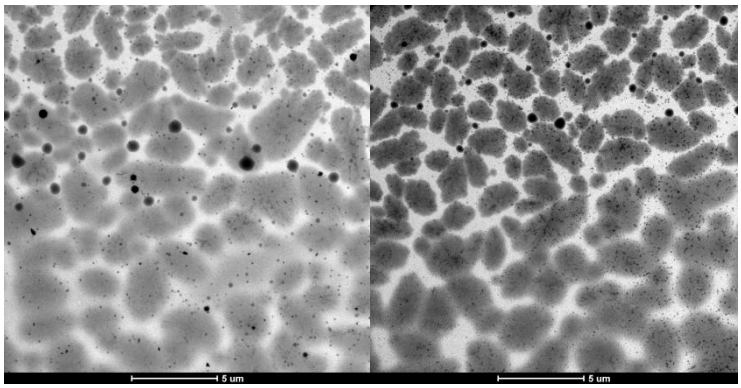

Figure 4-9 BFTEM images of MDMO-PPV:PCBM 1:4 active layers of solar cells showing the border of the CaAl electrode. The CaAl electrode was positioned at the bottom of the pictures. The annealing times were 8h (left) and 16h (right) at 110°C. (scale bar = 5 µm)

The kinetics of the clustering seems to be the same below and next to the CaAl electrode. After 8 hours of annealing, a few regions where clustering is not complete yet, are visible for both the area next to as well as below the

electrode. After 16 hours of annealing the clustering is complete everywhere in the sample. This is confirmed by Figure 4-10, showing a sample that was annealed for only 4 hours. The number of clusters is the same throughout the sample, however, below the CaAl, these clusters seem a little bit more spread out.

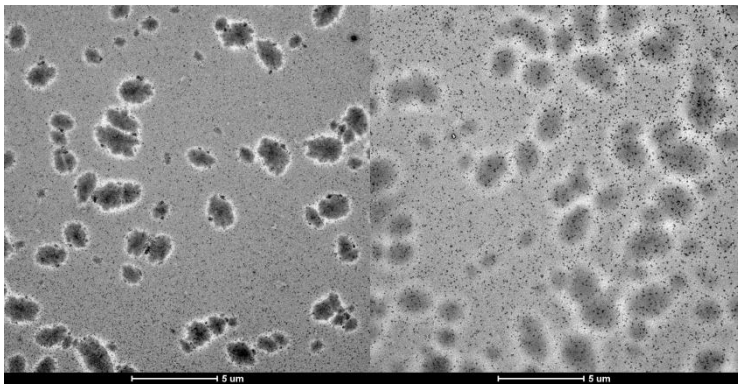

Figure 4-10 BFTEM images of MDMO-PPV:PCBM 1:4 active layers of solar cells annealed for 4h at 110 °C. The left TEM sample was made from an area next to the CaAl electrode, the right TEM sample was made from an area below the CaAl electrode. (scale bar = 5 µm)

Note that the clustering speed in Figure 4-9 and Figure 4-10 is lower than in Figure 4-5. This is attributed to the use of different batches of MDMO-PPV and PCBM at the time of this experiment.

4.7 Summary

To conclude, this chapter has shown that MDMO-PPV:PCBM 1:4 solar cells are not stable upon annealing. A large decrease in the performance of the solar cells coincides with a change in active layer morphology. Especially the short circuit current seems to be linked to these changes in morphology. Initially, the PCBM is well dispersed throughout the polymer matrix; phase separation on a small scale (50 – 100 nm), which is favourable for the solar cell performance, is visible. Upon annealing, PCBM starts to diffuse and forms large (> 1 µm) clusters. The diffusion of PCBM out of the polymer matrix results in a decrease of the interfacial area between polymer and PCBM, which causes a less efficient exciton dissociation. This leads to the decrease in J_{sc} as

observed by the ex-situ and in-situ monitoring of the photovoltaic performance.

4.8 References

[1] S.E. Shaheen, C.J. Brabec, N.S. Sariciftci, *Appl. Phys. Lett.* 78, **2001**, 841

[2] T. Martens, T. Munters, L. Goris, J. D'Haen, K. Schouteden, M. D'Olieslaeger, L. Lutsen, D. Vanderzande, W. Geens, J. Poortmans, L. De Schepper, J.V. Manca, *Appl. Phys. A.* 79 **2004**, 27

[3] M.T. Rispens, A. Meetsma, R. Rittberger, C.J. Brabec, N.S. Sariciftci, J.C. Hummelen, *Chem. Commun.* **2003**, 2116

[4] B. Conings, S. Bertho, K. Vandewal, A. Senes, J. D'Haen, J. Manca, R.A.J. Janssen, *Appl. Phys. Lett.* 96, **2010**, 163301

[5] S. Schuller, P. Schilinsky, J. Hauch, C.J. Brabec, *Appl. Phys. A.* 79, **2004**, 37

[6] R. De Bettignies, J. Leroy, M. Firon, C. Sentein, *Synth. Met.* 156, **2006**, 510

[7] J. Philibert, *Diffusion et transport de matière dan les solides*, Les éditions de physique, **1990**

[8] M. Jorgensen, K. Norrman, F.C. Krebs, *Sol. Energy Mater. Sol. Cells*

[9] X. Yang, A. Alexeev, M.A.J. Michels, J. Loos, *Macromolecules* 38, **2005**, 4290

Chapter 5

Comparative study of stability

This chapter compares the stability of solar cells based on different conjugated polymers. The popular P3HT:PCBM solar cells may exhibit an initial improvement of performance upon annealing, when they are subjected to prolonged annealing, they show a comparable degradation as the MDMO-PPV:PCBM solar cells in chapter 4. Preparing P3HT:PCBM solar cells in different ways does not render more stable devices.

Two routes are discussed which may improve thermal stability. The first one is the implementation of functionalized side chains in P3HT. The second one is the use of a polymer with higher T_g. Both methods show an improved thermal stability of the devices, coinciding with a more stable active layer morphology where the diffusion of PCBM is hindered.

5.1 Commercial P3HT

5.1.1 As produced

Figure 5-1 shows the decay of the short circuit current for solar cells based on P3HT[c] for several annealing temperatures. A clear difference can be observed in these decay characteristics as compared to MDMO-PPV (Figure 4-4). Solar cells based on MDMO-PPV showed a monotonous decay. For P3HT based solar cells, J_{sc} increases for relatively short annealing times. After a certain time, which depends on the annealing temperature, J_{sc} starts to decrease (as can be observed for T = 110 °C and 150 °C).

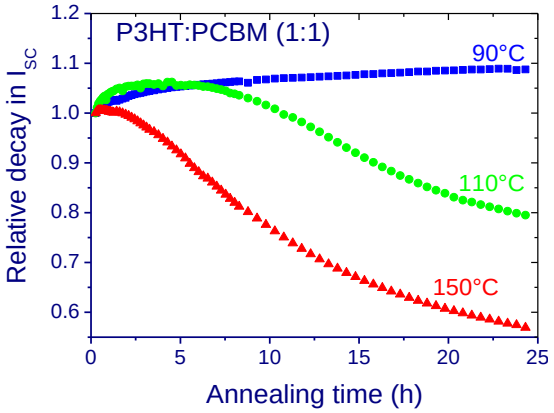

Figure 5-1 Relative decay of the short circuit current at different annealing temperatures for P3HT:PCBM (1:1) solar cells.

This evolution of J_{sc} for P3HT:PCBM 1:1 solar cells can also be linked to the active layer morphology. Bright Field TEM images show that after 4 hours of annealing at 110 °C, PCBM starts to cluster (Figure 5-2a). For this material however more information can be gathered from the SAED patterns of the P3HT:PCBM matrix in between the clusters. Figure 5-2b shows the residual intensities of these patterns for annealing at 110 °C for several hours. The original diffraction patterns suffered from a large background that resembled inelastic scattering. To improve the signal-to-noise ratio, integration across the complete diffraction ring was done, from which a calculated background due to

[c] P3HT was supplied by Merck, $M_w = 35 \cdot 10^3$ g/mol, PD = 1.8

inelastic scattering was subtracted (under the assumption that the blend in between the clusters is quasi-amorphous[1]). The residual intensities (for more details concerning the calculation, see section 2.1.4) of the SAED pattern of the non-annealed active layer shows distinct peaks at d-values of 2 Å, 3.1 Å and 4.6 Å corresponding to nanocrystalline PCBM.[2] In addition, for annealing times between 0.5h and 8h, some evolution in the intensity can be seen at 3.8 Å. The peak appearing here can be attributed to the superposition of the (002) and (020) reflections from the crystal planes of semi-crystalline P3HT.[3] After 16 hours of annealing, the P3HT peak is very pronounced in the SAED pattern. At the same time, the peaks corresponding to nanocrystalline PCBM are reducing. At this point, P3HT has formed fiber-like crystalline structures that can be seen clearly in a Bright Field TEM image (Figure 5-2c). On the other hand, PCBM is vanishing from the P3HT:PCBM matrix and gathering in the PCBM-clusters.

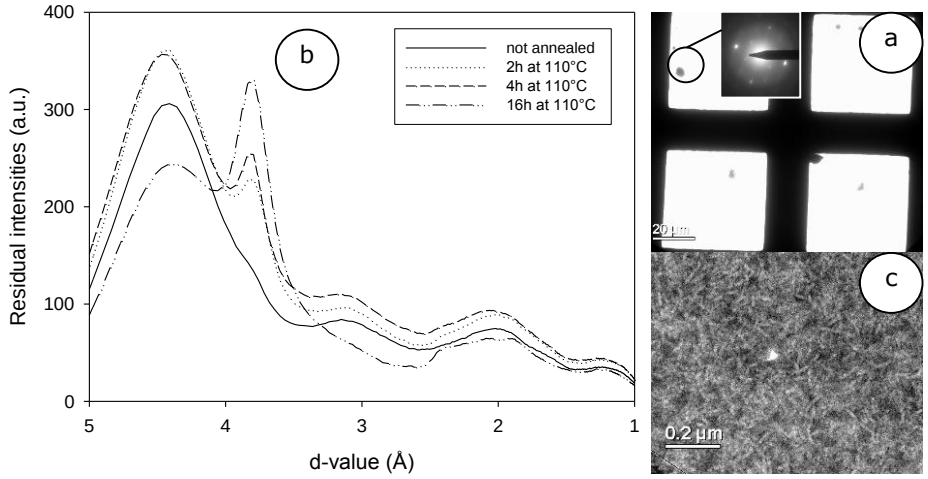

Figure 5-2 Evolution of a P3HT:PCBM (1:1) active layer during an annealing treatment at 110 °C, (a) after 4 hours some PCBM-clusters appear, (b) residual intensities of the SAED-patterns of the bulk, (c) P3HT-fibers are clearly visible after 16h.

It is clear that in P3HT:PCBM active layers, two processes take place.[4] One of them, namely the local crystallization of P3HT into fiber-like structures, leads to better charge transport,[5,6] resulting in a higher J_{sc}. The other process, as in

blends with MDMO-PPV, is again the clustering of PCBM, which at later times results in a decrease of J_{sc} mainly due to a lower interfacial area between P3HT and PCBM.

It is now clear that also for P3HT:PCBM 1:1 solar cells, the behavior upon thermal annealing is largely based upon the morphology evolution. For a good understanding of the lifetime of the devices, the previous measurements were quite short (~24 hours). Therefore, the experiment was redone for a longer time period. Note that for the remainder of this chapter, P3HT from another supplier was used.[d] In Figure 5-3, the degradation of J_{sc} in these solar cells shows the same characteristics as before (in Figure 5-1) but the degradation kinetics are slightly different (probably due to the change of the supplier).

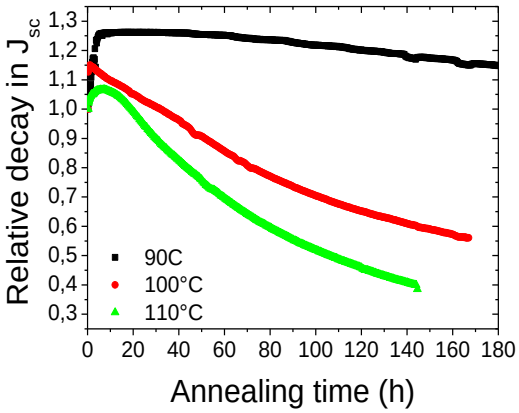

Figure 5-3 Relative decay of the short circuit current at different annealing temperatures for P3HT:PCBM (1:1) solar cells.

BFTEM images (Figure 5-30) show that for this P3HT, large PCBM clusters are formed upon annealing, quite similarly to the case of MDMO-PPV (Figure 4-5). The clustering speed of the PCBM is however a lot faster than the degradation speed of the J_{sc}. The residual intensities of the SAED patterns (Figure 5-4) indicate that the area in between the PCBM clusters is the most important for the degradation in J_{sc}. The P3HT peak at 3.8 Å for these devices grows very slowly, and is not as pronounced as in Figure 5-2. The PCBM peak at 4.6 Å reduces very slowly but is never really gone, not even after 68 hours of

[d] P3HT was supplied by Rieke, $M_w = 70.8 \cdot 10^3$ g/mol, PD = 2.1

annealing. The crystallization of P3HT, increasing the J_{sc}, is in competition with the diffusion of PCBM out of the polymer matrix, decreasing the J_{sc}. The evolution of J_{sc} is the combination of both processes. For short annealing times, the crystallization of P3HT has the upper hand but for long annealing times, the PCBM diffusion takes over. With lower PCBM content in the polymer matrix, J_{sc} will eventually deteriorate severely.

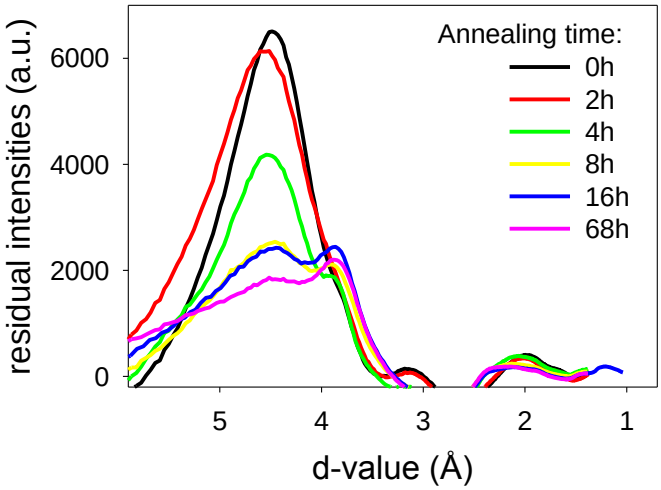

Figure 5-4 Residual intensities of SAED patterns of P3HT:PCBM 1:1 active layers annealed at 110°C.

5.1.2 Slow drying

P3HT:PCBM 1:1 solar cells obtain their best performance when P3HT has a high crystallinity and when a phase separation on a small scale is present between P3HT and PCBM.[7,8] The high crystalllinity of P3HT is believed to increase photovoltaic efficiency by an increase of the hole mobility within the polymer.[5,6] The first method to obtain this crystallinity was a thermal annealing step. The previous section however has showed that severe thermal annealing will lead to phase separation on a large scale of P3HT and PCBM and this reduces the photovoltaic performance.

Through solvent annealing or slow drying, it is possible to obtain crystalline P3HT while avoiding the thermal annealing step.[9] For this method, a solvent with a high boiling point is necessary. In this section, P3HT:PCBM 1:1 solar

cells are discussed that were prepared through slow drying from an ortho-dichlorobenzene (odCB) solution. Note that the boiling point of odCB is 180 °C while CB has a boiling point of 131 °C. The solution of P3HT:PCBM 1:1 in odCB was spin-coated for only 20s to obtain a homogeneous layer. Due to the short spin-coating time, the odCB was not evaporated completely and the wet samples were left to dry in closed petri-dishes. This gives the P3HT:PCBM blend the opportunity to self-organize.

Figure 5-5 compares this device to devices spin-coated from CB (as produced and with post-production thermal treatment). The current density of the devices was almost three times as high as for the P3HT:PCBM 1:1 devices that were spin-coated from CB (without annealing step). Also the devices with a post-production thermal treatment had a lower J_{sc}. The open circuit voltage decreased slightly as compared to the other solar cells,[10] but the overall efficiency was a lot better.

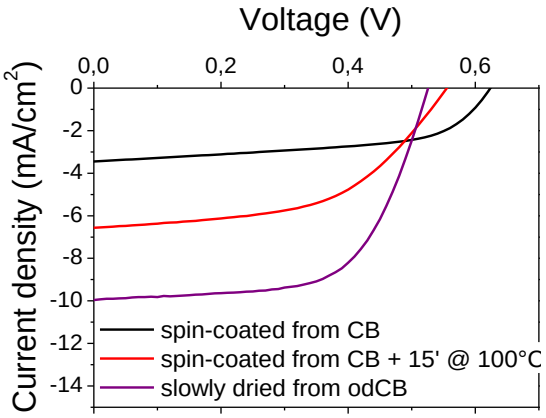

	J_{sc} (mA/cm^2)	V_{oc} (V)	FF	η (%)
---	3.5	0.62	0.57	1.2
---	6.6	0.55	0.53	1.9
---	9.9	0.53	0.63	3.3

Figure 5-5 J-V curve of a slowly dried P3HT:PCBM 1:1 device (purple) compared to P3HT:PCBM 1:1 devices spin-coated from CB, as produced (black) and with post-production thermal treatment (red).

Figure 5-6 shows that slow drying of P3HT:PCBM 1:1 indeed gives the desired small scale phase separation without the necessity of a thermal annealing step. The BFTEM image of the slowly dried film contains bright fiber-like features that correspond to crystalline P3HT, whereas the as produced P3HT:PCBM 1:1 active layer, spin-coated from CB, appears completely

featureless. A bright diffraction ring in the SAED pattern of the slowly dried P3HT:PCBM 1:1 confirms the presence of crystalline P3HT (inset in Figure 5-6 and 0h-curve in Figure 5-8).

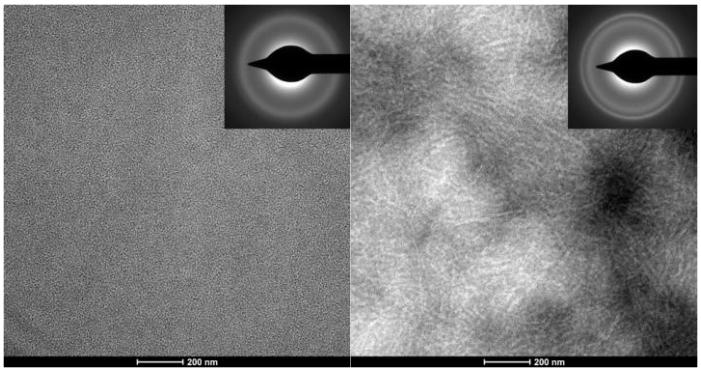

Figure 5-6 BFTEM image of P3HT:PCBM 1:1 active layers produced by spin-coating from CB (left) or by slow drying from odCB (right). Scale bar = 200 nm.

In literature, it is sometimes suggested that P3HT:PCBM solar cells, that contain crystalline P3HT before annealing are thermally more stable.[11] To verify this, slowly dried P3HT:PCBM 1:1 solar cells were subjected to a thermal treatment at 3 high temperatures (see Figure 5-7). The thermal stability of these devices did not seem better than for the devices spin-coated from P3HT:PCBM. J_{sc} decreased strongly upon annealing, and this decay happened faster for higher annealing temperatures.

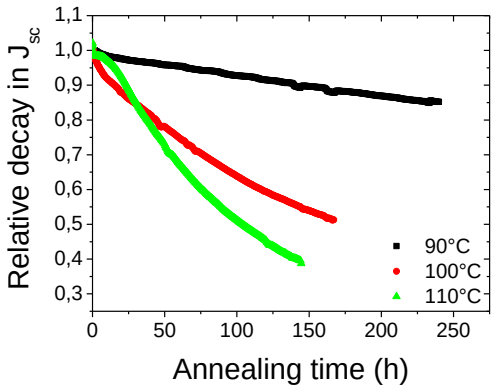

Figure 5-7 Relative decay in J_{sc} at different annealing temperatures for P3HT:PCBM 1:1 solar cells, slowly dried from odCB.

For short annealing times, no significant increase in J_{sc} was observed, as opposed to the P3HT:PCBM spin-coated devices. This was expected, since P3HT had already crystallized into fiber-like structures due to the slow drying process. The instability is confirmed by the SAED patterns (Figure 5-8). The PCBM peak at 4.6 Å decreases upon annealing but similar to the Figure 5-4 it is never completely gone. The crystalline P3HT peak at 3.8 Å is very pronounced for these devices. This indicated that the self organization of P3HT is more effective through slow drying than it was through thermal annealing (Figure 5-4). This is also reflected in the better performance of this device (Figure 5-5).

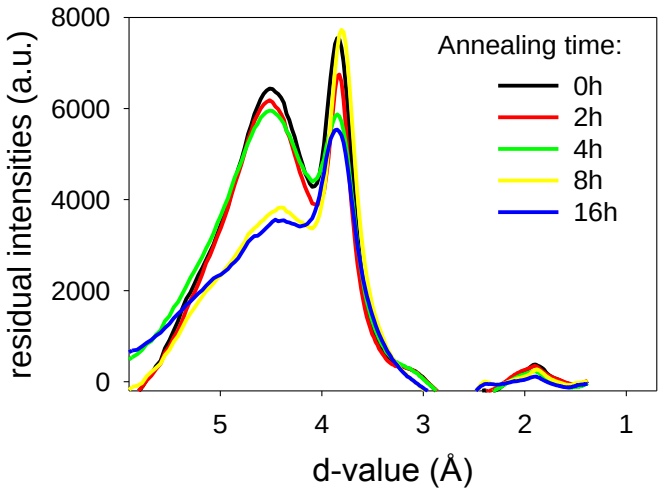

Figure 5-8 Residual intensities of SAED patterns of slowly dried P3HT:PCBM 1:1 active layers annealed at 110 °C.

5.1.3 Using less PCBM

When making P3HT:PCBM solar cells, the 1:1 weight ratio is the most common.[12,13] Using more PCBM would not be beneficial to photovoltaic performance since it leads to very fast PCBM clustering.[14] PCBM also reduces the crystallinity of P3HT, making a post-production treatment necessary to regain this crystallinity. Using less PCBM could thus be an option, as long as enough PCBM would be present to create percolation paths for electron diffusion towards the electrodes.

In Figure 5-9 it can be seen that a reduction of the PCBM content is indeed not detrimental for the photovoltaic performance of the as produced devices. On the contrary, J_{sc} increases with lower PCBM content. As expected, this is caused by the amount of crystalline P3HT present in the film. SAED patterns (Figure 5-10) indicate that a film consisting purely out of P3HT has a high crystallinity. Adding more PCBM reduces the P3HT crystallinity (the diffraction peak at 3.8 Å in Figure 5-10 becomes smaller).

At a P3HT:PCBM weight ratio of 1:0.4, J_{sc} is still increasing but the overall efficiency has dropped slightly. At this point, probably not enough PCBM is present anymore to provide good percolation paths for the electrons and more recombination will take place leading to a lower fill factor.

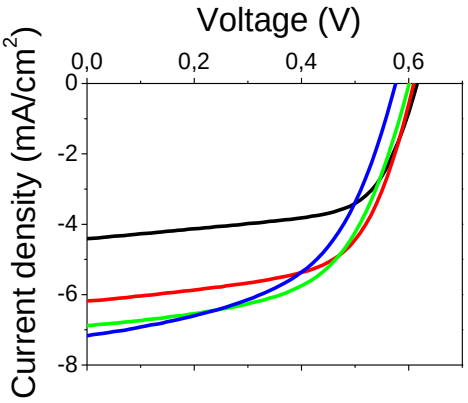

P3HT:PCBM				
Weight ratio:	**J_{sc}** (mA/cm^2)	**V_{oc}** (V)	**FF**	**η** (%)
1:1	4.4	0.62	0.63	1.7
1:0.8	6.2	0.61	0.61	2.3
1:0.6	6.9	0.60	0.58	2.4
1:0.4	7.2	0.58	0.52	2.2

Figure 5-9 J-V curves of P3HT:PCBM 1:x photovoltaic devices, spin-coated from CB (left) with the photovoltaic parameters (right).

Ma et al.[15] reported about P3HT:PCBM 1:0.8 solar cells that were thermally stable. Figure 5-11 however shows that decreasing the PCBM content does not increase the stability of J_{sc}. On the contrary, when decreasing the PCBM content from 1:1 to 1:0.6, the J_{sc} decreases slightly faster. If comparable kinetics of PCBM diffusion are assumed for the different devices, then the P3HT:PCBM matrix in devices with an originally low PCBM content will be depleted of PCBM faster than devices that originally had a high PCBM content. The might explain the slightly faster decrease in J_{sc}.

The degradation of the 1:0.4 device differed a little from the other devices.

While the devices with a weight ratio of 1:0.6 or higher showed a pronounced increase in J_{sc} (due to enhanced P3HT crystallization upon annealing), this increase was negligible for the 1:0.4 device.

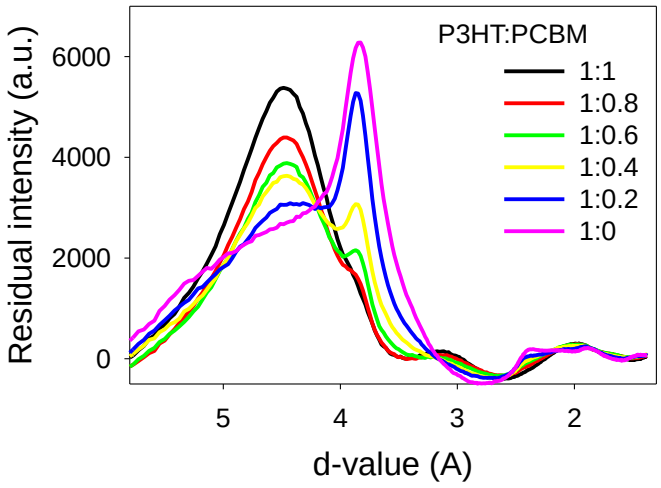

Figure 5-10 Residual intensities of SAED patterns of P3HT:PCBM 1:x spin-coated from CB.

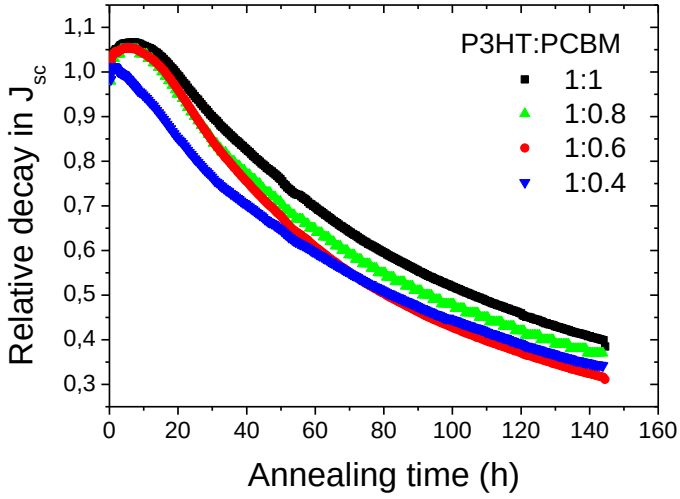

Figure 5-11 Relative decay in J_{sc} at 110 °C for different weight ratios of P3HT:PCBM, spin-coated from chlorobenzene.

BFTEM images of the active layer morphology of these devices (Figure 5-12) after 68 hours of annealing at 110 °C show that PCBM diffuses into clusters for

all the P3HT:PCBM weight ratios. The shape of the formed clusters differs slightly; for low PCBM content, they are a little bigger and more symmetric than for higher PCBM content. This seems plausible since for a high PCBM content, more seeds where crystallization can start, are present.

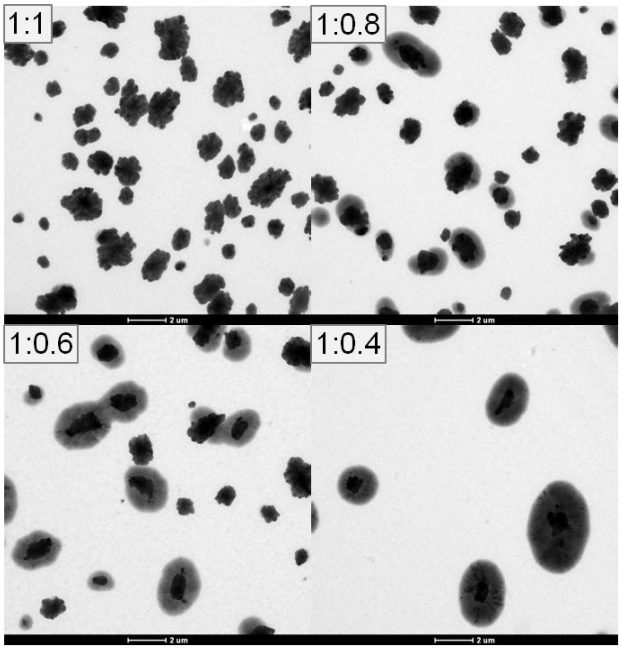

Figure 5-12 BFTEM images of P3HT:PCBM 1:x annealed for 68 hours at 110 °C. (scale bar = 2 µm)

5.2 P3HT fibers prepared in solution

In chapter 3, the use of P3XT fibers prepared in solution, for photovoltaic devices was discussed. The best performing solar cells (i.e. prepared from a solution at ~ 45 °C) were subjected to a degradation experiment. The original morphology of the active layers based on the fibrillar P3HT:PCBM 1:1, resembled the morphology of a slowly dried P3HT:PCBM 1:1 (section 5.1.2). In Figure 5-13, the bright P3HT fibers are visible against a dark PCBM rich background because of their lower density (1.1 g/cm^3) as compared with PCBM (1.5 g/cm^3).[16]

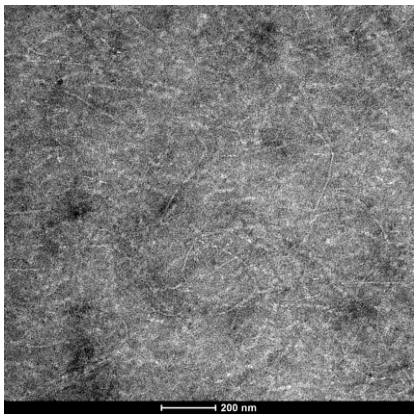

Figure 5-13 Fiber-P3HT:PCBM 1:1, spin-coated from p-xylene. (Scale bar = 200 nm)

Also for this variation of the P3HT:PCBM solar cell, the initial crystallinity of the P3HT did not improve the thermal stability. On the contrary, Figure 5-14, reveals that the devices break down completely after a certain annealing time. The higher the annealing temperature is, the shorter the time becomes when the devices fail.

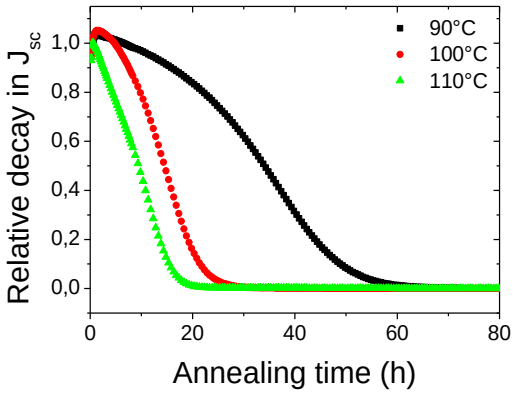

Figure 5-14 Relative decay in J_{sc} at different annealing temperatures of fiber-P3HT:PCBM 1:1 solar cells, spin-coated from para-xylene.

In the active layers of these solar cells, large PCBM clusters appear in the BFTEM images upon annealing (Figure 5-30). In between the clusters, the amount of PCBM can be linked to the residual intensities of the SAED patterns (Figure 5-15). The as produced layer, exhibits a very strong P3HT peak at

3.8 Å, corresponding to the P3HT fibers. Already after 4 hours of annealing at 110 °C, some amount of PCBM has diffused out of the matrix. The green and the red curve in Figure 5-15 correspond to 2 different areas in the sample that was annealed for 4 hours. In this sample, PCBM clusters were spread across the whole sample. At some places in between these clusters, the PCBM had almost vanished (e.g. the red curve), while in other places there was still a fair amount of PCBM present (e.g. the green curve). After 8 hours of annealing, the PCBM peak had vanished completely, indicating that no PCBM was left in the matrix.

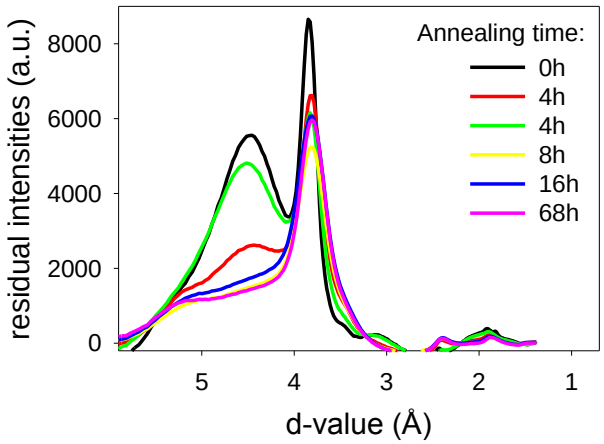

Figure 5-15 Residual intensities of SAED patterns of fiber-P3HT:PCBM 1:1 active layers annealed at 110 °C.

For an annealing temperature of 110 °C, the evolution of V_{oc} upon annealing is shown in Figure 5-16. The largest decrease happened in the first few minutes, when the temperature was still increasing until 110 °C was reached. This decrease of V_{oc} for higher temperatures is seen before.[17,18] Upon cooling down at the end of the experiment, V_{oc} regained this initial decrease largely (note that the temperature at the end of this experiment went down to 55 °C for the last point in the graph) while the first point in the graphs corresponds to room temperature.

Though J_{sc} reduced to values close to zero for these solar cells (Figure 5-14), V_{oc} only decreased a little. The devices still behaved as diodes, though the photovoltaic effect was gone.

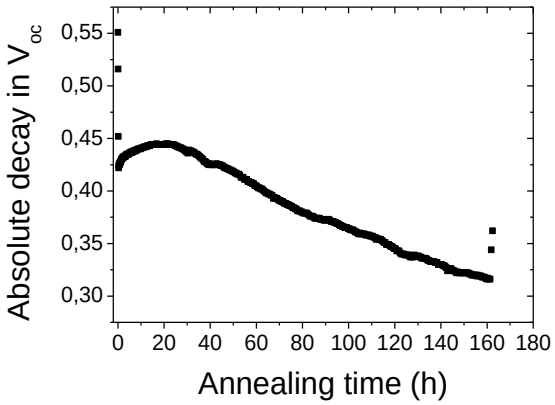

Figure 5-16 Evolution of V_{oc} of fiber-P3HT:PCBM 1:1 solar cells upon annealing at 110°C.

5.3 Side-chain functionalized P3HT

The previous sections have shown that the morphology and photovoltaic properties of P3HT:PCBM solar cells are intrinsically thermally unstable. Several routes can be followed to obtain high efficiency devices (see sections 5.1.2, 5.1.3, 5.2) but these routes do not improve the thermal stability. In this section, the donor polymer was intrinsically changed, i.e. the side chains of P3HT were functionalized.

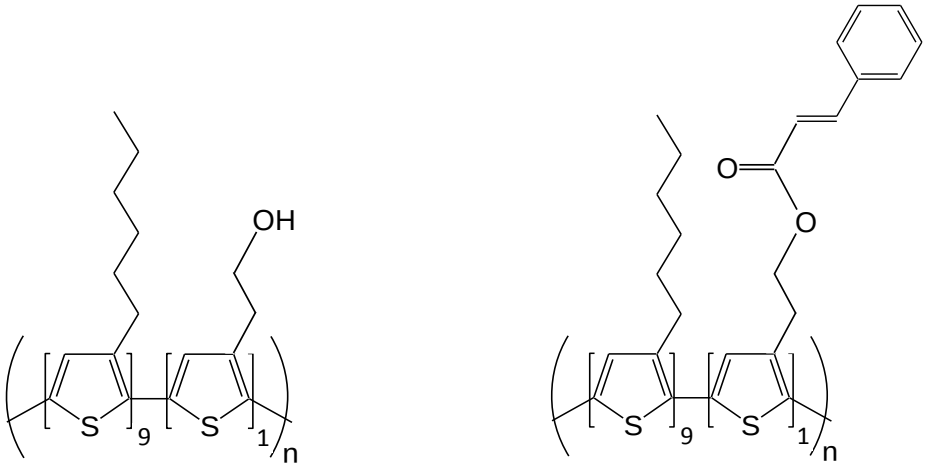

Figure 5-17 BCT037 (left) and BCT040 (right): two copolymers with 10% functionalized side-chains.

BCT037[e] and BCT040[f] (Figure 5-17) are 2 copolymers based on P3HT that were synthesized by Bert Campo of the Organic Chemistry group at UHasselt. More details concerning the synthesis of the materials and their chemical specifications can be found elsewhere.[19]

5.3.1 Photovoltaic performance

BCT037 and BCT040 are for 90% similar to P3HT, only 10% of the side chains is different. Before testing the effect on stability of this functionalization, the performance of both polymers in organic solar cells was checked. To this end, solar cells were made according to the same procedure as for the commercial P3HT. BCT037 and BCT040 were dissolved in chlorobenzene, together with PCBM in a 1:1 weight ratio. These blends were then spin-coated as active layer in devices with the structure depicted in Figure 4-1 with active layer thicknesses of ~100 nm.

The as produced devices exhibit fairly low efficiencies (Figure 5-18), but after a thermal treatment of 15' at 100 °C, both materials achieve efficiencies comparable to the slowly dried P3HT:PCBM 1:1 (section 5.1.2) or the fiber-P3HT:PCBM 1:1 (section 3.2.3). A modification of 10% of the side-chains of P3HT thus does not have a large effect on the photovoltaic performance.

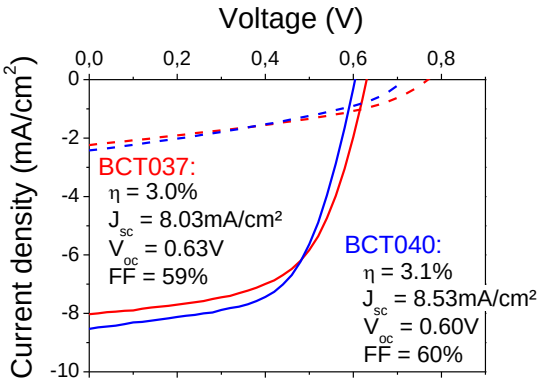

Figure 5-18 J-V curve of BCT037:PCBM 1:1 and BCT040:PCBM 1:1 solar cells, as produced (dashed line) and annealed for 15' at 100 °C.

[e] BCT037: M_w = 68100, PD = 2.2, T_g = 30 °C
[f] BCT040: M_w = 74500, PD = 2.2, T_g = 19 °C

5.3.2 Stability

Solar cells based on BCT037 and BCT040 were subjected to a thermal treatment at different temperatures. J_{sc} turned out to be a lot more stable for these materials (Figure 5-19, Figure 5-20). There was only a small decrease in J_{sc} and this decrease was quite similar for the different annealing temperatures.

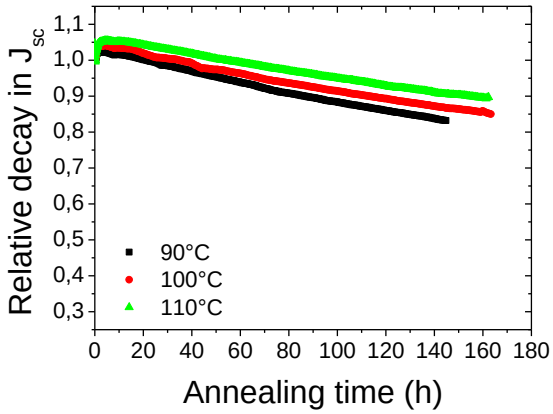

Figure 5-19 Relative decay in J_{sc} at different annealing temperatures of BCT037:PCBM 1:1 solar cells, spin-coated from chlorobenzene.

Since these devices had already had an annealing treatment of 15' at 100 °C, no significant increase in J_{sc} was observed for short annealing times. Only at 110 °C, a small but significant increase in J_{sc} was observed. Apparently, this temperature (higher than the initial thermal treatment at 100°C) induced a small increase in the P3HT crystallinity.

Also for these P3HT derivates, the stability of J_{sc} can be linked to the active layer morphology. BFTEM images (Figure 5-30) do not show the diffusion of PCBM into large clusters, the active layer morphology seems quite stable. This is confirmed by the SAED patterns (Figure 5-21, Figure 5-22) where the intensity of the PCBM diffraction peak at 4.6 Å does not change. Even after 68 hours of annealing at 110 °C, PCBM is still present in the matrix.

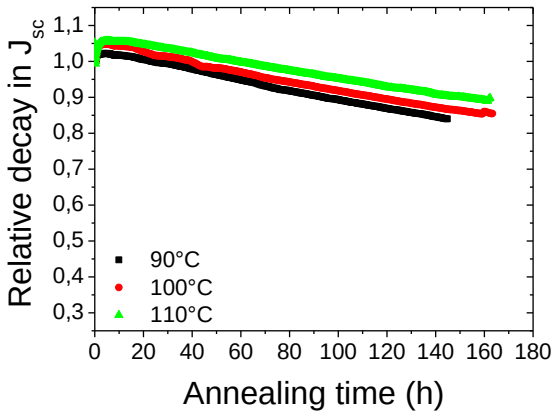

Figure 5-20 Relative decay in J_{sc} at different annealing temperatures of BCT040:PCBM 1:1 solar cells, spin-coated from chlorobenzene.

Remarkable for these materials is that the peak at 3.8 Å (due to crystalline P3HT[3]) becomes smaller for longer annealing times. It should be noted however that this diffraction peak is very sensitive to the electron beam of the electron microscope. After long exposure times, the peak extinguishes. For the collection of the SAED patterns throughout this work, the exposure of the samples to the electron beam was always limited as much as possible and for reproducibility the recordings were always repeated at different areas in the samples. For these long annealed samples based on functionalized P3HT, the peak at 3.8 Å was always as small as in Figure 5-21 and Figure 5-22. This indicates that either the crystallinity of P3HT has decreased, or that these samples are even more sensitive to beam irradiation than other samples. BFTEM images of these samples (Figure 5-23) still show bright structures that correspond to crystalline P3HT. This makes it more plausible that the samples have become more sensitive to beam irradiation.

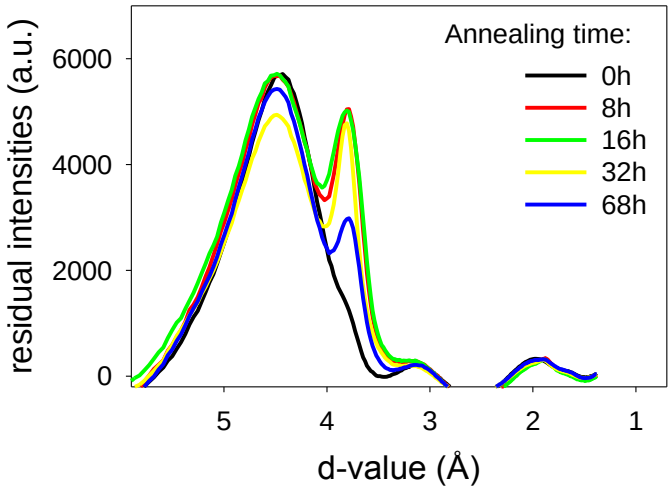

Figure 5-21 Residual intensities of SAED patterns of BCT037:PCBM 1:1 active layers annealed at 110°C.

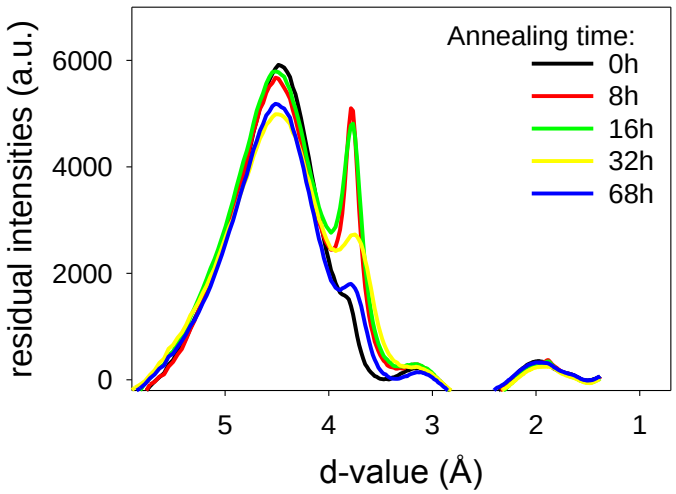

Figure 5-22 Residual intensities of SAED patterns of BCT040:PCBM 1:1 active layers annealed at 110 °C.

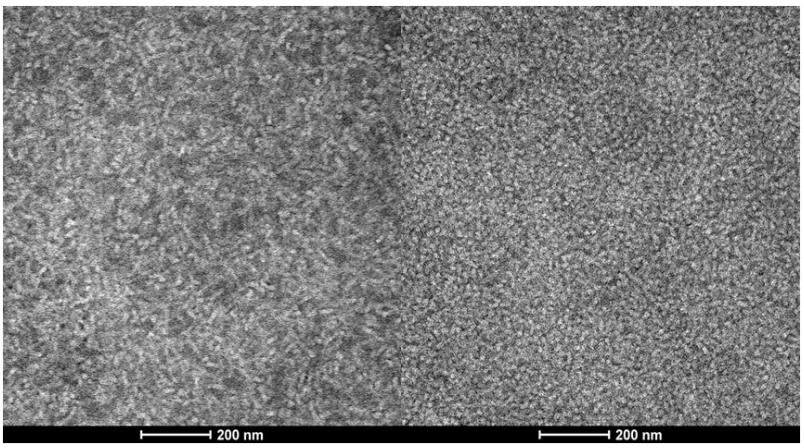

Figure 5-23 BFTEM of BCT037:PCBM 1:1 (left) and BCT040:PCBM 1:1 after 68h at 110 °C. Scale bar = 200 nm.

5.4 High T_g PPV

The previous chapter discussed the thermal instability of MDMO-PPV:PCBM 1:4 solar cells. The behaviour of these solar cells was less complicated than the PAT-based solar cells since MDMO-PPV is an amorphous polymer and upon annealing no crystallization takes place. Also for this family it is possible to achieve better thermal stability of photovoltaic performance. This section demonstrates the use of a PPV-derivative with a high glass transition temperature (T_g) of ~ 138 °C as compared to MDMO-PPV (T_g ≈ 68 °C). More details about this material were already discussed in section 1.5.4.

5.4.1 Photovoltaic performance

In order to demonstrate that 'High T_g PPV' is suitable as donor material in bulk heterojunction solar cells, Figure 5-24 shows a comparison of the current-voltage characteristic of a solar cell prepared with either 'High T_g PPV' or the reference material MDMO-PPV. For the preparation of the solar cells, both materials were dissolved in chlorobenzene together with PCBM in a 1:4 weight ratio. Active layers of about 100 nm of the 'High T_g PPV':PCBM 1:4 or the MDMO-PPV:PCBM 1:4 blend were then spin-coated to produce devices as depicted in Figure 4-1.

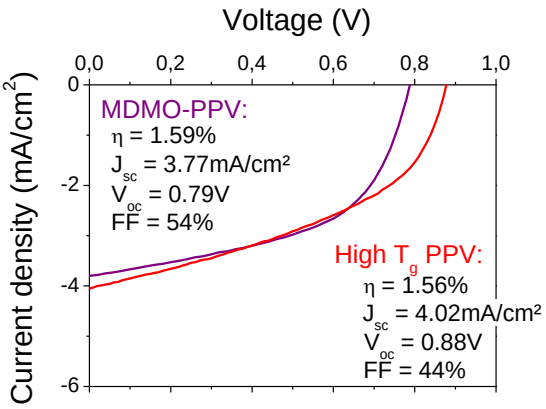

Figure 5-24 Current-voltage characteristics 'High T_g PPV':PCBM 1:4 and MDMO-PPV:PCBM 1:4 solar cells.

Solar cells based on 'High T_g PPV' gave an overall efficiency around 1.5%. Remarkable was the high open circuit voltage close to 0.9 V. The efficiency of solar cells based on these 2 PPV derivatives was rather comparable.

5.4.2 Stability

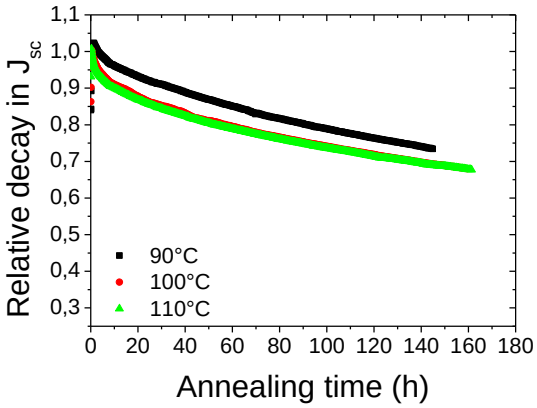

Figure 5-25 Relative decay in J_{sc} at different annealing temperatures of High T_g PPV:PCBM 1:4 solar cells, spin-coated from chlorobenzene.

Figure 5-26 shows BFTEM-images of the evolution of the active layers of MDMO-PPV:PCBM (1:4) and 'High T_g PPV':PCBM (1:4) during annealing at 110 °C. In the MDMO-PPV:PCBM (1:4) layers, large clusters are formed upon annealing. The SAED patterns of these clusters (insets in Figure 5-26) indicate

that they are in fact groups of PCBM-crystals. Annealing gives the PCBM molecules, within the MDMO-PPV:PCBM matrix, the opportunity to assemble in large clusters. This reduces the interfacial area between MDMO-PPV and PCBM, leading to less efficient exciton dissociation and a lower short circuit current (as was demonstrated in Figure 4-4). It is immediately clear from Figure 5-26 that the active layer of 'High T_g PPV':PCBM 1:4 is much more stable. It is not until after 16 hours of annealing at 110 °C that a solitary PCBM-cluster is found.

Comparing the two PPV-derivates, morphology changes are much more pronounced for the MDMO-PPV:PCBM blend. A fast PCBM-clustering occurs while for the 'High T_g blend' only negligible PCBM-clustering is observed. This difference is directly resulting from the difference in glass transition temperature. Due to the higher glass transition temperature of 'High T_g PPV', its matrix is firmer. This strongly restricts the possible migration and segregation of the PCBM molecules leading to a more stable active layer. These morphology changes coincide with the decay of the short circuit current in Figure 5-25. The slower decay of J_{sc} observed for the 'High T_g PPV':PCBM based solar cells can be attributed to a more stable active layer morphology.

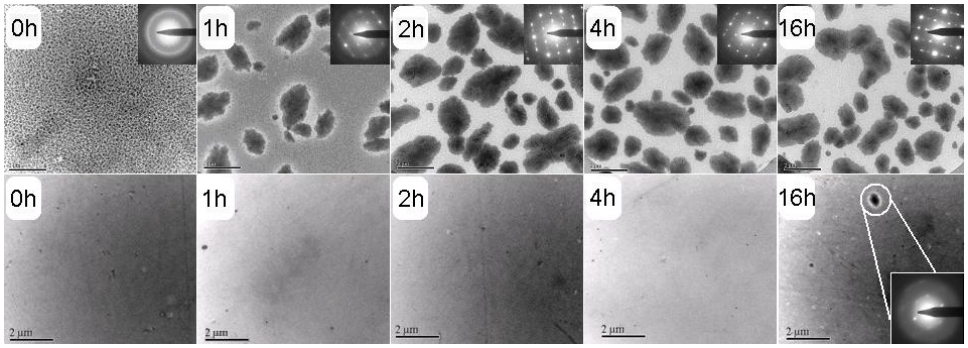

Figure 5-26 Morphology changes in the active layer of MDMO-PPV:PCBM 1:4 (top, similar to Figure 4-5) and 'High T_g PPV':PCBM 1:4 (bottom) as a result of annealing at 110 °C. The solar cells were annealed at 110 °C for 0h, 1h, 2h, 4h and 16h yielding formation of large PCBM-clusters for the MDMO-PPV based active layers while maintaining a more stable morphology for the 'High T_g PPV' based active layers. Scale bar = 2 µm.

5.5 Degradation reflected in UV-Vis

The better thermal stability of 'High T_g PPV' as compared to MDMO-PPV and P3HT is also confirmed by optical spectroscopy. Figure 5-27 shows the absorption spectra of MDMO-PPV:PCBM (1:4), 'High T_g PPV':PCBM (1:4) and P3HT:PCBM (1:1) films. An annealing treatment of 16 hours at 110 °C results in a quite remarkable change of the absorption spectrum of the MDMO-PPV:PCBM blend. The disappearance of the PCBM-absorption in the spectrum of this blend reflects the growth of PCBM crystallites as observed by TEM in the previous paragraph. Indeed, since the optical spectrometer works in a transmission mode, the dense PCBM crystals give rise to tremendous light scattering. As a result, the total transparent film area is reduced, explaining the appearance of an overall background in the spectrum.

Only the polymer regions – essentially PCBM free – contribute to the spectrum. The absorption of the 'High T_g PPV':PCBM film is stable during long thermal treatments, which directly reflects the higher thermal stability of its morphology.

The absorption spectra for the P3HT:PCBM blend reflect the dual crystallization behavior. For the as-produced P3HT:PCBM blend the PCBM-absorption is lower than for the PPV-derivatives because a lower amount of PCBM is used (a polymer:PCBM ratio of 1:1 instead of 1:4). However, also for this blend, the PCBM-absorption is reduced upon annealing, indicating the clustering of PCBM. For this blend, also a redshift for P3HT is observed, which indicates the ordering of P3HT into the fiber-like crystalline structures that were visible in de Bright Field TEM images.[20]

An essential step in the PV effect, the electron transfer from polymer to fullerene, can be monitored by the degree of photoluminescence (PL) quenching, which is close to complete in the unannealed blend films (see Figure 5-28). In the pure MDMO-PPV film, a drastic change in shape and peak intensity is observed in the first few minutes of the treatment at 110 °C after which the spectrum remains unaltered for hours.

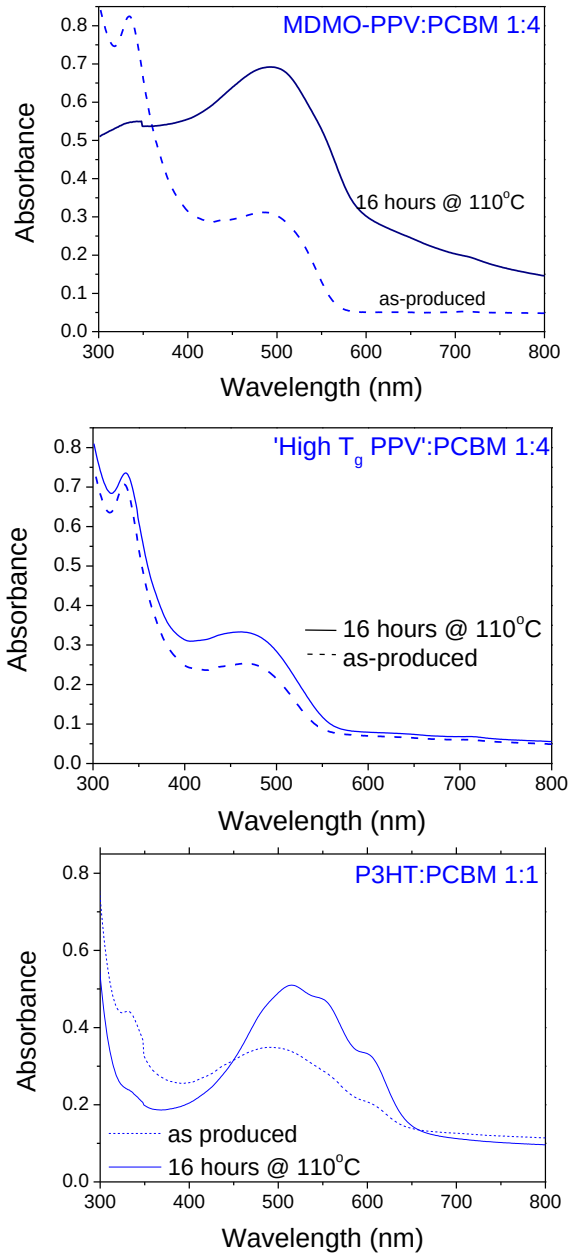

Figure 5-27 UV-VIS absorption spectra of MDMO-PPV:PCBM (1:4), 'High T_g PPV':PCBM (1:4) and P3HT:PCBM (1:1) films. Both the spectra of the as-produced films and after a heat treatment of 16 hours at 110 °C are shown.

This initial change is not related to degradation of the polymer, but should rather be ascribed to local rearrangements of the polymer chains. (While not discernable in the figure, the same fast change in shape is observed upon heating in the blend of MDMO-PPV with PCBM). No such initial effect is found in the 'High T_g PPV' film, and only a minor change is observed in both shape and intensity even after 16h of annealing at 110 °C.

A thermal treatment of 16h increases the emission intensity of each of the blends, pointing to decreasing charge transfer efficiency. This is much more pronounced in the blend with MDMO-PPV compared to 'High T_g PPV', which correlates well with the higher stability of the morphology in the latter. The decrease in charge transfer efficiency is attributed to the clustering of the PCBM, reducing the interfacial area between the two components of the blend. The TEM investigation has clearly demonstrated the importance of segregation and clustering in MDMO-PPV:PCBM blends, which is hardly observed for 'High T_g PPV':PCBM blends.

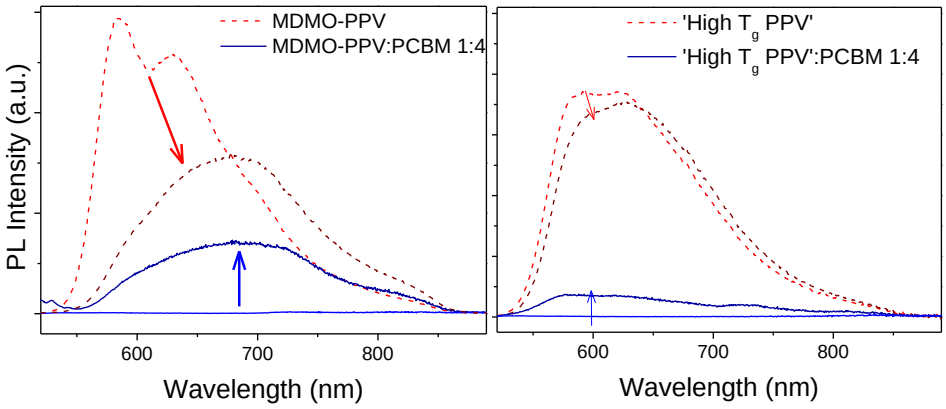

Figure 5-28 PL spectra from pure and blended MDMO-PPV and 'High T_g PPV' (1:4 ratio). The arrows indicate the effect of thermal heating during 16 hours at 110 °C. Note that the major effect in the pure MDMO-PPV film occurs within 3 minutes.

5.6 Comparison of stability for several conjugated polymers

This chapter demonstrated the different behavior of some conjugated polymers used in photovoltaic devices upon annealing. Figure 5-29 and Figure 5-30 summarize the results. All materials are compared for an annealing temperature of 110 °C. Clearly the fiber-P3HT:PCBM 1:1 were the least stable. The solar cells just went dead after 20 hours of annealing at 110 °C. BFTEM images showed big, butterfly-shaped PCBM clusters and in the SAED patterns, taken in between the clusters, the PCBM was completely gone, indicating that all PCBM was assembled in the clusters.

For commercial P3HT, it did not matter how the solar cells were prepared. Solar cells that were simply spin-coated turned out to be as unstable as devices that were prepared through slow drying or with less PCBM. Figure 5-30 indicates that indeed the course of PCBM clustering in the active layer does not depend on the production procedure of the solar cells. For these solar cells, J_{sc} did not decrease all the way down to zero which agrees with the SAED patterns (Figure 5-4, Figure 5-8, Figure 5-10) where still a small amount of PCBM was present.

As for MDMO-PPV:PCBM 1:4 solar cells in the previous chapter, the diffusion of PCBM in the active layer played a big role in the thermal stability of the solar cells. The stability could be improved by using materials that counteract the diffusion of PCBM within the active layer.

Within the PPV family, the use of a polymer with higher glass transition temperature produced an active layer that was much more stable coinciding with a more stable J_{sc}. The higher T_g made the polymer:PCBM matrix more solid and hampered in this way the free movement of the PCBM molecules. The best performing materials according to Figure 5-29 were 2 PAT-derivatives. Within the PAT-family, the functionalization of 10% of the side chain of P3HT turned out to be a good way to inhibit PCBM diffusion; BFTEM images (Figure 5-30) show no PCBM clusters in the active layer. With the stabilization of the active layer, also J_{sc} turned out to be a lot more stable.

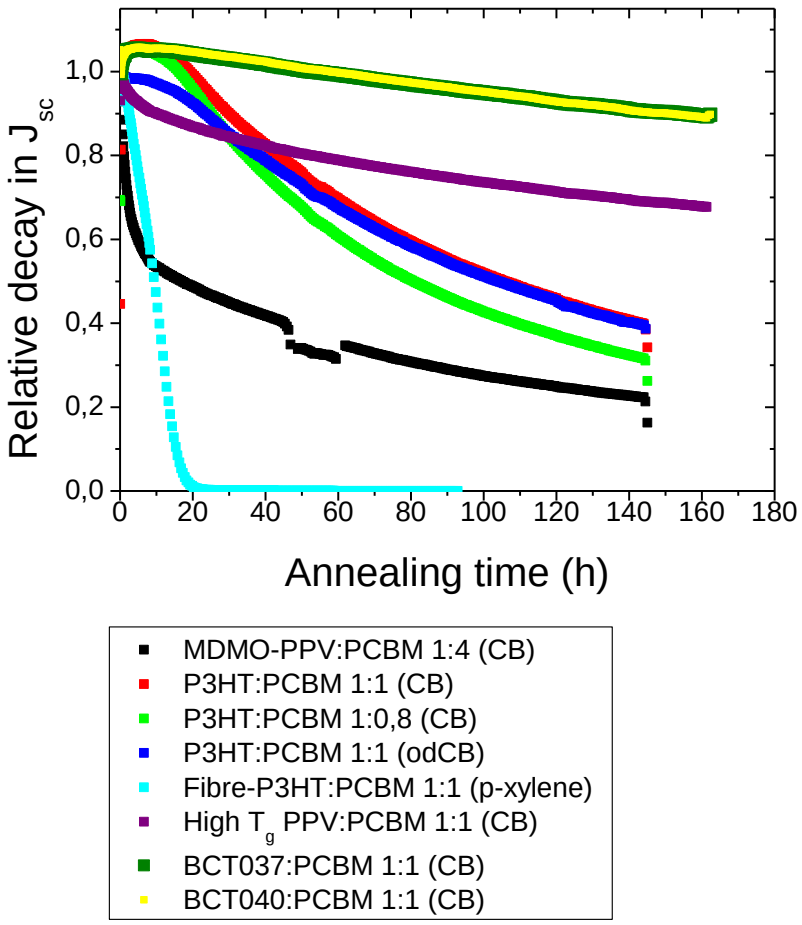

Figure 5-29 Comparison of the stability of J_{sc} for several conjugated polymers at an annealing temperature of 110 °C.

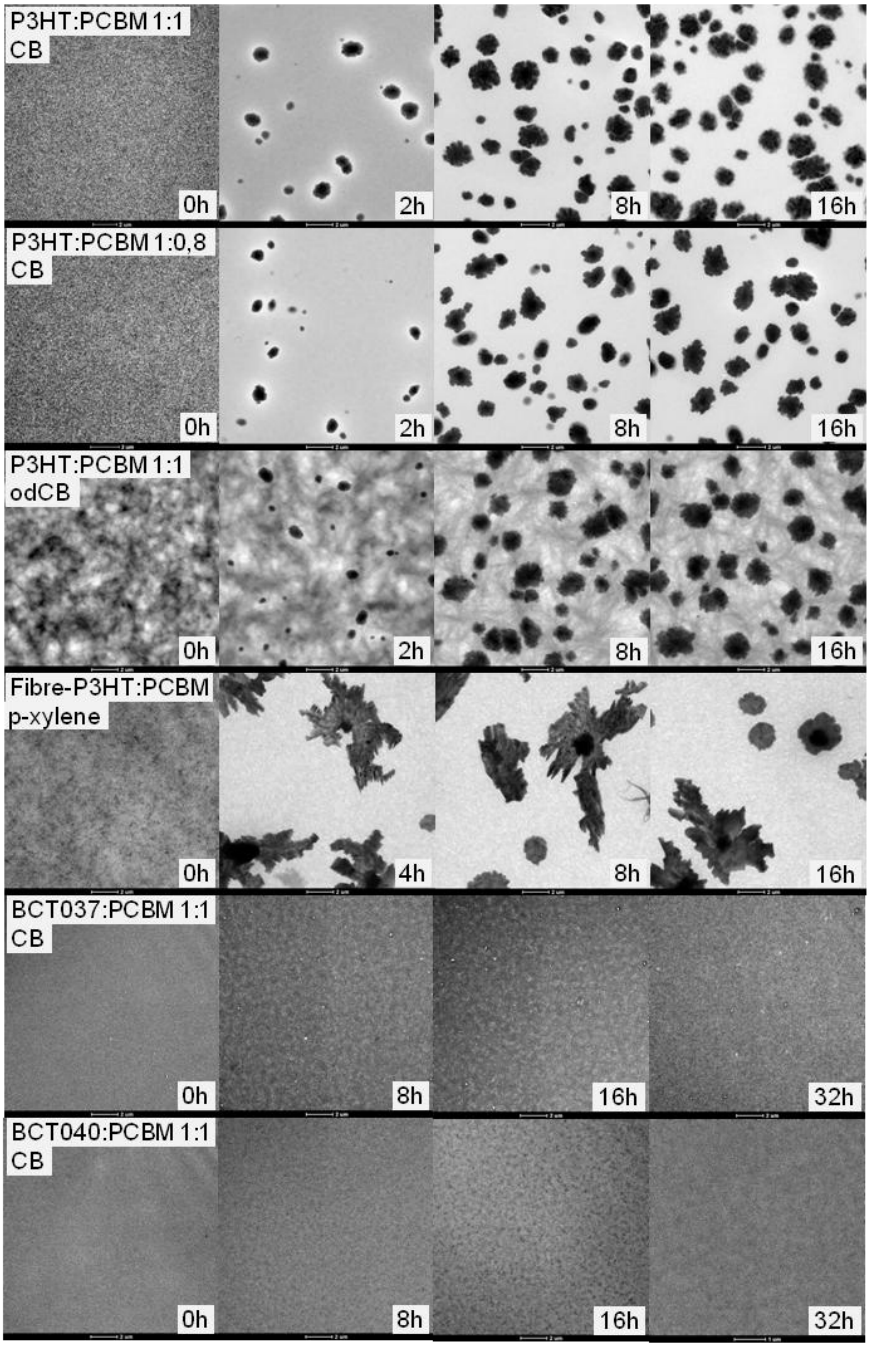

Figure 5-30 Evolution of the active layer morphology during annealing at 110°C of derivatives of P3HT blended with PCBM. (scale bar = 2µm)

5.7 References

[1] L. Reimer, *Transmission Electron Microscopy*, Springer, Berlin, **1989**
[2] M.T. Rispens, A. Meetsma, R. Rittberger, C.J. Brabec, N.S. Sariciftci, J.C. Hummelen, *Chem. Commun.* **2003**, 2116
[3] S. Hugger, R. Thomann, T. Heinzel, T. Thurn-Albrecht, *Colloid Polym. Sci.* 282, **2004**, 932
[4] A. Swinnen, I. Haeldermans, P. Vanlaeke, J. D'Haen, J. Poortmans, M. D'Olieslaeger, J.V. Manca, *Eur. Phys. J. Appl. Phys.* 36, **2007**, 251
[5] J.-F. Chang, B. Sun, D.W. Breiby, M.M. Nielsen, T.I. Solling, M. Giles, I. McCulloch, H.Sirringhaus, *Chem. Mater.* 16, **2004**, 4772
[6] R.J. Kline, M.D. McGehee, E.N.Kadnikavo, J. Liu, J.M.J. Fréchet, M.F. Toney, *Macromol.* 38, **2005**, 3312
[7] F. Padinger, R.S. Rittberger, N.S. Sariciftci, *Adv. Funct. Mater.* 13, **2003**, 85
[8] Y. Kim, S.A. Choulis, J. Nelson, D.D.C. Bradley, S. Cook, J.R. Durrant, *Appl. Phys. Lett.* 86, **2005**, 063502
[9] P. Vanlaeke, G. Vanhoyland, T. Aernouts, D. Cheyns, C. Deibel, J. Manca, P. Heremans, J. Poortmans, *Thin Solid Films* 511, **2006**, 358
[10] T.J. Savenije, J.E. Kroeze, X. Yang, J. Loos, *Thin Solid Films* 511, **2006**, 2
[11] C. Lin, E.-Y. Lin, F.-Y. Tsai, *Adv. Funct. Mater.* 20, **2010**, 834
[12] M. Al-Ibrahim, O. Ambacher, S. Sensfuss, G. Gobsch, *Appl. Phys. Lett.* 86, **2005**, 201120
[13] Y. Kim, S.A. Choulis, J. Nelson, D.D.C. Bradley, S. Cook, J.R. Durrant, *J. Mater. Sci.* 40, **2005**, 1371
[14] A. Swinnen, I. Haeldermans, M. v. Ven, J. D'Haen, G. Vanhoyland, S. Areso, M. D'Olieslaeger, J. Manca, *Adv. Funct. Mater.* 16, **2006**, 760
[15] W. Ma, C. Yang, X. Gong, K. Lee, A.J. Heeger, *Adv. Funct. Mater.* 15, **2005**, 1617
[16] S. van Bavel, E. Sourty, G. de With, J. Loos, *Nano Lett.* 9, **2009**, 507
[17] V. Dyakonov, *Physica E* 14, **2002**, 53
[18] D. Chirvase, Z. Chiguvare, M. Knipper, J. Parisi, V. Dyakonov, J.C. Hummelen, *J. Appl. Phys.* 93, **2003**, 3376
[19] B. Campo, *Side-chain Functionalized Poly(3-hexylthiophene)-based Copolymers: Synthesis and Characterization of Derivaties for Application in Polymer Solar Cells*, PhD Thesis UHasselt, D/2009/2451/56, **2009**
[20] P. Vanlaeke, A. Swinnen, I. Haeldermans, G. Vanhoyland, T. Aernouts, D. Cheyns, C. Deibel, J. D'Haen, P. Heremans, J. Poortmans, J.V. Manca, *Sol. Energy Mater. Sol. Cells* 90, **2006**, 2150

Chapter 6

Summary and outlook

This chapter summarizes the results presented in the previous chapters and gives an outlook towards the future.

6.1 Summary

Over the last decade, great improvements have been made within the field of organic BHJ solar cells. It has become clear that the active layer morphology plays a key role in achieving competitive devices. Within this work, the active layer morphology of several polymer:PCBM systems is correlated with the performance and stability of the corresponding solar cells. The morphology of polymer:fullerene blends has to be tuned to obtain state-of-the-art photovoltaic performance. But, an important general conclusion of this work is that the polymer:fullerene blended films are not stable. An increase of temperature can induce and accelerate PCBM diffusion and phase separation. In this work, also some solutions for this problem are investigated.

Chapter 2 discussed the techniques used in this thesis for studying the morphology of the active layers. With BFTEM, the bulk morphology of a sample can be displayed. SAED gives information about the ordering within the samples. Also UV-Vis can be applied to calculate the amount of P3XT fibers present in the active layer.

In chapter 3, it was shown that P3XT fibers, prepared in solution, can be used to prepare photovoltaic devices that do not need a post-production annealing treatment. The P3XT fibers were PAT derivatives with side chains ranging from 4 to 9 carbon atoms. A drawback of this method was the need to use different solvents for each material to obtain the fibers in solution. For some of these solvents, the solubility of PCBM was not optimal and this clearly had an effect on the active layer morphology. When PCBM had a high solubility in the solvent, good intermixing of PCBM and polymer was obtained. For low PCBM solubility, the PCBM assembled in large (> 500nm) chunks. A method, based on solution heating, was presented, which allowed to control the amount of P3XT fibers in the P3XT:PCBM blend. The photovoltaic properties and the morphology of the various P3XT materials applied in solar cells, have been investigated. J_{sc} largely depended on the morphology of the P3XT:PCBM blends. When good intermixing of P3XT and PCBM was obtained, J_{sc} reached an optimum. V_{oc} was correlated with the P3XT fiber content. Upon increasing

the solution temperature, and in this way decreasing the fiber content, V_{oc} increased. It was demonstrated before[1] that the aggregation of P3HT into fibers increases the polymer's oxidation potential. Since V_{oc} is related to the HOMO level of the donor material, the increase in V_{oc} for the P3XT:PCBM solar cells was attributed to a decrease in fibrillar P3XT upon solution heating. The efficiencies for the different P3XT (X = 4 to 9) ranged from 0.6% to 3.1%; the best performance was obtained with P36T. This efficiency did not increase linearly with fiber content, but formed an optimum at average fiber contents, also observed by van Bavel et al.[2] for state-of-the-art P3HT:PCBM solar cells.

Though efficiencies of organic BHJ solar cells are gradually increasing towards values necessary for large scale consumption, their stability is still poor compared to their inorganic counterparts. Chapter 4 discussed the thermal stability of MDMO-PPV:PCBM solar cells. It was seen that upon thermal annealing, a thermally accelerated demixing of MDMO-PPV and PCBM takes place. The reduced interfacial area, resulting from this process, leads to less efficient exiton dissociation (which happens at the polymer-PCBM interface). This is reflected in the photovoltaic performance where a strong decrease in J_{sc} is observed. An Arrhenius model is used to describe the degradation kinetics at the various ageing temperatures and to extrapolate the lifetime of the solar cells to other temperatures. An activation energy of 0.87 eV was found.

In chapter 5, the stability of several polymer:PCBM systems was compared. First the stability of the popular P3HT was studied. Though this material initially behaves positive during an annealing treatment (P3HT crystallizes for short annealing times leading to improved charge transport and better photovoltaic performance), its long time stability turns out to be quite poor. For long annealing at elevated temperatures, a demixing of P3HT and PCBM occurs. This can be correlated again to a decrease in J_{sc}. Small changes in the preparation method of the solar cells (i.e. using less PCBM or applying a slow drying treatment) can improve the initial performance of the solar cells, because of the instant crystallization of P3HT, but do not lead to enhanced thermal stability. Introducing functionalized side chains in the polymer structure did prove to enhance the thermal stability. An implementation of

only 10% of these side chains turned out to be enough to hamper the free movement of PCBM molecules in the polymer matrix and in this way stabilize the performance of the device. Also using a polymer with a high glass transition temperature (above the operating temperatures of the device) induced a more stable morphology coinciding with a more stable performance.

6.2 Outlook

This work demonstrates that controlling the active layer morphology of polymer:PCBM solar cells, is essential not only for achieving devices with a high efficiency but also for obtaining devices with a good stability. The ideal morphology consists of a polymer:PCBM blend that is phase separated on a small scale (in the order of the exciton diffusion length) and that contains percolation paths (that serve as 'highways') towards the electrodes for both electrons and holes.

It was demonstrated that the morphology can be stabilized e.g. by using a donor polymer with high glass transition temperature (section 5.4) or by inserting functionalized side chains in the donor polymer (section 5.3). The higher T_g of the donor polymer resulted in a more rigid matrix which hampered the free movement of the PCBM molecules. The effect of using functionalized side chains is however not fully understood yet. Bert Campo[3] (Organic Chemistry, UHasselt) discovered a correlation between the crystallization behavior of the functionalized polymer:PCBM blends and the clustering of PCBM upon annealing. Apparently, the functionalized copolymers have a lower tendency to self-organize which is reflected in an augmented thermal stability of the polythiophene:PCBM blend morphology where the crystallization of PCBM is hampered. However, not all functionalizations lead to better morphological stability. Jan Duchateau[4] (Organic Chemistry, UHasselt) created several functionalized MDMO-PPV derivates (Figure 6-1) which turned out to be a lot more unstable than the original material.

When blended with PCBM in a 1:4 weight ratio, the initial morphology of the active layers (Figure 6-2, top) was quite similar to that of MDMO-PPV:PCBM though the scale of phase separation changed slightly. After annealing at

100°C for 15 minutes however, large differences were observed (Figure 6-2, bottom). PCBM clustered at a very fast rate and thin but widespread crystals were formed (see also Appendix A.2).

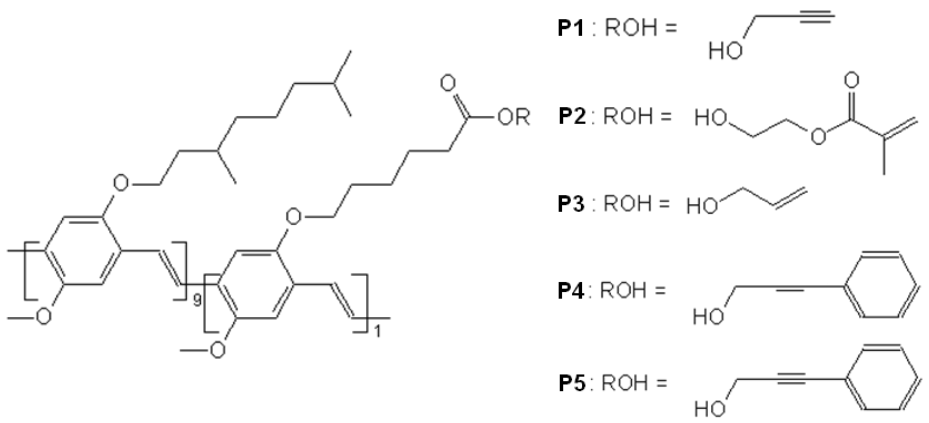

Figure 6-1 MDMO-PPV derivatives with 10% functionalized side chains designed by Jan Duchateau.[4]

This indicates that very small changes in the donor polymer (only 10% of the side chains were functionalized) can have a large influence on the active layer morphology. More insight into the mechanisms that drive these morphology changes is necessary in order to be able to distinguish the side chains that could be beneficial for the stability of the devices.

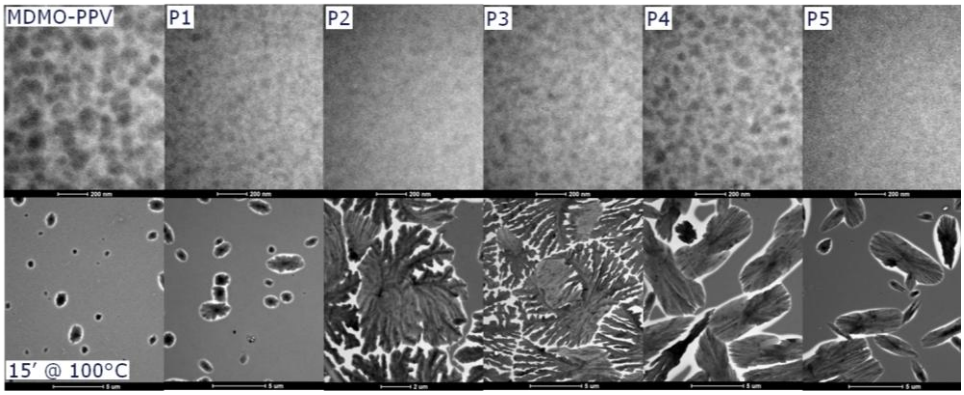

Figure 6-2 Morphology of functionalized polymers in Figure 6-1 blended with PCBM in a 1:4 ratio as produced (top, scale bar = 200 nm) and annealed for 15 minutes at 100°C (bottom, scale bar = 5 µm).

This work focused especially on the influence of active layer morphology on the short circuit current of solar cells. However, also the open circuit voltage and the fill factor are influenced by a thermal treatment and need further investigation. The changes in V_{oc}, related to changes in morphology, are currently being investigated in our lab.

Morphology changes of P3HT:PCBM blends are also affected by the crystallization rate of the P3HT:PCBM blends. Current activities, in collaboration with the VUB aim to correlate this crystallization rate to the observed performance degradation of the solar cells.

Another factor that could influence the stability of polymer:fullerene blends is the molecular weight M_w of the polymer. Since the glass transition temperature increases upon increasing M_w,[5] it might be expected that the thermal stability will also increase with increasing M_w.

Beside high temperatures, operational solar cells are also subjected to oxygen and other atmospherical gasses, humidity and UV-light. These degradation mechanisms should also be studied, which will be done in the future with environmental chambers.

This work has provided a qualitative relation between the morphology of polymer:PCBM blends and the performance and stability of the corresponding devices. In order to obtain a quantitative relationship, a physical model based on the Poisson, drift-diffusion and continuity equations is currently under construction.

6.3 References

[1] T.J. Savenije, J.E. Kroeze, X. Yang, J. Loos, *Thin Solid Films* 511, **2006**, 2

[2] S. van Bavel, E. Sourty, B. de With, J. Loos, *EMC 2008, Vol. 2 Mater. Sci.*, **2008**, 795

[3] B. Campo, *Side-chain Functionalized Poly(3-hexylthiophene)-based Copolymers: Synthesis and Characterization of Derivaties for Application in Polymer Solar Cells*, PhD Thesis UHasselt, D/2009/2451/56, **2009**

[4] J. Duchateau, *Design, Synthesis and Characterization of Functionalized Poly(p-Phenylene Vinylene) Copolymers: The Development of a Universal Method towards Advanced conjugated Polymers for Device Applications*, PhD Thesis UHasselt, D/2009/2451/57, **2009**

[5] L.-P. Blanchard, J. Hesse, S.L. Malhotra, *Can. J. Chem.* 52, **1974**, 3170

Appendix A: Additional TEM features (i.e. possibilities of the Tecnai G2 Spirit Twin)

A.1 EDX

Energy dispersive X-ray spectroscopy (EDX) is a technique used for the elemental investigation of a sample. In TEM, the incident beam consists of electrons with very high energies. If one of these electrons collides with an electron of a sample atom, the latter will be knocked out of its shell, creating a hole in the electron shell. If such a hole appears in the inner shell of a sample atom, it is not in a stable state anymore. To stabilize the atom, an electron from an outer shell will drop into the inner shell. However, because the outer shells are at a higher energy state, the atom must lose some energy. It does this in the form of X-rays.

The X-rays emitted from the sample atom are characteristic in energy and wavelength to the element of the atom and also to which shell has lost an electron and which shell has replaced it. The observed X-rays can be used for the identification of the chemical elements present in the material.

Figure A-1 shows BFTEM images of MDMO-PPV:PCBM 1:4 active layers of solar cells. These TEM samples were prepared directly from the photovoltaic devices. As can be seen in the BFTEM images, they contained some impurities at some areas in the samples. Through EDX the composition of the active layers could be deduced.

In the sample without impurities (Figure A-1, bottom), the largest peak corresponds to carbon (C). This is not surprising since the film contains mostly organic material (MDMO-PPV and PCBM). The oxygen (O) peak also comes from these organic materials. The second largest peak corresponds to copper (Cu) and can be attributed to the Cu-grid on which the sample is deposited. Finally, a small amount of sulphur (S) is present; this has to be related to some PEDOT-PSS that was not removed completely by the etching in HF and H_2O.

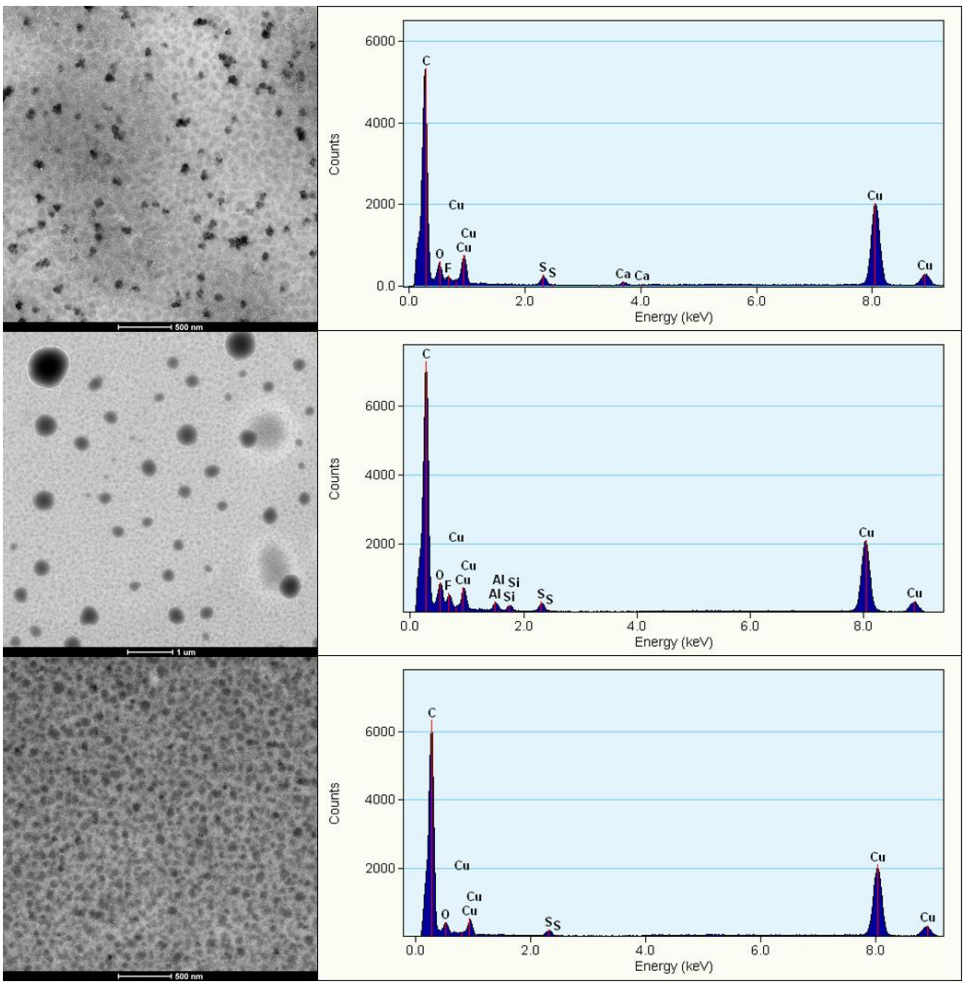

Figure A-1 BFTEM images of MDMO-PPV:PCBM 1:4 active layers of solar cells together with their EDX profiles showing that the impurities in the layers correspond to remainders of the CaAl contact.

Throughout the sample 2 kinds of impurities were found. Some small (~ 80 nm) chunks, visible in the top image of Figure A-1, seemed to correspond to remainders of Ca from the CaAl electrode. Next to the peaks that appeared in the 'clean' sample, a small Ca peak could be seen in the EDX profile. Another remainder of the HF etching was a small fluorine (F) peak. At other places some bigger (0.2 – 1 µm) sphere shaped structures were present. These structures could be remainders of Al from the CaAl electrode (an Al peak

appears in the EDX pattern). However, a Si peak in the EDX pattern indicated that the glass substrate has also reacted with the HF during etching and some residue of this reaction is present in the TEM sample.

A.2 HRTEM

High Resolution Transmission Electron Microscopy (HRTEM) is a technique that allows the imaging of the crystalline structure of a sample. For HRTEM a larger objective diaphragm than in BFTEM is used (Figure A-2). Together with the transmitted beam, also some diffracted beams are allowed to pass through the objective diaphragm. When electrons pass through the sample and are diffracted, their relative phases change. When the diffracted beam(s) eventually interfere(s) with the transmitted beam, this will create phase contrast in the image plane. In this way, it is possible to visualize the lattice planes of a crystalline sample.

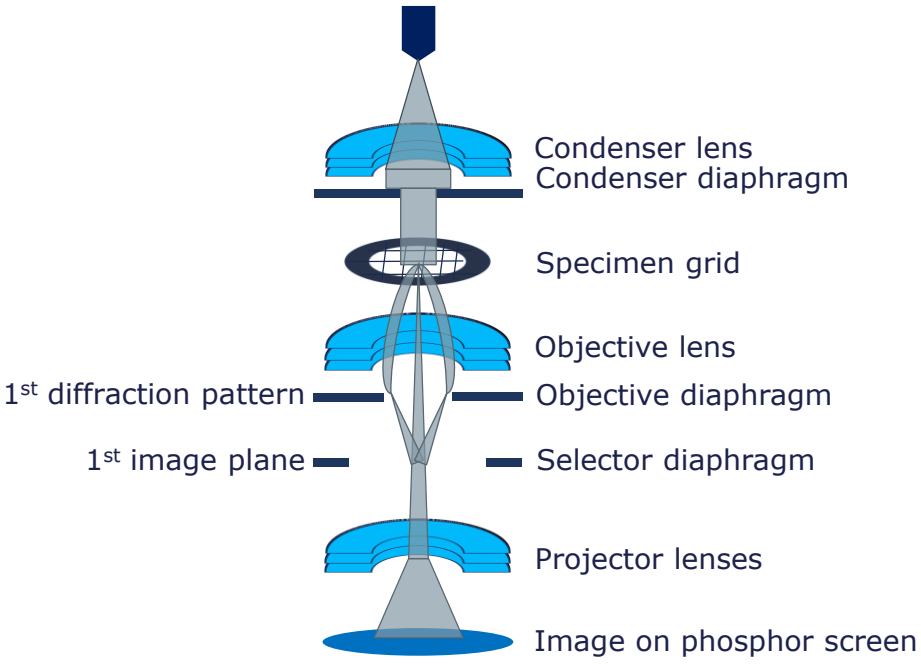

Figure A-2 Schematic representation of a TEM operating in High Resolution mode.

In this work, PCBM needles, formed upon annealing of a polymer:PCBM film (see chapters 4 and 5), came across very frequently. Therefore, it was attempted to visualize their structure with HRTEM. One important condition in HRTEM is that the samples are as thin as possible (at most a few tens of nanometers). Because PCBM needles tend to grow out of the matrix and reach thicknesses of over 200 nm,[1] it was not always possible to perform HRTEM on PCBM needles. Too much diffraction of the electron beam on these thick needles takes place which makes it impossible to visualize the lattice planes. However, it was also seen before that the dimensions and the shape of PCBM needles can be tuned by using different materials or different preparation conditions. By adding functionalized side chains to MDMO-PPV, Jan Duchateau[2] succeeded in making a polymer that, when mixed with PCBM in a blend, gave very large but also very thin PCBM needles upon annealing (Figure A-3).

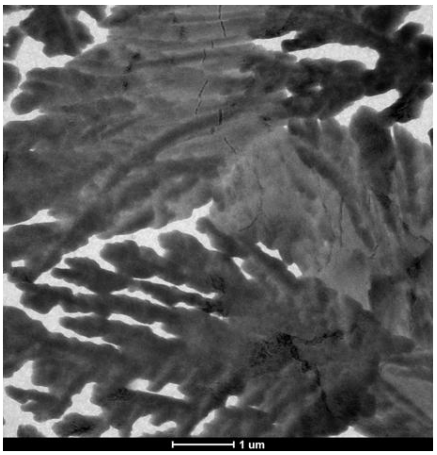

Figure A-3 Functionalized MDMO-PPV:PCBM 1:4 forms large and thin PCBM needles upon annealing. Scale bar = 1 µm.

These thin PCBM needles made it possible to obtain a HRTEM image. Figure A-4 clearly shows parallel lines representing the lattice planes of triclinic PCBM.[3] The distance between the lattice planes was 0.85 nm corresponding to the (1 1 -1) crystal planes.

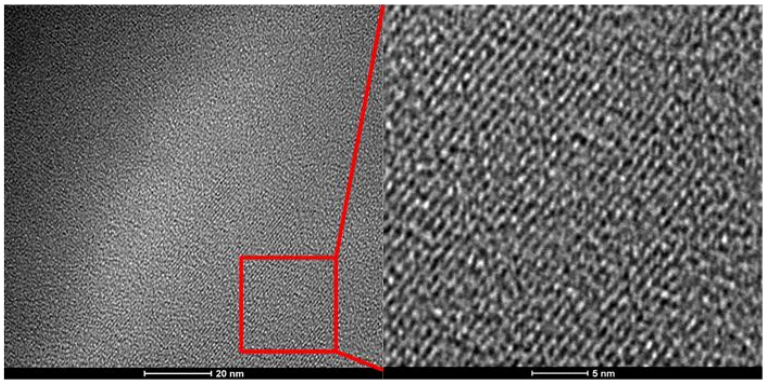

Figure A-4 HRTEM image of a PCBM cluster showing the lattice planes of PCBM. Scale bar = 20 nm (left) and 5 nm (right).

A.3 STEM

In the STEM (Scanning Transmission Electron Microscopy) mode of the microscope images are acquired by moving a focused beam in a raster across the specimen and collecting a signal at each pixel coordinate. The signals for all pixels together make the STEM image.

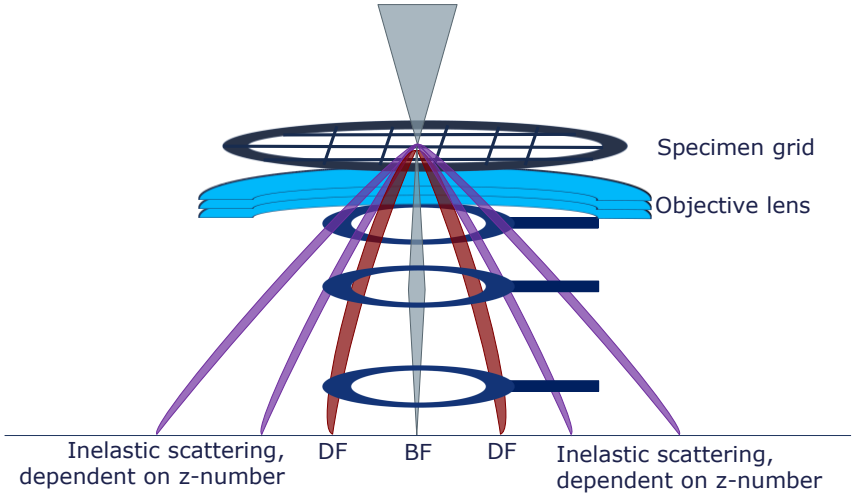

Figure A-5 Schematic representation of a TEM in STEM mode with a ring-shaped HAADF detector.

When a High Angle Annular Dark Field (HAADF) detector is used in STEM mode, Z-contrast can be obtained. The operating principle is depicted in Figure

A-5. The HAADF detector is ring-shaped. The camera length[7] of the detector determines the structures that are highlighted. For long camera lengths, electrons that are elastically scattered (Bragg reflections) can be displayed. For shorter camera lengths, electrons that are inelastically scattered at high angles are displayed. The intensity is then proportional to the product of thickness (=number of scattering atoms) and the square of the atomic number (= Z-contrast).[4]

Figure A-6 shows 2 HAADF images of identical MDMO-PPV:PCBM 1:4 samples, spin-coated from chlorobenze. The left image was obtained at IMO with the FEI Tecnai G^2 Spirit Twin. The right image was obtained at TU/e with a Fei Tecnai G^2 20 by S. van Bavel.[5] Clearly, the right image shows a lot more details. The bright areas that correspond to PCBM rich regions are interconnected by small wires. In this way a percolation network is formed within the MDMO-PPV:PCBM 1:4 layer.

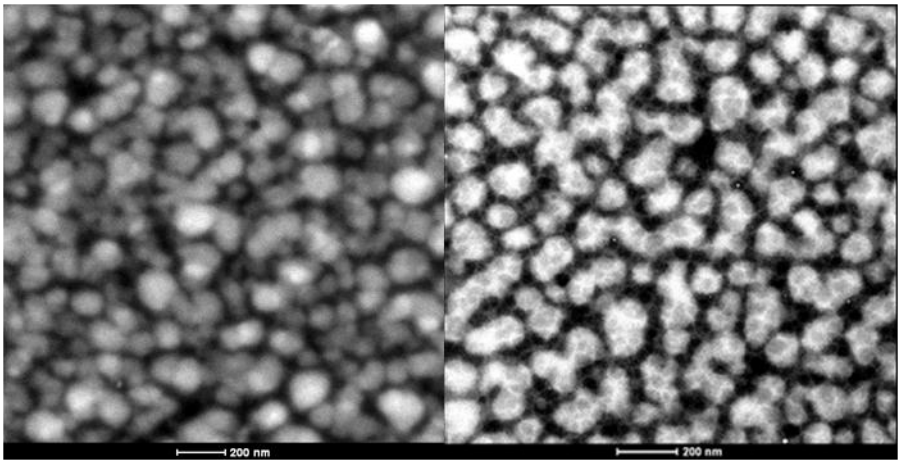

Figure A-6 HAADF image of an MDMO-PPV:PCBM 1:4 film, spin-coated from CB. The left image was obtained at IMO, the right picture was obtained at TU/e.[5] Scale bar = 200 nm.

The lower resolution of the image taken at IMO could be caused by a difference in operating voltage. While the FEI Tecnai G^2 Spirit Twin operated at

[7] In reality, the position of the HAADF detector is fixed. The camera length is changed by adjusting the electromagnetic lenses.

120 kV, the Fei Technai G^2 20 operated at 200 kV resulting in reduction of the spherical aberrations and thus a better resolution.

A.4 Tomography

Tomography is a method for 3D reconstruction of the interior of an object from its projections. Tomography can be used with different imaging techniques (BFTEM, DFTEM, STEM). The technique consists in tilting the sample around a rotation axis and recording images at different angles. In most TEMs, it is not possible to rotate a sample 180°; a missing wedge exists. Figure A-7 demonstrates that this leads to a loss of information.

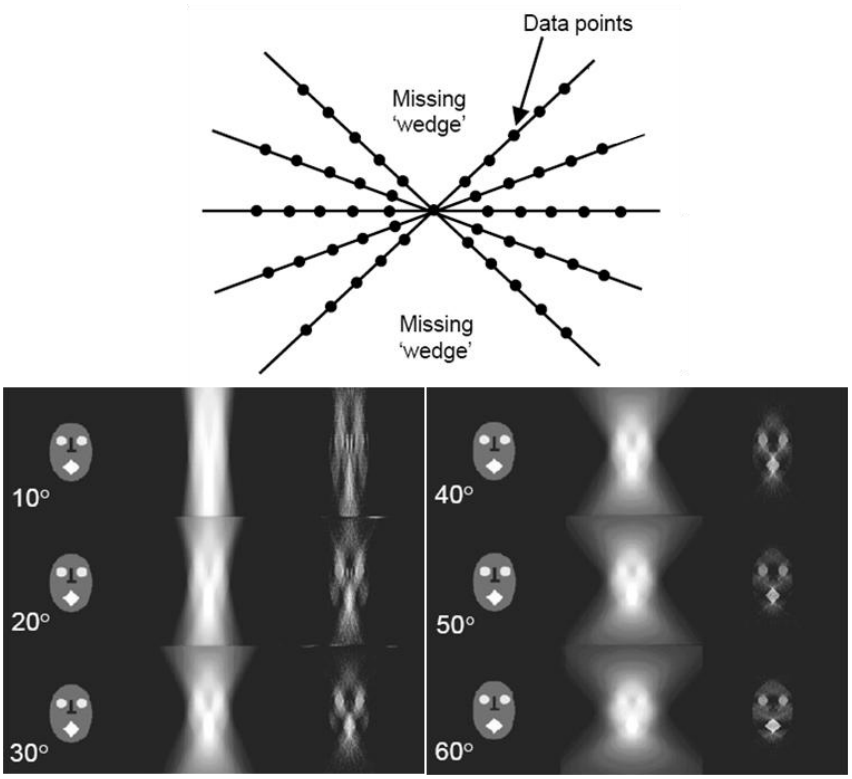

Figure A-7 The missing wedge in tomography (top) and the effect on imaging (bottom): the original object is shown in the left-hand column, the direct back-projection reconstruction in the middle and the weighted back-projection reconstruction in the right-hand column. Increasing the tilt range from ± 10° to ± 60° results in a much better reconstruction.[6]

An important condition for obtaining a good tomography series is that the sample does not move upon rotation. Since mostly a small amount of drift is present, the microscope corrects for this by cross-correlating images at subsequent angles and automatically moving the sample if necessary. After acquisition of a tilting series, some drift in the images still remains. This is corrected again by calculating the cross-correlation of the subsequent images. When the images are aligned correctly, reconstruction of the volume is done by weighted back-projection.

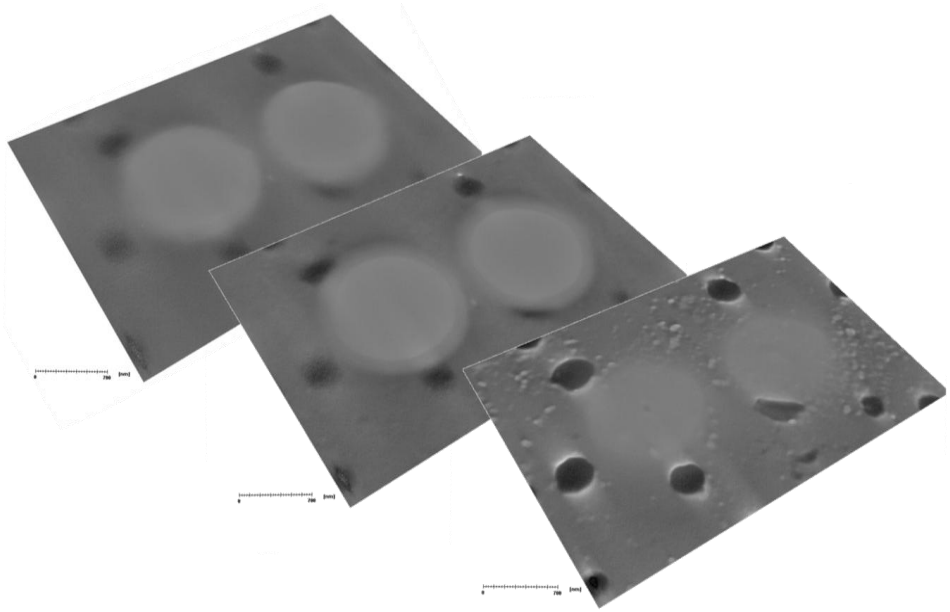

Figure A-8 STEM tomography on MDMO-PPV:PCBM 1:4 doctor bladed from toluene. Left: top of the film, middle: half-way the film, right: bottom of the film at the glass substrate. Scale bar = 600 nm.

Figure A-8 and Figure A-9 show reconstructions of an MDMO-PPV:PCBM 1:4 blend that was doctor bladed from toluene on a glass substrate. Tomography was performed in STEM mode. The 2 bright spheres in the images correspond to large (>500 nm) PCBM rich areas. In Figure A-8, the reconstructed slice of the bottom of the sample shows some grains originating from the rough surface of the glass substrate. The dark areas correspond to holes in the samples. In the middle slice, the PCBM spheres have a light border. During the

evaporation of the toluene, PCBM has apparently diffused toward the big sphere leaving behind a border that is depleted of PCBM. The top slice of the image is becoming very fuzzy. At this point, the PCBM sphere sticks out above the film. This is confirmed by Figure A-9 that shows reconstructed slices in three dimensions.

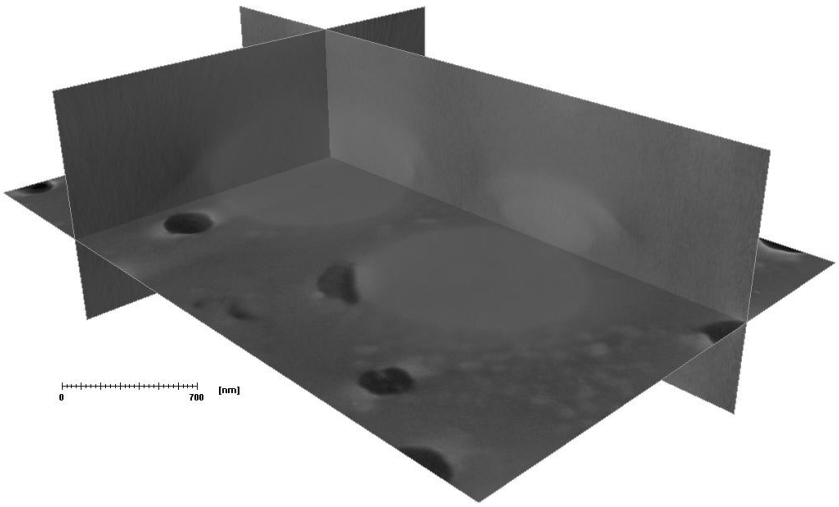

Figure A-9 STEM tomography on MDMO-PPV:PCBM 1:4 showing cross-sections in 3 directions. Scale bar = 600 nm.

S. van Bavel[7] used BFTEM tomography to study annealed P3HT:PCBM layers. It was observed that more crystalline P3HT was present at the bottom of the layer that at the top. The amount of crystalline P3HT in the film was determined to be 60%.

A.5 References

[1] A. Swinnen, I. Haeldermans, M. Van de Ven, J. D'Haen, G. Vanhoyland, S. Aresu, M. D'Olieslaeger, J. Manca, *Adv. Funct. Mater*. **2006**, 760

[2] J. Duchateau, *Design, Synthesis and Characterization of Functionalized Poly(p-Phenylene Vinylene) Copolymers: The Development of a Universal Method towards Advanced Conjugated Polymers for Device Applications*, PhD Thesis UHasselt, D/2009/2451/57, **2009**

[3] M.T. Rispens, A. Meetsma, R. Rittberger, C.J. Brabec, N.S. Sariciftci, J.C. Hummelen, *Chem. Commun.* 17, **2003**, 2116

[4] T. Walther, Y. Qiu, A.G. Cullis, *J. Phys. Conf. Ser.* 241, **2010**, 012068
[5] S. van Bavel, E. Sourty, B. de With, J. Loos, *EMC 2008, Vol. 2 Mater. Sci.*, **2008**, 795
[6] P.A. Midgley, M. Weyland, *Ultramicroscopy* 96, **2003**, 413
[7] S. van Bavel, E. Sourty, G. de With, J. Loos, *Nano Lett.* 9, **2009**, 507

Appendix B: Paper 1

Influence of thermal ageing on the stability of polymer bulk heterojunction solar cells

S. Bertho, I. Haeldermans, A. Swinnen, W. Moons, T. Martens, L. Lutsen, D. Vanderzande, J. Manca, A. Senes, A. Bonfiglio, *Solar Energy Materials and Solar Cells* 91, 2007, 385-389

Available online at www.sciencedirect.com
ScienceDirect
Solar Energy Materials & Solar Cells 91 (2007) 385–389
Solar Energy Materials and Solar Cells
www.elsevier.com/locate/solmat

Influence of thermal ageing on the stability of polymer bulk heterojunction solar cells

Sabine Bertho[a,*], Ilse Haeldermans[a], Ann Swinnen[a], Wouter Moons[a], Tom Martens[a], Laurence Lutsen[b], Dirk Vanderzande[a,b], Jean Manca[a,b], Alessia Senes[c], Annalisa Bonfiglio[c]

[a]*Institute for Materials Reseach (IMO), Hasselt University, Wetenschapspark 1, B-3590 Diepenbeek, Belgium*
[b]*IMEC vzw, Division IMOMEC, Wetenschapspark 1, B-3590 Diepenbeek, Belgium*
[c]*University of Cagliari, Italy*

Available online 22 November 2006

Abstract

A new approach is presented in order to improve the thermal stability of polymer: [6-6]-phenyl C_{61} butyric acid methyl ester (PCBM) bulk heterojunction solar cells. The central idea in this approach is the use of a polymer with high glass transition temperature (T_g), well above the normal operating temperatures of the devices. In this paper, a PPV-derivative with a T_g of 150 °C was used as an electron donor and the thermal stability of the obtained solar cells was compared with solar cells based on the reference material poly[2-methoxy-5-(3′,7′-dimethyloctyloxy)-1,4-phenylene vinylene] (MDMO-PPV) with a T_g of 45 °C. The use of the material with higher glass transition temperature resulted in a significant improvement of the thermal stability of the photovoltaic parameters. Furthermore, a systematic transmission electron microscope (TEM) study demonstrates that the better thermal stability of performance coincides with a more stable active layer morphology. Both improvements are attributed to the reduced free movement of the electron donor material (PCBM) within the active layer of the solar cell.

Keywords: Organic photovoltaics; Thermal stability; Glass transition temperature

1. Introduction

Over the last decade, great improvements have been made in the field of organic solar cells. An important breakthrough came with the introduction of a blend of an electron-donor-type polymer and suitable electron-acceptor material as active layer [1,2]. Compared to former bilayer structures, the contact area between the donor and acceptor material was enlarged, resulting in more efficient exciton dissociation and AM 1.5 power conversion efficiencies in the range of 1%. Improvement of film morphology by altering the casting conditions of poly[2-methoxy-5-(3′,7′-dimethyloctyloxy)-1,4-phenylene vinylene] (MDMO-PPV):[6-6]-phenyl C_{61} butyric acid methyl ester (PCBM) based photoactive layers resulted in 2.5–2.9% efficient organic solar cells [3,4]. Nowadays, efficiencies of 5% are achieved through the use of high mobility donor polymers (e.g. P3HT) and through a continued nanoscale control of the morphology of the donor–acceptor interpenetrating networks [5]. One of the general bottlenecks of organic solar cells is their poor stability. A low resistance towards oxygen, UV-light, high temperatures, etc. results in a degradation of the solar cells [6–10]. It has been reported by Neugebauer et al. that the use of fullerenes in a blend with a polymer gave an improved stability compared with single component devices due to a slower degradation of the polymer in the mixture [11,12]. However, recent studies show that the fullerenes induce a thermal instability of the active layer morphology, yielding observations such as phase separation and PCBM clustering [13,14]. Annealing treatments bring along the demixing of polymer and PCBM, resulting in a reduced interfacial area and less efficient exciton dissociation. Due to this link between the active layer morphology and the performance of solar cells, several

*Corresponding author. Tel.: +3211268887.
E-mail address: sabine.bertho@uhasselt.be (S. Bertho).

0927-0248/$ - see front matter © 2006 Elsevier B.V. All rights reserved.
doi:10.1016/j.solmat.2006.10.008

solutions have been proposed to improve the thermal stability of organic solar cells by nanomorphology control. A possible approach is the use of diblock-copolymers, consisting of donor- and acceptor blocks, which could render stable phase separated structures on the scale of the respective block lengths [15,16]. In P3HT-based solar cells, the thermal stability could be improved by using a low fullerene content in the active layer [5]. This prevented clustering of PCBM under an annealing treatment without hampering the crystallization of P3HT. In this study, a novel approach is presented, based on the use of a high T_g polymer as electron donor. For this purpose, we use a PPV with a high glass transition temperature ($T_g \approx 150\,^{\circ}C$). This 'high T_g PPV' (Fig. 1) is a copolymer designed by Merck. The synthetic route is described by Becker et al. [17]. The thermal stability of the photovoltaic output parameters and of the bulk morphology for the obtained solar cells is compared with reference MDMO-PPV:PCBM solar cells.

2. Experimental

Bulk heterojunction solar cells were made according to standard preparation guidelines. Indium tin oxide (ITO, 100 nm) coated glass plates were cleaned 10 min in an ultrasonic bath with successively: soap, demineralised water, acetone and boiling isopropanol. A 60 nm thick poly(3,4-ethylenedioxythiophene-polystyrenesulfonate (PEDOT-PSS

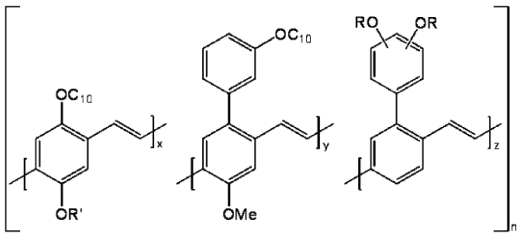

Fig. 1. 'High T_g PPV': a copolymer designed by Merck with a glass transition temperature of about 150 °C [17].

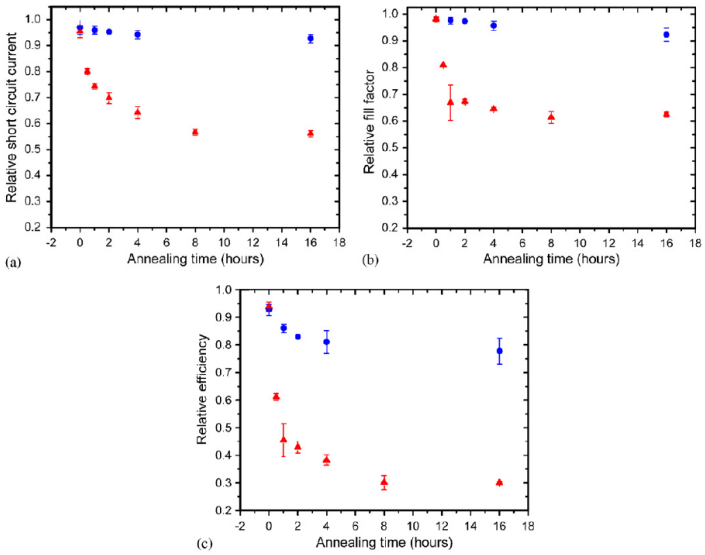

Fig. 2. Decay of the relative short circuit current (a), the fill factor (b), and the efficiency (c) as a result of annealing at 110 °C of MDMO-PVV:PCBM solar cells (triangles) and 'high T_g PPV':PCBM solar cells (circles).

(Bayer)) layer was spincoated on the ITO structure. The substrates were dried for 20 min on a hotplate at 120 °C. The active layer, with thickness of 120 nm, consisting of a blend of donor polymer (MDMO-PPV (Merck) or 'high T_g PPV' (Merck)) and acceptor material (PCBM (Nano-C)) was spincoated on top of the PEDOT-PSS layer. The blends were spincoated from a solution in chlorobenzene with a polymer:PCBM ratio of 1:4. The concentrations of the solutions were, respectively, 0.5 and 0.3 wt% (weight percentage of polymer in chlorobenzene solvent) for MDMO-PPV and 'high T_g PPV'. To obtain good dissolving, the MDMO-PPV:PCBM solution was stirred over night at 50 °C; the 'high T_g PPV':PCBM solution was stirred for a week at 50 °C. Finally, the Al top electrode of 80 nm was evaporated on top of the active layer. The IV-characteristics were measured with an Oriel solar simulator equipped with a xenon short arc lamp with a power of 150 W. The annealing treatment was carried out on a hotplate in a glovebox with nitrogen atmosphere and in the dark to avoid degradation due to oxygen and UV radiation.

After the IV-measurements, the active layer of the solar cells was studied with a transmission electron microscope (TEM)(Philips CM12-STEM).

3. Results and discussion

Fig. 2 shows the decay of the short circuit-current, the fill factor and the efficiency of solar cells with an active layer of either 'high T_g PPV':PCBM (1:4) or MDMO-PPV:PCBM (1:4). For each point in the graphs, corresponding to a different annealing time, a new sample containing four solar cells has been used.

Directly after preparation of the solar cells, IV-characterization was performed to obtain the initial values of the solar cell parameters. Each device was then annealed (at 110 °C, in a dark, nitrogen atmosphere) for a specific time interval (between 0 and 16 h). After 35 h, when all annealing treatments were finished, IV-characterization of all solar cells was redone. The final solar cell parameters were normalized with respect to the initial values. Note that the annealing temperature is above the glass transition temperature of the used MDMO-PPV ($T_g \approx 45$ °C) but below the glass transition temperature of the 'high T_g PPV' ($T_g \approx 150$ °C).

The first point of the graphs in Fig. 2 corresponds to the degradation of the devices due to storage at room temperature (shelf life), while the following points are obtained through annealing at 110 °C. The decay of the photovoltaic parameters due to shelf storage ageing (0 h annealing time) lies in the same range for both kinds of solar cells, well above 90% of the initial values. In the further course of the graphs, there is a clear deviation for the two different materials used. The short-circuit current of the 'high T_g PPV' solar cells showed a small decrease due to annealing, nevertheless, its value stayed above 90% of the initial value after 16 h of annealing at 110 °C. For MDMO-PPV based solar cells, 16 h of annealing resulted in a decrease down to less than 60% of the initial short-circuit current. The decay in fill factor for both kinds of devices roughly follows the same pattern as the decay in short-circuit current. This results in the fact that the overall efficiency, being proportional to the short-circuit current

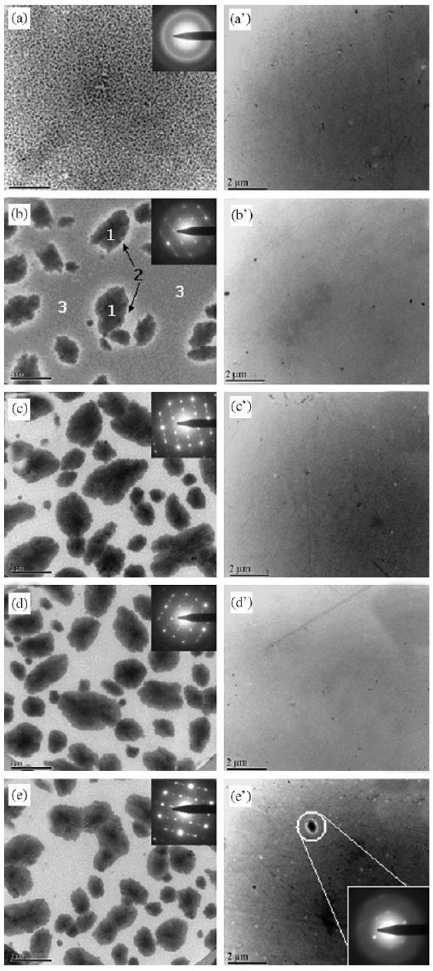

Fig. 3. TEM images of the active layer of MDMO-PPV:PCBM 1:4 solar cells (a–e) and 'high T_g PPV':PCBM 1:4 solar cells (a′–e′). The solar cells were annealed at 110 °C for 0 h (a, a′), 1 h (b, b′), 2 h (c, c′), 4 h (d, d′) and 16 h (e, e′) yielding formation of large PCBM-clusters for the MDMO-PPV based active layers while maintaining a more stable morphology for the 'high T_g PPV' based active layers (scale bar: 2 μm).

and the fill factor, is much more stable for 'high T_g PPV' based solar cells (a decrease down to about 80% after 16 h of annealing) as compared to MDMO-PPV based solar cells (a decrease down to about 30% after 16 h of annealing).

Efficiencies of MDMO-PPV:PCBM based solar cells have evolved over the last decade to values up to 2.9% [4]. In this study, the initial efficiencies for the MDMO-PPV:PCBM as well as for the 'high T_g PPV':PCBM solar cells were in the range of 1–2% (without LiF and without process optimisation). In realistic outdoor conditions, the poor thermal stability of the MDMO-PPV:PCBM together with operating conditions in full sunlight (possibly up to 75 °C) will result in a gradual decrease of the efficiency. Though the initial values of efficiency have the same order of magnitude for both materials, we expect that, because of its better thermal stability, the 'high T_g PPV':PCBM solar cells will outperform MDMO-PPV:PCBM based solar cells under full sunlight conditions in the long run.

Furthermore, a systematic TEM study, demonstrates that the better thermal stability of the performance for the 'high T_g PPV' solar cells coincides with a more stable morphology of the active layer. Fig. 3 shows TEM images of the active layer of the MDMO-PPV based solar cells (a–e) and the 'high T_g PPV' based solar cells (a′–e′).

As mentioned already by Yang et al. [14] large (>1 μm) PCBM-clusters (dark areas, indicated as area 1 in Fig. 3b) are formed upon annealing in the MDMO-PPV:PCBM active layers. The selected area electron diffraction (SAED) patterns of these clusters (insets in Fig. 3) indicate that they are in fact groups of single crystals. After 1 h of annealing at 110 °C, a light border (area 2 in Fig. 3b) is visible around the PCBM-crystals. The SAED pattern of this region was compared with the SAED pattern of the area in between the crystals (area 3 in Fig. 3b). Fig. 4 shows the residual intensity of the SAED patterns of both regions as a function of the *d*-value.

The area in between the crystals (area 3) shows intensity peaks at *d*-values corresponding to PCBM [18]. In the SAED pattern of the light border around the PCBM-cluster (area 2), the PCBM peaks have disappeared. Only a broad, low-intensity profile is present, which is typical for amorphous MDMO-PPV. We conclude that this light border around the PCBM-clusters is depleted of PCBM while the area in between the crystals still consists of a homogeneous MDMO-PPV:PCBM blend. After 2 h of annealing the homogeneous MDMO-PPV:PCBM matrix has vanished. All the PCBM has diffused out of the blend and is assembled in the PCBM-clusters. The TEM images of the active layer of the 'high T_g PPV' solar cells (Fig. 3a′–e′) show a more stable morphology. It is not until after 16 h of annealing at 110 °C that a PCBM-cluster is found. The corresponding SAED pattern again confirms that it is a group of PCBM single crystals.

The difference in PCBM crystallization rate in MDMO-PPV:PCBM active layers and 'high T_g PPV':PCBM active layers is interpreted qualitatively as a result of the difference in glass transition temperature of MDMO-PPV and 'high T_g PPV'. As long as the solar cells are kept below the glass transition temperature of the polymer, the matrix is stiff and gives the PCBM molecules hardly any possibility to move freely. When a thermal treatment is applied above the glass transition temperature, it causes the matrix to become soft, making it easy for PCBM molecules to assemble.

In summary, from the comparison of the thermal stability between standard MDMO-PPV solar cells and solar cells based on a material with high glass transition

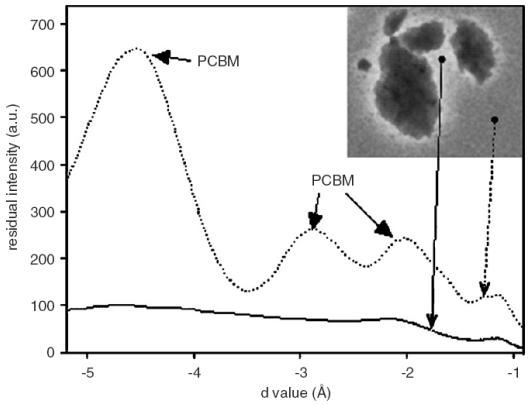

Fig. 4. Residual intensity of the SAED patterns of the light border around a PCBM-cluster (solid line) and the grey area in between the PCBM-clusters (dotted line).

temperature, it can be stated that 'high T_g PPV' solar cells clearly show a better thermal stability of performance and bulk morphology. This is interpreted as a more stable active layer morphology, where the free movement of the PCBM molecules is hampered due to a stiffer 'high T_g PPV':PCBM matrix. The proposed approach towards thermally more stable bulk heterojunction solar cells based on the use of high T_g polymers has, therefore, proven to be effective and is hence a promising route for further developments towards high efficiency, high stability organic solar cells.

Acknowledgements

The research was carried out in the framework of the IWT-project 030220 ''Nanosolar'', the FWO-project G025204 and the European project Molycell. Sabine Bertho is research assistant of the Fund for Scientific Research, Flanders (Belgium) (F.W.O.). Hasselt University is acknowledged for providing PhD-grants to Ilse Haeldermans. We thank Dr. H. Becker of Merck OLED Materials GmbH for the supply of the 'high T_g PPV'.

References

[1] G. Yu, J. Gao, J.C. Hummelen, F. Wudl, A.J. Heeger, Science 270 (1995) 1789.
[2] L.S. Roman, M.R. Andersson, T. Yohanms, Adv. Mater. 9 (1997) 1164.
[3] S.E. Shaheen, C.J. Brabec, N.S. Sariciftci, F. Padinger, T. Fromherz, J.C. Hummelen, Appl. Phys. Lett. 78 (2001) 841.
[4] T. Munters, T. Martens, L. Goris, V. Vrindts, J. Manca, L. Lutsen, W. De Ceuninck, D. Vanderzande, L. De Schepper, J. Gelan, N.S. Sariciftci, C.J. Brabec, Thin Solid Films 403–404 (2002) 247.
[5] W. Ma, C. Yang, X. Gong, K. Lee, A.J. Heeger, Adv. Funct. Mater. 15 (2005) 1617.
[6] H. Neugebauer, C.J. Brabec, J.C. Hummelen, R.A.J. Janssen, N.S. Sariciftci, Synth. Met. 102 (1999) 1002.
[7] F. Padinger, T. Fromherz, P. Denk, C.J. Brabec, J. Zettner, T. Hierl, N.S. Sariciftci, Synth. Met. 121 (2001) 1605.
[8] J.M. Kroon, M.M. Wienk, W.J.H. Verhees, J.C. Hummelen, Thin Solid Films 403–404 (2002) 223.
[9] F.C. Krebs, J.E. Carlé, N. Cruys-Bagger, M. Andersen, M.R. Lilliedal, M.A. Hammond, S. Hvidt, Sol. Energy Mater. Sol. Cells 86 (2005) 499.
[10] S. Schuller, P. Schilinsky, J. Hauch, C.J. Brabec, Appl. Phys. A 79 (2004) 37.
[11] H. Neugebauer, C. Brabec, J.C. Hummelen, N.S. Sariciftci, Sol. Energy Mater. Sol. Cells 61 (2000) 35.
[12] N. Camaioni, G. Ridolfi, G. Casalbore-Miceli, G. Possamai, L. Garlaschelli, M. Maggini, Sol. Energy Mater. Sol. Cells 76 (2003) 107.
[13] X. Yang, J.K.J. van Duren, M.R. Rispens, J.C. Hummelen, R.A.J. Janssen, M.A.J. Michels, J. Loos, Adv. Mater. 16 (2004) 802.
[14] X. Yang, J.K.J. van Duren, R.A.J. Janssen, M.A.J. Michels, J. Loos, Macromolecules 37 (2004) 2151.
[15] H. Hoppe, N.S. Sariciftci, J. Mater.Res. 19 (2004) 1924.
[16] Z. Zhu, S. Hadjikyriacou, D. Waller, R. Gaudiana, J. Macromol. Sci., Part A: Pure Appl. Chem. 41 (2004) 1467.
[17] H. Becker, H. Spreitzer, W. Kreuder, E. Kluge, H. Schenk, I. Parker, Y. Cao, Adv. Mater. 42 (2000) 42.
[18] M.T. Rispens, A. Meetsma, R. Rittberger, C.J. Brabec, N.S. Sariciftci, J.C. Hummelen, Chem. Commun. 17 (2003) 2116.

Appendix C: Paper 2

Effect of temperature on the morphological and photovoltaic stability of bulk heterojunction polymer:fullerene solar cells

S. Bertho, G. Janssen, T.J. Cleij, B. Conings, W. Moons, A. Gadisa, J. D'Haen, E. Goovaerts, L. Lutsen, J. Manca, D. Vanderzande, *Solar Energy Materials and Solar Cells* 92, 2008, 753-760

Available online at www.sciencedirect.com
ScienceDirect
Solar Energy Materials & Solar Cells 92 (2008) 753–760
Solar Energy Materials and Solar Cells
www.elsevier.com/locate/solmat

Effect of temperature on the morphological and photovoltaic stability of bulk heterojunction polymer:fullerene solar cells

Sabine Bertho[a,*], Griet Janssen[b], Thomas J. Cleij[a], Bert Conings[a], Wouter Moons[a], Abay Gadisa[c], Jan D'Haen[a], Etienne Goovaerts[b], Laurence Lutsen[c], Jean Manca[a,c], Dirk Vanderzande[a,c]

[a]*Institute for Materials Research, Hasselt University, Wetenschapspark 1, B-3590 Diepenbeek, Belgium*
[b]*Physics Department, University of Antwerp, Universiteitsplein 1, B-2610 Antwerp, Belgium*
[c]*IMECvzw, IMOMEC, B-3590 Diepenbeek, Belgium*

Received 31 October 2007; received in revised form 7 January 2008; accepted 8 January 2008
Available online 4 March 2008

Abstract

In high performance polymer:fullerene bulk heterojunction solar cells the nanoscale morphology of interpenetrating acceptor:donor materials is optimized through appropriate preparation conditions such as annealing and choice of solvent, but this initial state-of-the-art morphology will not remain stable during long-term operation. We report the effects of prolonged storage at elevated temperatures on both the morphology and the photovoltaic performance for the model systems MDMO-PPV:PCBM and P3HT:PCBM as compared to 'High T_g PPV':PCBM based solar cells, where the 'High T_g PPV' is characterized by its high glass transition temperature (138 °C). In situ monitoring of the photocurrent–voltage characteristics at elevated temperatures, in combination with a systematic transmission electron microscopy (TEM) study and complementary optical spectroscopy, reveals distinct degradation kinetics and morphological changes that indicate the occurrence of different underlying physico-chemical mechanisms.

Keywords: Organic photovoltaics; Thermal stability; Glass transition temperature; Morphology

1. Introduction

In the historical development towards state-of-the-art polymer:fullerene bulk heterojunction solar cells the nanoscale morphology of the photoactive film always played a crucial role [1–4]. In bulk heterojunction solar cells the morphology of the donor–acceptor interpenetrating networks is fine tuned in order to optimize the combination of both exciton dissociation and charge transport. Moreover, the short exciton diffusion length in these material systems (5–10 nm) demands proximity of the donor and acceptor regions on nanoscale. The nanoscale morphology of the interpenetrating acceptor:donor materials is optimized through appropriate preparation conditions such as annealing conditions and choice of solvents. For the model system MDMO-PPV:PCBM, improvement of the film morphology has been obtained by switching to the use of chlorobenzene as a solvent, resulting in 2.5–2.9% efficient organic solar cells [3,4]. Nowadays, efficiencies of 5% are achieved through the use of high mobility donor polymers (e.g. P3HT) and through a continued nanoscale control of the morphology of the donor–acceptor interpenetrating networks—which in some cases has been realized by the introduction of an additional annealing step [5,6]. However, in this paper it will be demonstrated that this initial optimized morphology will not remain stable during long-term operation or during storage at elevated temperatures, and therefore becomes one of the multiple stability issues encountered in organic solar cells. Organic solar cells degrade because of their low resistance towards oxygen, light, high temperatures, etc. [7–16]. We will focus here on the instability of organic solar cells that results from morphological changes in the active layer due

*Corresponding author. Tel.: +3211268887.
E-mail address: sabine.bertho@uhasselt.be (S. Bertho).

0927-0248/$ - see front matter © 2008 Elsevier B.V. All rights reserved.
doi:10.1016/j.solmat.2008.01.006

to a thermal treatment [17–19]. In particular, the relation between the morphological instability and the glass transition temperature of the donor materials is studied in more detail. We investigated the effect of temperature on the morphology as well as on the photovoltaic performance of three polymer:fullerene material systems—the model systems MDMO-PPV:PCBM and P3HT:PCBM as compared to 'High T_g PPV':PCBM, based on a conjugated polymer with a high glass transition temperature. The photovoltaic output (i.e. the short circuit current, open circuit voltage, fill factor, and efficiency) was studied in situ at various annealing temperatures. Complementary with this in situ electrical monitoring of the degradation kinetics, the evolution of the active layer morphology was studied with transmission electron microscopy (TEM) and optical and photoluminescence (PL) absorption spectroscopy results are discussed.

2. Experimental

Bulk heterojunction solar cells with three different conjugated polymers (MDMO-PPV(Poly[2-methoxy-5-(3′,7′-dimethyloctyloxy)-1,4-phenylene vinylene]) with $T_g \approx 50\,^{\circ}C$, P3HT(poly(3-hexylthiophene)) with $T_g \approx 6\,^{\circ}C$ [20–23] and 'High T_g PPV' with $T_g \approx 138\,^{\circ}C$, all supplied by Merck) as electron donor materials and PCBM ([6-6]-phenyl C_{61} butyric acid methyl ester (Nano-C)) as acceptor material were made according to the following preparation guidelines. The devices had an ITO/PEDOT-PSS/polymer:PCBM/Al structure. Each device had an active area of 25.0 mm^2. Indium tin oxide (ITO, 100 nm) coated glass plates were successively cleaned in a soap solution, demineralized water and acetone, each for 10 min in an ultrasonic bath. This was followed by cleaning in boiling isopropanol for 10 min. A 60 nm thick Poly(3,4-ethylenedioxythiophene-polystyrenesulfonate (PEDOT-PSS (Bayer)) layer was spincoated on the clean glass/ITO substrates. The substrates were dried for 20 min on a hotplate at 120 °C. The active layer, with thickness of 120 nm, consisting of a blend of polymer and PCBM in chlorobenzene was spincoated on top of the PEDOT-PSS layer. The polymer:PCBM ratio for MDMO-PPV, 'High T_g PPV', and P3HT were, respectively, 1:4, 1:4, and 1:1 (these ratios were chosen because they resulted in the best solar cell performance). The concentrations of the solutions were, respectively, 0.5, 0.3, and 1.0 wt% (weight percentage of polymer in chlorobenzene solvent) for MDMO-PPV, 'High T_g PPV', and P3HT. To obtain complete dissolution of MDMO-PPV:PCBM and P3HT:PCBM, these solutions were stirred overnight at 50 °C; the 'High T_g PPV':PCBM solution was stirred for 3 days at 50 °C. The solar cells were completed by evaporating 80 nm of Al on top of the active layer.

The current–voltage (IV) characteristics were measured with an Oriel solar simulator equipped with a xenon short arc lamp with a power of 150 W. The influence of thermal annealing on the photovoltaic performance was measured in a set-up that measures IV characterizations at regular time intervals (illumination with a White 5500 K LED (Lamina)) while the samples were kept under continuous annealing. In between the measurements, the samples were kept in the dark.

Values for the glass transition temperature (T_g) of the 'High T_g PPV' were determined by UV–Vis spectroscopy. To this end, an Ocean Optics USB2000 spectrometer with fiber optics arrangement was used. Samples were prepared by spincoating the polymer from a 1.0 wt% solution in chlorobenzene onto a quartz substrate. Subsequently, the substrate was placed in a Linkam TMS94/THMS600 controlled heating/freezing stage, which was positioned in the optical path of the UV–Vis spectrophotometer. The sample was then heated from room temperature to 200 °C (heating rate: 5 °C/min) and subsequently cooled (cooling rate: 5 °C/min) to room temperature. Each measurement point was obtained by averaging 500 individual UV–Vis absorption spectra. The second heating run was used for the determination of T_g.

The active layer morphology was studied with a transmission electron microscope (Philips CM12-STEM). A Varian Cary absorption spectrometer and a Varian Cary Eclipse fluorometer (excitation wavelength of 485 nm) were used for the optical absorption and PL measurements, respectively.

3. Results and discussion

3.1. 'High T_g PPV'

As described earlier, 'High T_g PPV' is characterized by its rather high glass transition temperature as compared to MDMO-PPV and P3HT. This means that its blend with PCBM allows a wide window for investigation of thermal degradation under elevated temperature conditions. However, while P3HT and MDMO-PPV are well studied materials, 'High T_g PPV' is not well known, and therefore requires an appropriate introduction. Fig. 1 shows the chemical structure of the conjugated polymer that we call 'High T_g PPV' for simplicity. The material is a copolymer designed by Merck. The synthetic route is described elsewhere by Becker et al. [24].

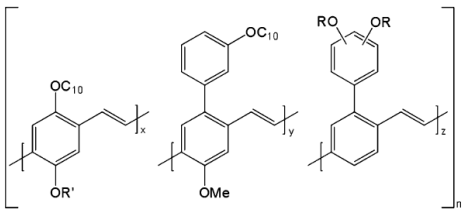

Fig. 1. 'High T_g PPV': a copolymer designed by Merck with a high glass transition temperature [24].

The glass transition temperatures of MDMO-PPV and P3HT (respectively, 50 and 6 °C) were determined through differential scanning calorimetry (DSC) measurements. The glass transition temperature of 'High T_g PPV' was indicated by Merck to be about 150 °C, but no T_g could be observed with conventional DSC measurements. Therefore, the T_g value of 'High T_g PPV' was verified by the following method. Many conjugated polymers exhibit typical thermochromic properties. In PPV-type polymers, this thermochromism allows for a direct determination of previously inaccessible T_g values. This is a result of the fact that these thermochromic effects are directly correlated with temperature dependent deviations from planarity of the conjugated system, which occur above the glass transition temperature T_g. Below T_g the backbone conformation no longer changes and as a result no thermochromism but only ground-state aggregation phenomena are observed. As a result, for PPV-type polymers an accurate value for T_g can be determined from temperature dependent UV–Vis absorption spectra. A T_g measurement of 'High T_g PPV' is displayed in Fig. 2. By plotting the wavelength λ at half-maximum of the π–π^* transition as a function of temperature, two linear fits with different slopes are obtained. For these fits the measurements close to T_g, i.e. at 130 and 140 °C were omitted. The intersection of the obtained fits gives an accurate estimate of the T_g of the polymer. For 'High T_g PPV' it was determined to be 138 °C. Furthermore, from Fig. 2 it is evident that the T_g is well defined, since the entire transition occurs within the limited temperature range of 120–150 °C.

In order to demonstrate that 'High T_g PPV' is suitable as donor material in bulk heterojunction solar cells, Fig. 3 shows an *IV* characteristic of a solar cell prepared with 'High T_g PPV'. Such solar cells gave an overall efficiency around 1.5%. Remarkable though is the high open circuit voltage of 0.83 V.

3.2. *In situ monitoring of photovoltaic degradation kinetics*

In the following, several experiments are performed at elevated temperatures to speed up the degradation processes inside the solar cells presented above. Fig. 4 shows the relative decay of the photovoltaic parameters of a solar cell with an MDMO-PPV:PCBM 1:4 blend as active layer for an annealing temperature of 110 °C. As can be inferred from the figure, the open circuit voltage (V_{oc}) is barely sensitive to the thermal treatment performed over a long period of time. This is consistent with the fact that V_{oc} mainly depends on material properties, namely the ionization potential of the donor polymer and electron affinity of the acceptor fullerene molecule. Only a relatively small decrease in V_{oc} (less than 10%) is observed. A larger decrease is observed in the short circuit current (I_{sc}) and the fill factor (FF). The efficiency of the solar cell, proportional to I_{sc}, V_{oc}, and FF, shows the largest decrease.

Fig. 5 shows the decay of the short circuit current for solar cells based on the three materials (MDMO-PPV,

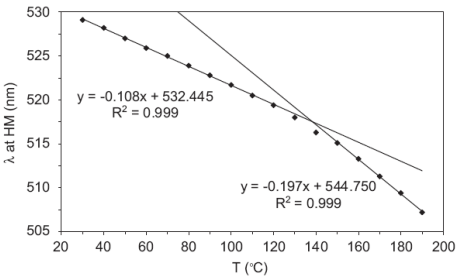

Fig. 2. Graph of the wavelength λ at half-maximum of the π–π^* transition as a function of temperature; two linear fits with different slopes are obtained. The intersection of the obtained fits gives a T_g for 'High T_g PPV' of 138 °C.

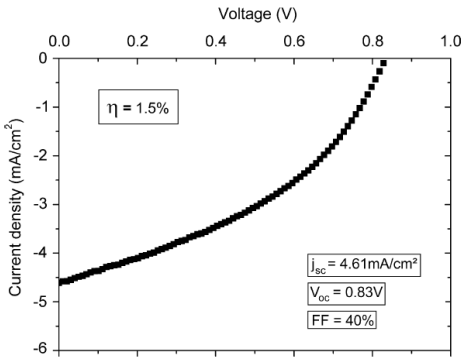

Fig. 3. The current–voltage characteristics obtained from a 'High T_g PPV':PCBM solar cell under AM 1.5 illumination.

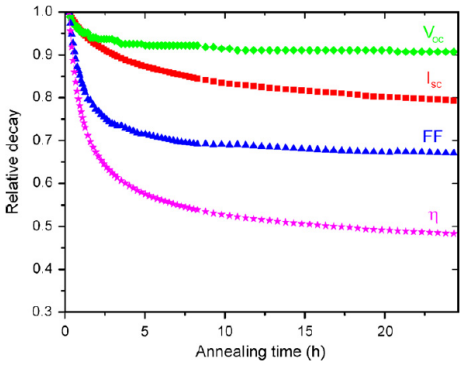

Fig. 4. Relative decay of the short circuit current (I_{sc}), open circuit voltage (V_{oc}), fill factor (FF) and efficiency (η) of an MDMO-PPV:PCBM 1:4 solar cell at 110 °C.

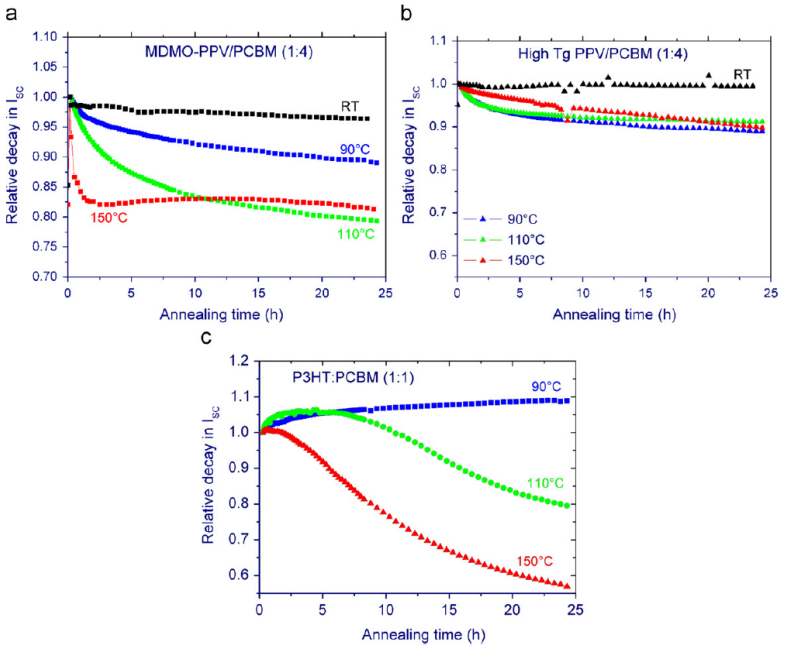

Fig. 5. Relative decay of the short circuit current at several annealing temperatures for solar cells based on (a) MDMO-PPV:PCBM (1:4), (b) 'High T_g PPV':PCBM (1:4) and (c) P3HT:PCBM (1:1).

'High T_g PPV', and P3HT) for several annealing temperatures. At room temperature, the short circuit current of the PPV-derivatives stays rather constant for several hours. Once the samples are annealed, a clear difference can be observed in the decay characteristics of the three materials. Solar cells based on MDMO-PPV show a monotonous decay. For P3HT based solar cells, I_{sc} increases for relatively short annealing times. After a certain time, which depends on the annealing temperature, I_{sc} starts to decrease (as can be observed for $T = 110$ and 150 °C). On the contrary, solar cells based on 'High T_g PPV' remain rather stable, with no large impact of the annealing temperature up to 150 °C.

3.3. Morphology vs. thermal annealing

Previous studies have already shown a strong correlation between the morphology of the active layer of solar cells and their performance [3,25]. Here we will demonstrate that the behavior of the short circuit current of the solar cells depicted in Fig. 5 can also be linked to morphology changes taking place in the active layer. Fig. 6 shows Bright Field TEM-images of the evolution of the active layers of MDMO-PPV:PCBM (1:4) and 'High T_g PPV':PCBM (1:4) during annealing at 110 °C. In earlier work [26], it was already presented that the active layer morphology of 'High T_g PPV':PCBM is much more stable than MDMO-PVV:PCBM. The high glass transition temperature of 'High T_g PPV' results in a firm polymer:PCBM matrix, where the demixing of the two components is hampered. This difference in morphological stability coincides with the observed decay of the short circuit current in Fig. 5. The slower decay of I_{sc} for the 'High T_g PPV':PCBM based solar cells can be attributed to a more stable active layer morphology.

The evolution of I_{sc} for P3HT:PCBM 1:1 solar cells shown in Fig. 5 can also be linked to the active layer morphology. Bright Field TEM images show that after 4 h of annealing at 110 °C, PCBM starts to cluster (Fig. 7a). For this material, however, more information can be gathered from the SAED patterns of the P3HT:PCBM matrix in between the clusters. Fig. 7b shows the residual intensities of these patterns for annealing at 110 °C for several hours. The original diffraction patterns suffered from a large background that resembled inelastic scattering. To improve the signal-to-noise ratio, integration across the complete diffraction ring was done, from which a calculated background due to inelastic scattering was

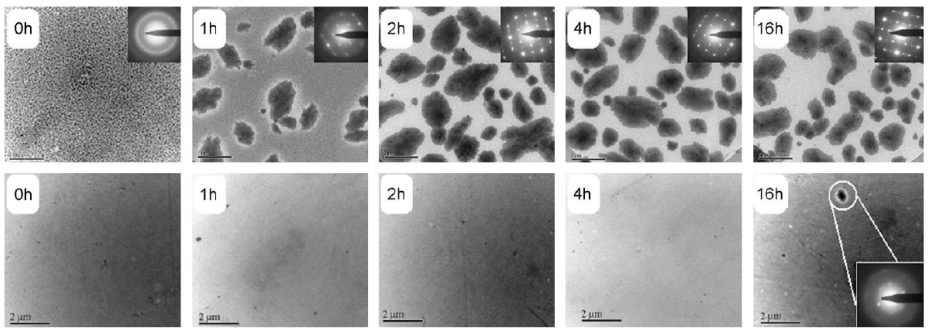

Fig. 6. Morphology changes in the active layer of MDMO-PPV:PCBM 1:4 (top) and 'High T_g PPV':PCBM 1:4 (bottom) as a result of annealing at 110 °C. The active layers were annealed at 110 °C for 0, 1, 2, 4, and 16 h yielding formation of large PCBM-clusters for the MDMO-PPV based active layers while maintaining a more stable morphology for the 'High T_g PPV' based active layers (scale bar: 2 μm).

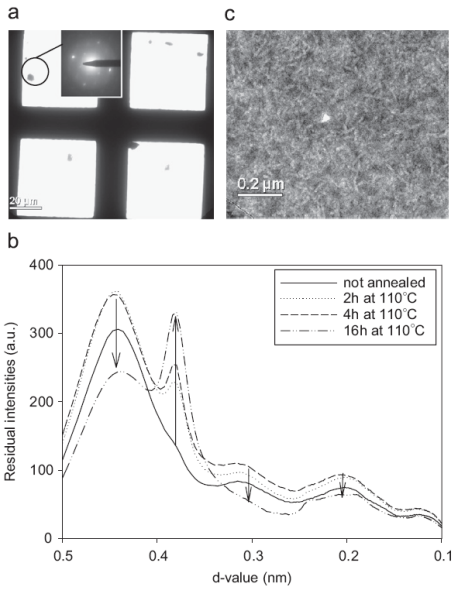

Fig. 7. Evolution of a P3HT:PCBM (1:1) active layer during an annealing treatment at 110 °C, (a) after 4 h some PCBM-clusters appear, (b) residual intensities of the SAED-patterns of the bulk, and (c) P3HT-fibers are clearly visible after 16 h.

subtracted (under the assumption that the blend in between the clusters is quasi-amorphous [27]). The residual intensities of the SAED pattern of the non-annealed active layer show distinct peaks at *d*-values of 2, 3.1, and 4.6 Å corresponding to nanocrystalline PCBM [28]. In addition, for annealing times between 0.5 and 8 h (not all curves are shown for clarity), some evolution in the intensity can be seen at 3.8 Å. The peak appearing here can be attributed to the superposition of the (0 0 2) and (0 2 0) reflections from the crystal planes of semi-crystalline P3HT [23]. After 16 h of annealing, the P3HT peak is very pronounced in the SAED pattern. At the same time, the peaks corresponding to nanocrystalline PCBM are reducing. At this point, P3HT has formed fiber-like crystalline structures that can be seen clearly in a Bright Field TEM image (Fig. 7c). On the other hand, PCBM is vanishing from the P3HT:PCBM matrix and gathering in the PCBM-clusters.

It is clear now that in P3HT:PCBM active layers, two processes take place [29]. One of them, namely the local crystallization of P3HT into fiber-like structures, leads to better charge transport, resulting in a higher I_{sc}. The other process, as in blends with MDMO-PPV, is again the clustering of PCBM, which at later times results in a decrease of I_{sc} mainly due to a lower interfacial area between P3HT and PCBM.

3.4. Thermal stability reflected in absorption and emission

The better thermal stability of 'High T_g PPV' as compared to MDMO-PPV and P3HT is also confirmed by optical spectroscopy. Fig. 8 shows the absorption spectra of MDMO-PPV:PCBM (1:4), 'High T_g PPV':PCBM (1:4), and P3HT:PCBM (1:1) films. An annealing treatment of 16 h at 110 °C results in a quite remarkable change of the absorption spectrum of the MDMO-PPV:PCBM blend. The disappearance of the PCBM-absorption (around 350 nm) in the spectrum of this blend reflects the growth of PCBM crystallites as observed by TEM in the previous paragraph.

Indeed, since the optical spectrometer works in a transmission mode, the dense PCBM crystals give rise to tremendous light scattering. As a result, the total transparent

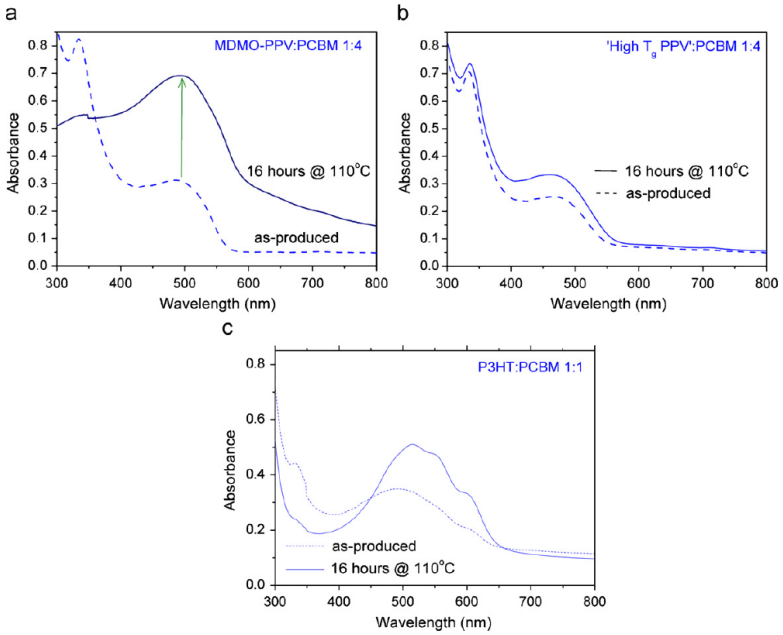

Fig. 8. UV–VIS absorption spectra of (a) MDMO-PPV:PCBM (1:4), (b) 'High T_g PPV':PCBM (1:4), and (c) P3HT:PCBM (1:1) films. Both the spectra of the as-produced films and after a heat treatment of 16 h at 110 °C are shown.

film area is reduced, explaining the appearance of an overall background in the spectrum. Only the polymer regions—essentially PCBM free—contribute to the spectrum. The absorption of the 'High T_g PPV':PCBM film is stable during long thermal treatments, which directly reflects the higher thermal stability of its morphology.

The absorption spectra for the P3HT:PCBM blend reflect the dual crystallization behavior. For the as-produced P3HT:PCBM blend the PCBM-absorption is lower than for the PPV-derivatives because a lower amount of PCBM is used (a polymer:PCBM ratio of 1:1 instead of 1:4). However, also for this blend, the PCBM-absorption is reduced upon annealing, indicating the clustering of PCBM. For this blend, also a redshift for P3HT is observed, which indicates the ordering of P3HT into the fiber-like crystalline structures that were visible in the Bright Field TEM images [30].

An essential step in the PV effect, the electron transfer from polymer to fullerene, can be monitored by the degree of PL quenching, which is close to complete in the unannealed blend films (see Fig. 9, as-produced films). In the pure MDMO-PPV film, a drastic change in shape and peak intensity is observed in the first few minutes of the treatment at 110 °C after which the spectrum remains unaltered for hours. This initial change is not related to degradation of the polymer, but should rather be ascribed to local rearrangements of the polymer chains. (While not discernable in the figure, the same fast change in shape is observed upon heating in the blend of MDMO-PPV with PCBM.) No such initial effect is found in the 'High T_g PPV' film, and only a minor change is observed in both shape and intensity even after 16 h of annealing at 110 °C.

A thermal treatment of 16 h increases the emission intensity of each of the blends, pointing to decreasing charge transfer efficiency. This is much more pronounced in the blend with MDMO-PPV compared to 'High T_g PPV', which correlates well with the higher stability of the morphology in the latter. The decrease in charge transfer efficiency is attributed to the clustering of the PCBM, reducing the interfacial area between the two components of the blend. The TEM investigation has clearly demonstrated the importance of segregation and clustering in MDMO-PPV:PCBM blends, which is hardly observed for 'High T_g PPV':PCBM blends.

4. Conclusion

For the three materials (MDMO-PPV, P3HT, and 'High T_g PPV'), a clear correlation between the morphological evolution of the active layer of solar cells and the

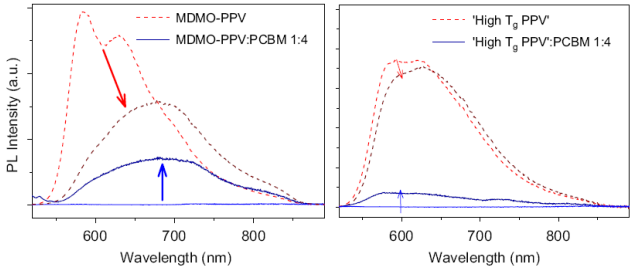

Fig. 9. PL spectra from pure and blended MDMO-PPV and 'High T_g PPV' (1:4 ratio). The arrows indicate the effect of thermal heating during 16 h at 110 °C. Note that the major effect in the pure MDMO-PPV film occurs within 3 min.

degradation of their characteristics is demonstrated. The active layers based on MDMO-PPV show a rapid formation of PCBM-clusters upon annealing. The smaller interfacial area between electron acceptor and electron donor results in a lower photocurrent output. P3HT shows a dual crystallization behavior: on the one hand, P3HT crystallizes, which leads to improved charge conduction and a higher photocurrent output; on the other hand, PCBM groups into clusters, again reducing the interfacial area between electron acceptor and donor regions, which results in a decrease in photocurrent. Comparing the three materials, morphology changes are strongly suppressed in the 'High T_g PPV' active layers which leads to the demonstrated high thermal stability of the device characteristics. Due to the higher glass transition temperature of 'High T_g PPV', its matrix is firmer. This strongly restricts the possible migration and segregation of the PCBM molecules leading to a more stable active layer and consequently to a more stable photovoltaic behavior.

The thermal stability of the MDMO-PPV and 'High T_g PPV' polymer films is also reflected in the stability of the UV–Vis absorption spectra. The charge transfer, monitored by the degree of PL quenching, is much less affected by the thermal treatment in the blends with 'High T_g PPV' than with MDMO-PPV, which is directly related to their very different morphological evolution.

Acknowledgments

The research was carried out in the framework of the IWT-project 030220 "Nanosolar", the FWO-project G.0252.04 and the interregional project OLED+. The work, as part of the project "SOHYDs" within the European Science Foundation EUROCORES Programme, was also supported with funds by the FWO (G.0685.06) and the EC Sixth Framework Programme, under contract no. ERAS-CT-2003-980409. Sabine Bertho is research assistant of the Fund for Scientific Research, Flanders (Belgium) (F.W.O.). We thank Dr. H. Becker of Merck OLED Materials GmbH for the supply of the 'High T_g PPV'.

References

[1] G. Yu, J. Gao, J.C. Hummelen, F. Wudl, A.J. Heeger, Science 270 (1995) 1789.
[2] L.S. Roman, M.R. Andersson, T. Yohanms, Adv. Mater. 9 (1997) 1164.
[3] S.E. Shaheen, C.J. Brabec, N.S. Sariciftci, F. Padinger, T. Fromherz, J.C. Hummelen, Appl. Phys. Lett. 78 (2001) 841.
[4] T. Munters, T. Martens, L. Goris, V. Vrindts, J. Manca, L. Lutsen, W. De Ceuninck, D. Vanderzande, L. De Schepper, J. Gelan, N.S. Sariciftci, C.J. Brabec, Thin Solid Films 403–404 (2002) 247.
[5] W. Ma, C. Yang, X. Gong, K. Lee, A.J. Heeger, Adv. Funct. Mater. 15 (2005) 1617.
[6] F. Padinger, T. Fromherz, P. Denk, C.J. Brabec, J. Zettner, T. Hierl, N.S. Sariciftci, Synth. Met. 121 (2001) 1605.
[7] H. Neugebauer, C.J. Brabec, J.C. Hummelen, R.A.J. Janssen, N.S. Sariciftci, Synth. Met. 102 (1999) 1002.
[8] J.M. Kroon, M.M. Wienk, W.J.H. Verhees, J.C. Hummelen, Thin Solid Films 403–404 (2002) 223.
[9] F.C. Krebs, J.E. Carlé, N. Cruys-Bagger, M. Andersen, M.R. Lilliedal, M.A. Hammond, S. Hvidt, Sol. Energy Mater. Sol. Cells 86 (2005) 499.
[10] S. Schuller, P. Schilinsky, J. Hauch, C.J. Brabec, Appl. Phys. A. 79 (2004) 37.
[11] H. Neugebauer, C. Brabec, J.C. Hummelen, N.S. Sariciftci, Sol. Energy Mater. Sol. Cells 61 (2000) 35.
[12] N. Camaioni, G. Ridolfi, G. Casalbore-Miceli, G. Possamai, L. Garlaschelli, M. Maggini, Sol. Energy Mater. Sol. Cells 76 (2003) 107.
[13] H. Hoppe, N.S. Sariciftci, J. Mater. Res. 19 (2004) 1924.
[14] Z. Zhu, S. Hadjikyriacou, D. Waller, R. Gaudiana, J. Macromol. Sci. 41 (2004) 1467.
[15] F.C. Krebs, H. Spanggaard, Chem. Mater. 17 (2005) 5235.
[16] F.C. Krebs, K. Norrman, Prog. Photovolt. Res. Appl. 15 (2007) 697.
[17] X. Yang, J.K.J. van Duren, M.R. Rispens, J.C. Hummelen, R.A.J. Janssen, M.A.J. Michels, J. Loos, Adv. Mater. 16 (2004) 802.
[18] X. Yang, J.K.J. van Duren, R.A.J. Janssen, M.A.J. Michels, J. Loos, Macromolecules 37 (2004) 2151.
[19] X. Yang, J. Loos, S.C. Veenstra, W.J.H. Verhees, M. Wienk, J.M. Kroon, M.A.J. Michels, R.A.J. Janssen, Nano Lett. 5 (2005) 579.
[20] A. Swinnen, J. Zhao, G. Van Assche, D. Vanderzande, M. D'Olieslaeger, J.V. Manca, B. Van Mele, Proc. SPIE 6656 (2007) 665619.
[21] Y. Zhao, G. Yuan, P. Roche, M. Leclerc, Polymer 36 (1995) 2211.
[22] X. Hu, L. Xu, Polymer 41 (2000) 9147.
[23] S. Hugger, R. Thomann, T. Heinzel, T. Thurn-Albrecht, Colloid Polym. Sci. 282 (2004) 932.

[24] H. Becker, H. Spreitzer, W. Kreuder, E. Kluge, H. Schenk, I. Parker, Y. Cao, Adv. Mater. 42 (2000) 42.
[25] T. Martens, J. D'Haen, T. Munters, Z. Beelen, L. Goris, J. Manca, M. D'Olieslaeger, D. Vanderzande, L. De Schepper, R. Andriessen, Synth. Met. 138 (2003) 243.
[26] S. Bertho, I. Haeldermans, A. Swinnen, W. Moons, T. Martens, L. Lutsen, D. Vanderzande, J. Manca, A. Senes, A. Bonfiglio, Sol. Energy Mater. Sol. Cells 91 (2007) 385.
[27] L. Reimer, Transmission Electron Microscopy, Springer, Berlin, 1989.
[28] M.T. Rispens, A. Meetsma, R. Rittberger, C.J. Brabec, N.S. Sariciftci, J.C. Hummelen, Chem. Commun. 17 (2003) 2116.
[29] A. Swinnen, I. Haeldermans, P. Vanlaeke, J. D'Haen, J. Poortmans, M. D'Olieslaeger, J. Manca, Eur. Phys. J. 36 (3) (2006) 251–256.
[30] P. Vanlaeke, A. Swinnen, I. Haeldermans, G. Vanhoyland, T. Aernouts, D. Cheyns, C. Deibel, J. D'Haen, P. Heremans, J. Poortmans, J.V. Manca, Sol. Energy Mater. Sol. Cells 90 (2006) 2150.

Appendix D: Paper 3

Controlling the morphology of nanofiber-P3HT:PCBM blends for organic bulk heterojunction solar cells

S. Bertho, W.D. Oosterbaan, V. Vrindts, J. D'Haen, T.J. Cleij, L. Lutsen, J. Manca, D. Vanderzande, Organic Electronics 10 (2009) 1248-1251

Organic Electronics 10 (2009) 1248–1251

Contents lists available at ScienceDirect

Organic Electronics

journal homepage: www.elsevier.com/locate/orgel

Controlling the morphology of nanofiber-P3HT:PCBM blends for organic bulk heterojunction solar cells

Sabine Bertho [a,*], Wibren D. Oosterbaan [a], Veerle Vrindts [b], Jan D'Haen [a], Thomas J. Cleij [a], Laurence Lutsen [b], Jean Manca [a,b], Dirk Vanderzande [a,b]

[a] Hasselt University, Institute for Materials Research, Wetenschapspark 1, B-3590 Diepenbeek, Belgium
[b] IMEC vzw, IMOMEC, B-3590 Diepenbeek, Belgium

ARTICLE INFO

Article history:
Received 6 May 2009
Received in revised form 24 June 2009
Accepted 26 June 2009
Available online 3 July 2009

PACS:
84.60.Jt
42.70.Jk
81.05.Tp
64.75.Jk
68.37.Lp

Keywords:
Organic solar cells
Nanofibers
Transmission electron microscopy

ABSTRACT

Within the field of organic bulk heterojunction solar cells, the morphology of the active layer has a key role in obtaining high power conversion efficiencies. P3HT nanofibers, obtained in highly concentrated solutions, are able to give controlled morphologies directly upon deposition. Since the solar cell efficiency of fiber solar cells depends on the fiber content of the casting solution, it is important to control this parameter. Here, we demonstrate an easy way to control the fiber content in the casting solution, i.e. changing the solution temperature. By using solution heating, the overall molecular weight of the polymer in the blend is kept constant, fiber isolation is not needed and the use of solvent mixtures is avoided. The obtained optimal power conversion efficiency is shown to be linked to the morphology of the active layer, which is studied with Transmission Electron Microscopy (TEM).

1. Introduction

P3HT (poly(3-hexylthiophene)) has been a workhorse material for the development of organic solar cells. Its first breakthrough within the field came with the discovery of the beneficial effect of a heat-treatment of solar cells based on a P3HT:PCBM ([6-6]-phenyl C_{61}-butyric acid methyl ester) blend [1–3]. After this, efficiencies have gradually increased towards 5–6% through a control of the nanomorphology of the polymer:PCBM blend [4,5]. Lately, P3HT nanofibers obtained in highly concentrated solutions have been shown to give optimized morphologies directly upon deposition [6–8]. This makes traditional thermal treatment superfluous. The deposition of nanofibers is therefore a more appropriate method to be used with flexible substrates, such as poly(ethylene terephthalate) (PET), which have a low glass transition temperature. The solar cell efficiency of these fiber solar cells depends on the fiber content of the casting solution. Berson et al. [6] controlled the fiber content by mixing isolated fibers with well-dissolved low molecular weight (MW) P3HT; a ratio of 0.75 fiber to 0.25 well-dissolved polymer gave optimal efficiency. Li et al. [7] used the anti-solvent hexane to control the fiber content of P3HT in *o*-dichlorobenzene. Moulé et al. [8] added different amounts of nitrobenzene to a solvent mixture of P3HT:PCBM; this caused the formation of aggregated P3HT networks during the drying process of the devices. Here, we show that the fiber content can be easily controlled by solution temperature. In this way, the overall MW of the P3HT in the blend is kept constant. This is important, since it has been shown that MW influences the photovoltaic performance of P3HT:PCBM solar cells

* Corresponding author. Tel.: +32 (0) 11 268887; fax: +32 (0) 11 268899.
E-mail address: sabine.bertho@uhasselt.be (S. Bertho).

1566-1199/$ - see front matter © 2009 Elsevier B.V. All rights reserved.
doi:10.1016/j.orgel.2009.06.018

[9,10]. In this paper we can rule out this influence. Also fiber isolation is not needed and the use of solvent mixtures is avoided, which may allow for easier recycling of processing solvent. We found an optimal efficiency at a 42% fiber content of the casting solution and show that it can be linked to the morphology of the active layer.

2. Experimental

2.1. Preparation of P3HT fibers

P3HT was prepared via the Rieke method [11]. The regioregularity was determined at >94.5% and it had a M_n of 23.7 kg mol^{-1} (polydispersity index of 1.80) as determined by Analytical Size Exclusion Chromatography (SEC). The SEC was performed using a Spectra series P100 (Spectra Physics) pump equipped with two mixed-B columns (10 μm, 2 × 30 cm, Polymer Labs) and a Refractive Index detector (Shodex) at 60 °C. Chlorobenzene was used as the eluent at a flow rate of 1.0 mL/min. Molecular weight distributions are given relative to polystyrene standards. P3HT fibers were prepared by slow cooling of an orange coloured 0.7 wt% P3HT solution in *p*-xylene, as described elsewhere [11].

2.2. Solar cell fabrication

After the preparation of the P3HT fibers in the *p*-xylene solution, PCBM ([6-6]-phenyl C_{61}-butyric acid methyl ester (Solenne)) was added to the solution in a 1:1 weight ratio with P3HT to act as acceptor material. The casting solution was stirred for ~48 h at room temperature. The solar cells were prepared starting from indium tin oxide (ITO, 100 nm) coated glass plates that were successively cleaned in a soap solution, demineralised water and acetone, each for 10 min in an ultrasonic bath. This was followed by cleaning in boiling isopropanol for 10 min. A 25 nm thick poly(3,4-ethylenedioxythiophene–polystyrenesulfonate (PEDOT–PSS (Bayer)) layer was spin-coated on the clean glass/ITO substrates. The substrates were dried for 20 min on a hot plate at 120 °C. The active layer (P3HT:PCBM 1:1), was spin-coated at 750 rpm on top of the PEDOT–PSS layer. The solution from which the active layer was spin-coated, was heated gradually to several temperatures (between 37 and 50 °C). At each temperature used for the experiment, the solution was left to stabilize for at least 30 min before the active layer was spin-coated on top of the PEDOT–PSS layer. After deposition of the active layer, the devices were left in vacuum (10^{-6} mbar) to get rid of the remaining solvent. Finally, a calcium layer (~25 nm) and an aluminium layer (~70 nm) were evaporated to form the top contact of the solar cell. Each photovoltaic device had an active area of 25 mm^2. The *I–V*-characteristics were measured with an Oriel solar simulator equipped with a Xenon Short Arc lamp with a power of 150 W.

2.3. Morphology of the active layer studied with TEM

For each solution temperature, the morphology of the active layer was studied. A thin film, identical to the active layer of the solar cell, was deposited on a cleaned glass substrate, using the same procedure as for preparing the complete solar cell. This film was isolated by etching with 40% hydrofluoric acid (HF) to remove the glass substrate and then put on a copper TEM-grid. TEM-measurements were performed with a Philips CM12-STEM. The SAED patterns, recorded through TEM, originally suffered from a large background that resembled inelastic scattering. To improve the signal-to-noise ratio, integration across the complete diffraction ring was done, from which a fitted background due to inelastic scattering was subtracted (under the assumption that the blend in between the fibers is quasi-amorphous [12]).

2.4. Determination of the fiber content in the solution

At each solution temperature used for preparing a photovoltaic device, a small amount (<50 μL) of the casting solution was isolated just after spin-coating and diluted in ~3 mL of *p*-xylene of the same temperature. UV–Vis measurements (with a Varian Cary 500 Scan UV–Vis–NIR spectrophotometer) were performed on this highly diluted solution after cooling to room temperature. The obtained UV–Vis spectra were fitted as a sum of previously recorded spectra of PCBM, well-dissolved P3HT and fully fibrillar P3HT, all in *p*-xylene. The known relation between the latter two spectra allowed for the determination of the fiber content [11].

3. Results and discussion

Fig. 1 shows the photovoltaic (PV) parameters of solar cells with a nanofiber-P3HT:PCBM 1:1 active layer as a function of casting solution temperature together with the fiber content of the solution at each temperature. The graph shows that the fiber content of the solution is very sensitive to temperature. When raising the temperature from 37 to 50 °C, the fiber content of the solution decreases from 60% to 14%. The solar cell efficiency displays a quadratic dependence on temperature. An optimal efficiency of ~3.2% is found for a solution temperature of 45 °C. At this temperature, the fiber content was 42%. When comparing the different PV-parameters, it seems that the behavior of the efficiency is strongly related to the behavior of the short circuit current J_{sc}. The open circuit voltage V_{oc} of the solar cells has an increasing trend. The fill factor follows a rather rough course.

The origin of the dependence of the photovoltaic performance on the temperature of the casting solution can be found in the active layer morphology. Fig. 2 shows Bright Field Transmission Electron Microscopy (BFTEM) images of the active layers. The active layer spin-coated from a solution at a relatively low temperature (37 °C) shows large (up to 50 μm) needles (Fig. 2(a, left)). Spots in the Selected Area Electron Diffraction (SAED) patterns of the needles confirm that they are groups of PCBM single crystals [13]. In between the needles, fibers of P3HT are visible (Fig. 2(a, right)). They appear dark against a light background. SAED also gives information about this part of the active layer. In Fig. 3, the residual intensities of the

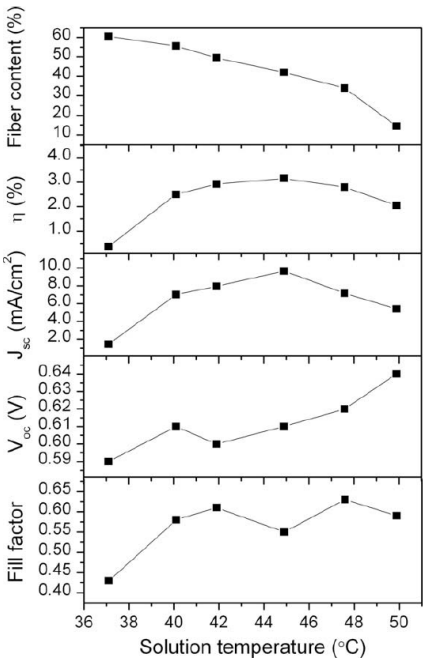

Fig. 1. Fiber content of the casting solution, efficiency η, short circuit current J_{sc}, open circuit voltage V_{oc} and fill factor of nanofiber-P3HT:PCBM (1:1) solar cells as a function of solution temperature.

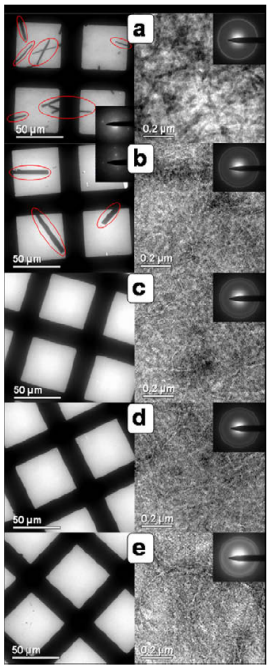

Fig. 2. Bright Field TEM images of P3HT:PCBM 1:1 spin-coated from a solution at 37.1 °C (a), 40.5 °C (b), 41.9 °C (c), 44.9 °C (d) and 49.9 °C (e), at low temperatures PCBM assembles in needle-like structures, P3HT fibers appear as dark or light areas depending on the presence of PCBM within the polymer matrix. The insets show the SAED patterns of either the PCBM needles (left) or the homogeneous P3HT:PCBM regions (right).

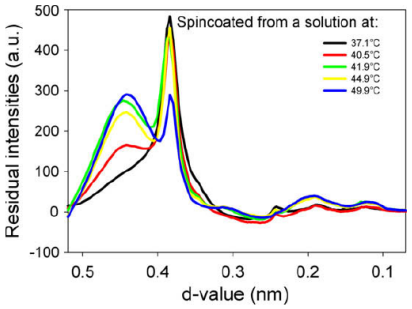

Fig. 3. Residual intensities of the SAED patterns of the polymer:PCBM matrix for several solution temperatures.

SAED patterns of the homogeneous areas of the active layers are shown (the area in between the PCBM crystals). These curves were obtained after integration across the diffraction ring followed by subtraction of a fitted background due to inelastic scattering (*cf.* Experimental). For the film spin-coated at 37 °C, the residual intensity SAED pattern shows a clear peak at 0.38 nm (Fig. 3). This peak can be attributed to the superposition of the (0 0 2) and (0 2 0) reflections from the crystal planes of semi-crystalline P3HT [14]. The remainder of the SAED pattern appears featureless and no peaks corresponding to PCBM can be distinguished. This indicates that the major part of PCBM is assembled in the needles. By slightly increasing the solution temperature to ~40 °C, a change in morphology is immediately observed. The PCBM needles have grown larger (Fig. 2b). We believe that the PCBM needles were formed in the casting solution during the long (>48 h) stirring at room temperature and elevated temperatures and not during spin-coating of the active layer. The spin-coating takes <120 s, which does not leave much time for the formation of such large needles. The long time available during stirring together with the perfect crystal shape and dependence of the crystal size on the temperature of the casting solution, all indicate that the crystals were formed during stirring of the casting solution by an Ostwald ripening process [15]. Higher temperatures accelerate the Ostwald ripening; therefore less but larger PCBM needles are visible at the solution temperature of ~40 °C. These needles have grown at the expense of the needles

that were present in solution at ~37 °C. For the solution temperature of ~40 °C, a small increase in the diffraction intensity at 0.46 nm can be seen in the SAED pattern of the area in between the needles (Fig. 3). This small peak indicates that some amount of nano-crystalline PCBM [16] is now present in between the fibers. Apparently a small part of the PCBM has dissolved in the *p*-xylene at this temperature; the PCBM is no longer completely grouped in the needles. This gives a higher yield of exciton dissociation at the polymer:PCBM interface and thus a higher J_{sc} and better solar cell performance (*cf.* Fig. 1). As opposed to the film made from a solution at 37 °C, the P3HT fibers are now visible as light areas in the BFTEM image (Fig. 2). This is caused by the presence of PCBM with a higher density in between the polymer matrix [2]. A further increase of the solution temperature leads to the disappearance of the PCBM needles (Fig. 2). For solution temperatures of ~42 °C, ~45 °C (Fig. 3) and ~48 °C (not shown) strong peaks corresponding to both P3HT (at 0.38 nm) and PCBM (at 0.2, 0.31 and 0.46 nm [16]) are present. These temperatures also correspond to the best photovoltaic performances (Fig. 1). Good charge transport due to crystalline P3HT, in combination with a large interfacial area between polymer and PCBM render good solar cells. At a solution temperature of ~50 °C, there is a slight drop in solar cell efficiency. At this point the fiber content has decreased strongly, which will likely result in less efficient hole transport.

4. Conclusion

We have demonstrated that the fiber content of the P3HT-fiber:PCBM casting solution can be easily controlled by temperature. Meanwhile, the dissolution of PCBM varies with temperature. The combined effect can be used to control the active layer morphology in photovoltaic devices and thus also their performance. An optimal solar cell efficiency was found at a solution temperature of ~45 °C when the fiber content was 42%. BFTEM images of the active layer morphology combined with SAED patterns revealed that this optimal photovoltaic efficiency occurred when the PCBM was dissolved completely at the highest possible fiber content. The initial increase in efficiency with temperature of the casting solution could be attributed to an increased solubility of PCBM in the casting solution. At temperatures lower than 41 °C, PCBM formed large (>50 μm) needles in the casting solution by Ostwald ripening, resulting in poorly mixed active layers and low solar cell efficiencies. At temperatures of 45 °C and higher, the PCBM was dissolved well and, after reaching its maximum, the solar cell efficiency started to decrease again with decreasing fiber content (due to the increasing solution temperature).

Acknowledgements

The research was carried out in the framework of the SBO-project 030220 "PolySpec", the FWO-project R-1226 and the interregional project OLED+. The work, as part of the project "SOHYDs" within the European Science Foundation EUROCORES Programme was also supported from funds by the FWO (G.0685.06) and the EC Sixth Framework Programme, under Contract No. ERAS-CT-2003-980409. Sabine Bertho is research assistant of the Fund for Scientific Research, Flanders (Belgium) (FWO).

References

[1] F. Padinger, R.S. Rittberger, N.S. Sariciftci, Adv. Funct. Mater. 13 (2003) 85.
[2] X. Yang, J. Loos, S.C. Veenstra, W.J.H. Verhees, M.M. Wien, J.M. Kroon, M.A.J. Michels, R.A.J. Janssen, Nano Lett. 5 (2005) 579.
[3] Y. Kim, S.A. Choulis, J. Nelson, D.D.C. Bradley, Appl. Phys. Lett. 86 (2005) 063502.
[4] X. Yang, G. Lu, L. Li, E. Zhou, Small 3 (2007) 611.
[5] W. Ma, C. Yang, X. Gong, K. Lee, A.J. Heeger, Adv. Funct. Mater. 15 (2005) 1617.
[6] S. Berson, R. De Bettignies, S. Bailly, S. Guillerez, Adv. Funct. Mater. 17 (2007) 1377.
[7] L. Li, G. Lu, X. Yang, J. Mater. Chem. 18 (2008) 1984.
[8] A.J. Moulé, K. Meerholz, Adv. Mater. 20 (2008) 240.
[9] W. Ma, J.Y. Kim, K. Lee, A.J. Heeger, Macromol. Rapid Commun. 28 (2007) 1776.
[10] P. Schilinsky, U. Asawapirom, U. Scherf, M. Biele, C.J. Brabec, Chem. Mater. 17 (2005) 2175.
[11] W.D. Oosterbaan, V. Vrindts, S. Berson, S. Guillerez, O. Douhéret, B. Ruttens, J. D'Haen, P. Adriaensens, J. Manca, L. Lutsen, D. Vanderzande, J. Mater. Chem., in press. doi:10.1039/b900670b.
[12] L. Reimer, Transmission Electron Microscopy, Springer-Verlag, Berlin, 1989.
[13] M.T. Rispens, A. Meetsma, R. Rittberger, C.J. Brabec, N.S. Sariciftci, J.C. Hummelen, Chem. Commun. (2003) 2116.
[14] S. Hugger, R. Thomann, T. Heinzel, T. Thurn-Albrecht, Colloid Polym. Sci. 282 (2004) 932.
[15] R. Boistelle, J.P. Astier, J. Cryst. Growth 90 (1988) 14.
[16] X. Yang, J.K.J. van Duren, M.T. Rispens, J.C. Hummelen, R.A.J. Janssen, M.A.J. Michels, J. Loos, Adv. Mater. 16 (2004) 802.